



This is to certify that the

thesis entitled

A TENTATIVE DOUBLE-SPRAY MODEL FEATURING SPRAY VAPORIZATION AND COUNTERFLOW DIFFLISION FLAMES presented by

MICHAEL YANG

has been accepted towards fulfillment of the requirements for

MASTER OF SCIENCE degree in MECHANICAL ENGINEERING

Major professor

Date 22. August, 1997

MSU is an Affirmative Action/Equal Opportunity Institution

0-7639

LIBRARY Michigan State University

PLACE IN RETURN BOX

to remove this checkout from your record.

TO AVOID FINES return on or before date due.

DATE DUE	DATE DUE	DATE DUE

1/98 c:/CIRC/DateDue.p65-p.14

A TENTATIVE DOUBLE-SPRAY MODEL FEATURING SPRAY VAPORIZATION AND COUNTERFLOW DIFFUSION FLAMES

 $\mathbf{B}\mathbf{y}$

Michael Yang

A THESIS

Submitted to
Michigan State University
in partial fulfillment of the requirements
for the degree of

MASTER OF SCIENCE

Department of Mechanical Engineering

1997

ABSTRACT

A TENTATIVE DOUBLE-SPRAY MODEL FEATURING SPRAY VAPORIZATION AND COUNTERFLOW DIFFUSION FLAMES

By

Michael Yang

The word "tentative" means purely theoretical. In this model we consider two gaseous streams (e.g., helium and nitrogen) approaching each other from opposite directions in a counterflow. The two opposed streams each carry a distribution of liquid droplets. Hence, we are examining the problem of a dual counterflow spray flame. We consider that the sprays consist of liquid fuel (e.g., hydrogen) and liquid oxidizer (e.g., oxygen), respectively. The sprays vaporize, and their subsequent gaseous phases diffuse toward a chemical reaction region near the stagnation plane, at which reactants burn.

At the outset, with the proper thermodynamic assumptions, we derive a set of steady-state, ordinary differential equations to describe the temperature of the gas flow and the mass fractions of each reactant. Then, we solve numerically the differential equations in three consequent cases, each more complicated than the one previous: (1) fast vaporization and fast chemistry, (2) finite-rate vaporization and fast chemistry, and (3) finite-rate vaporization and finite-rate chemistry. We compare the numerical results of our model to the fuel-spray-only and the purely-gaseous counterflow diffusion flame models.

Dedicated to my beloved Mother, Father, and Sister.



ACKNOWLEDGMENTS

This thesis strictly resembles the paper, "Counterflow Spray Diffusion Flames: Comparison between Asymptotic, Numerical, and Experimental Results," a masterpiece by Mr. Philippe Versaevel, Ecole Centrale de Paris, France, 1993. In other words, Mr. Versaevel's work is so excellent as well as promising and extendable, that it enables me to construct a similar, extended version upon itself. However, due to logistic limitations, the asymptotic and experimental methods applied by Mr. Versaevel are not covered in this thesis.

I shall be full-heartedly grateful to my academic advisor, Dr. Indrek S. Wichman, for his four-year-long guidance, encouragement, and... tolerance! He changed my life.

TO CHANGE A LIFE IS TO CHANGE A WORLD ENTIRE.

TABLE OF CONTENTS

	LIST OF FIGURES	vii
	NOMENCLATURE	xii
	INTRODUCTION	1
Chapter 1	MAIN ASSUMPTIONS	7
Chapter 2	GENERAL FORMULATION	9
	2.1. Governing Equations	9
	2.2. Nondimensionalization	11
Chapter 3	FAST VAPORIZATION AND FAST CHEMISTRY	14
-	3.1 Formulation by Coupling	15
	3.2 Formulation by Other Manipulations	18
	3.3 Locations of the Vaporization Fronts	23
	3.4 Location of the Flame Front	26
	3.5 Procedure to Determine the Profile	30
Chapter 4	FINITE-RATE VAPORIZATION AND FAST CHEMISTRY	35
_	4.1 Preliminary Relations	36
	4.2 Procedure to Determine the Profile	38
Chapter 5	FINITE-RATE VAPORIZATION AND FINITE-RATE CHEM-	
	ISTRY	45
	5.1 Procedure to Determine the Profile	45
Chapter 6	NUMERICAL RESULTS OF THE DOUBLE-SPRAY MODEL	55
•	6.1 Fast Vaporization and Fast Chemistry	56
	6.2 Finite-Rate Vaporization and Fast Chemistry	57
	6.3 Finite-Rate Vaporization and Finite-Rate Chemistry	61
Chapter 7	COMPARISON BETWEEN DOUBLE-SPRAY, FUEL-SPRAY-	
	ONLY, AND PURELY-GASEOUS MODELS	92

CONCLUSIONS	94
BIBLIOGRAPHY	95

LIST OF FIGURES

Figure 1	A representation of the tentative double-spray model	6
Figure 2	Five functions versus X: $\frac{F(X)}{1-X}$ and 1-X over [0, 0.5], $\frac{F(X)}{X}$ and X over [0.5, 1], and F(X) over [0, 1].	34
	120101 [010, 1], and 1 (12) 0 / 01 [0, 1].	٥.
Figure 3	A result of fast vaporization and fast chemistry in X-coordinate, with $Y_{OO} = 0.15$, $Y_{FF} = 0.03$ (i.e., $\phi = 1.6$). Upper diagram: T	
	[K]. Lower diagram: \tilde{Y}_{Fg} , \tilde{Y}_{Og} (_), \tilde{Y}_{Fl} , \tilde{Y}_{Ol} (), \tilde{Y}_{P} ().	65
Figure 4	A result of fast vaporization and fast chemistry in \tilde{x} -coordinate, with $Y_{OO} = 0.15$, $Y_{FF} = 0.03$ (i.e., $\phi = 1.6$). Upper diagram: T	
	[K]. Lower diagram: \tilde{Y}_{Fg} , \tilde{Y}_{Og} (_), \tilde{Y}_{Fl} , \tilde{Y}_{Ol} (), \tilde{Y}_{P} ().	66
Figure 5	Results of fast vaporization and fast chemistry in X-coordinate, with $Y_{OO} = 0.15$, $Y_{FF} = 0.015$, 0.03, 0.045, 0.06 (i.e., $\phi = 0.8$, 1.6, 2.4, 3.2, respectively). Upper diagram: T [K]. Lower diagram: \tilde{Y}_{Fg} , \tilde{Y}_{Og} (_), \tilde{Y}_{P} ().	67
Figure 6	Results of fast vaporization and fast chemistry in \tilde{x} -coordinate, with $Y_{OO} = 0.15$, $Y_{FF} = 0.015$, 0.03, 0.045, 0.06 (i.e., $\phi = 0.8$, 1.6, 2.4, 3.2, respectively). Upper diagram: T [K]. Lower diagram: \tilde{Y}_{Fg} , \tilde{Y}_{Og} (_), \tilde{Y}_{P} ().	68
Figure 7	Results of fast vaporization and fast chemistry in X-coordinate, with 6 sets of inputs: $Y_{OO} = 0.15$, $Y_{FF} = 0.015$ and 0.06 (i.e., $\phi = 0.8$ and 3.2); $Y_{OO} = 0.1$, $Y_{FF} = 0.01$ and 0.04 ($\phi = 0.8$ and 3.2); $Y_{OO} = 0.05$, $Y_{FF} = 0.005$ and 0.02 ($\phi = 0.8$ and 3.2).	

	Upper diagram: T [K]. Lower diagram: \tilde{Y}_{Fg} , \tilde{Y}_{Og} (_), \tilde{Y}_{P} ().	69
Figure 8	Results of fast vaporization and fast chemistry in \tilde{x} -coordinate, with 6 sets of inputs: $Y_{OO} = 0.15$, $Y_{FF} = 0.015$ and 0.06 (i.e., $\phi = 0.8$ and 3.2); $Y_{OO} = 0.1$, $Y_{FF} = 0.01$ and 0.04 ($\phi = 0.8$ and 3.2); $Y_{OO} = 0.05$, $Y_{FF} = 0.005$ and 0.02 ($\phi = 0.8$ and 3.2). Upper diagram: T [K]. Lower diagram: \tilde{Y}_{Fg} , \tilde{Y}_{Og} (_), \tilde{Y}_{P} ().	70
Figure 9	A result of finite-rate vaporization and fast chemistry in X-coordinate, with $Y_{OO} = 0.15$, $Y_{FF} = 0.03$, $1/D_{Ov} = 0.1$. Upper	
	diagram: T [K]. Lower diagram: Y_{Fg} , Y_{Og} (_), Y_{Fl} , Y_{Ol} (), Y_{P} ().	71
Figure 10	A result of finite-rate vaporization and fast chemistry in \tilde{x} -coordinate, with $Y_{OO} = 0.15$, $Y_{FF} = 0.03$, $1/D_{Ov} = 0.1$. Upper	
	diagram: T [K]. Lower diagram: \tilde{Y}_{Fg} , \tilde{Y}_{Og} (_), \tilde{Y}_{Fl} , \tilde{Y}_{Ol} (), \tilde{Y}_{P} ().	72
Figure 11	Results of finite-rate vaporization and fast chemistry in X-coordinate, with $Y_{OO}=0.15$, $Y_{FF}=0.03$, $1/D_{Ov}=0.0001$, 0.25,	
	0.5, 0.75, 1.0. Upper diagram: T [K]. Lower diagram: \tilde{Y}_{Fg} , \tilde{Y}_{Og}	
	(_), Y_{Fl} , Y_{Ol} (), Y_{P} ().	73
Figure 12	Results of finite-rate vaporization and fast chemistry in \tilde{x} -coordinate, with $Y_{OO} = 0.15$, $Y_{FF} = 0.03$, $1/D_{Ov} = 0.0001$, 0.25,	
	0.5, 0.75, 1.0. Upper diagram: T [K]. Lower diagram: \tilde{Y}_{Fg} , \tilde{Y}_{Og} (_), \tilde{Y}_{Fl} , \tilde{Y}_{Ol} (), \tilde{Y}_{P} ().	74
Figure 13	Results of finite-rate vaporization and fast chemistry shown as X-locations and temperatures versus a broad range of $1/D_{\rm Ov}$, with	
	$Y_{OO} = 0.15$, $Y_{FF} = 0.03$. Upper diagram: X_{Fv}^- , X_{Fv}^+ , X_{eq} ,	
	X_{Ov}^- , X_{Ov}^+ . Lower diagram: T_{Fl} , T_{Fv+} , T_{Ol} , T_{Ov-} , T_{eq} [K].	75
Figure 14	Results of finite-rate vaporization and fast chemistry shown as X -locations and temperatures versus a broad range of $1/D_{Ov}$, with	

	$Y_{OO} = 0.15$, $Y_{FF} = 0.015$, 0.03, 0.045, 0.06. Upper diagram:	
	X_{Ov}^- (_), X_{eq} (). Lower diagram: T_{Ov-} (_), T_{eq} () [K].	76
Figure 15	Results of finite-rate vaporization and finite-rate chemistry shown as temperature at the fast-chemistry flame front, T_f [K], ver-	
	sus strain rate, K [1/sec], with $Y_{OO} = 0.15$, $Y_{FF} = 0.025$, 0.00	
	and the original diameter of $O_2 = 1 \mu m$, $10 \mu m$, $20 \mu m$.	77
Figure 16	Results of finite-rate vaporization and finite-rate chemistry shown as temperature at the fast-chemistry flame front, T_f [K], ver-	
	sus strain rate, K [1/sec], with $Y_{OO} = 0.15$, $Y_{FF} = 0.025$, 0.026,	
	0.027, 0.028, 0.029, 0.03, 0.031, 0.032, 0.033, 0.034, 0.035, and the original diameter of $O_2 = 1~\mu$ m, $10~\mu$ m, $20~\mu$ m.	78
Figure 17	A result of finite-rate vaporization and finite-rate chemistry at	
	extinction in X-coordinate, with $Y_{OO} = 0.15$, $Y_{FF} = 0.035$,	
	K=150.88 /sec, and the original diameter of $O_2 = 1.0 \mu \text{ m}$. Upper	
	diagram: T [K]. Lower diagram: \hat{Y}_{Fg} , \hat{Y}_{Og} (_), \hat{Y}_{Fl} , \hat{Y}_{Ol} (), \hat{Y}_{P} ().	79
Figure 18	A result of finite-rate vaporization and finite-rate chemistry at extinction in \tilde{x} -coordinate, with $Y_{OO} = 0.15$, $Y_{FF} = 0.035$,	
	K=150.88 /sec, and the original diameter of $O_2 = 1.0 \mu \text{ m}$. Upper	
	diagram: T [K]. Lower diagram: \tilde{Y}_{Fg} , \tilde{Y}_{Og} (_), \tilde{Y}_{Fl} , \tilde{Y}_{Ol} (), \tilde{Y}_{P} ().	80
Figure 19	A result of finite-rate vaporization and finite-rate chemistry at extinction in X-coordinate, with $Y_{OO} = 0.15$, $Y_{FF} = 0.035$,	
	K=97.27 /sec, and the original diameter of $O_2 = 10 \mu \text{ m}$. Upper	
	diagram: T [K]. Lower diagram: \tilde{Y}_{Fg} , \tilde{Y}_{Og} (_), \tilde{Y}_{Fl} , \tilde{Y}_{Ol} (), \tilde{Y}_{P} ().	81
Figure 20	A result of finite-rate vaporization and finite-rate chemistry at extinction in \tilde{x} -coordinate, with $Y_{OO} = 0.15$, $Y_{FF} = 0.035$,	
	K=97.27 /sec, and the original diameter of $O_2 = 10 \mu \text{ m}$. Upper	
	diagram: T [K]. Lower diagram: \tilde{Y}_{Fg} , \tilde{Y}_{Og} (_), \tilde{Y}_{Fl} , \tilde{Y}_{Ol} (), \tilde{Y}_{P} ().	82

	extinction in X-coordinate, with $Y_{OO} = 0.15$, $Y_{FF} = 0.025$,	
	K=17.02 /sec, and the original diameter of $O_2 = 20 \mu$ m. Upper	
	diagram: T [K]. Lower diagram: \tilde{Y}_{Fg} , \tilde{Y}_{Og} (_), \tilde{Y}_{Fl} , \tilde{Y}_{Ol} (), \tilde{Y}_{P} ().	89
Figure 28	A result of finite-rate vaporization and finite-rate chemistry at extinction in \tilde{x} -coordinate, with $Y_{OO} = 0.15$, $Y_{FF} = 0.025$,	
	K=17.02 /sec, and the original diameter of $O_2 = 20 \mu$ m. Upper	
	diagram: T [K]. Lower diagram: \tilde{Y}_{Fg} , \tilde{Y}_{Og} (_), \tilde{Y}_{Fl} , \tilde{Y}_{Ol} (), \tilde{Y}_{P} ().	90
Figure 29	Results of finite-rate vaporization and finite-rate chemistry shown as (upper) the global equivalence ratio ϕ versus strain rate at extinction, K_{ext} [1/sec], and (lower) ϕ versus the highest flame	
	temperature at extinction, $T_{\text{max, ext}}$ [K], with $Y_{\text{OO}} = 0.15$, and the original diameter of $O_2 = 1 \mu \text{m}$, $10 \mu \text{m}$, $20 \mu \text{m}$.	91
Figure 30	Comparison between the Double-spray, Fuel-Spray-Only, and	
<i>3</i>	Purely-Gaseous Models	93

NOMENCLATURE

В	frequency factor for the chemical reaction
C_p	specific heat per unit mass of the gas mixture
d	original droplet diameter
D	diffusion coefficient
D_c	classical Damkohler number
D_{Fv}	vaporization Damkohler number for the fuel
D_{Ov}	vaporization Damkohler number for the oxidizer
K	strain rate of the counterflow
L_{F}	heat of vaporization per unit mass of fuel
L_{O}	heat of vaporization per unit mass of oxidizer
n	droplet number density
Q	heat released by combustion per unit mass of gaseous fuel
r	droplet radius
T	temperature of gas
T_a	activation temperature for the chemical reaction

T_{Fl}	boiling temperature of the fuel
T_{Ol}	boiling temperature of the oxidizer
v	axial velocity
x	axial coordinate
Y	mass fraction

Greek Symbols

 $\begin{array}{lll} \lambda & & \text{thermal conductivity of gas} \\ \\ \nu & & \text{stoichiometric coefficient} \\ \\ \varphi & & \text{global equivalence ratio (g.e.r.)} \\ \\ \rho & & \text{density} \\ \\ \rho_g & & \text{gas density} \end{array}$

Subscripts and Superscripts

FF relating to the origin of the fuel Fg relating to gaseous fuel relating to liquid fuel Flrelating to the fuel vaporization Fv relating to gaseous oxidizer OgOlrelating to liquid oxidizer relating to the origin of the oxidizer 00 relating to the oxidizer vaporization Ov

INTRODUCTION

Liquid fuel, especially when injected as a spray, is popular to many types of combustion engines. To investigate how the existence of the liquid phase of a reactant influences the combustion phenomenon, Philippe Versaevel [1] developed a simplified model by installing two nozzles injecting two gaseous nitrogen streams which approach each other from opposite directions in a counterflow. One of the opposed streams carries a distribution of liquid hydrocarbon droplets, considered as the fuel spray, and the other stream, which is purely gaseous, consists of an inert gas mixed with a certain amount of gaseous oxygen as the oxidizer. The fuel spray vaporizes, and then both the subsequent gaseous phase of fuel and the gaseous oxidizer diffuse and convect toward a chemical reaction region (denoted as the "flame zone") near the stagnation plane, at which reactants burn. This model, later referred to as the "fuel-spray-only" model in this thesis, is described as one-dimensional, steady-state, isobaric (under one atmosphere), constantstrain, fuel-lean, diffusional-flaming, and the distance between the origins of the fuel and oxidizer, which we regard as the two boundaries of the entire flow field being considered, is infinitely long compared to the thickness of the flame zone.

The spacecraft liquid rocket engines inspire us to consider the oxidizer as

well as the fuel as originally in liquid phase. However, in our research model, we do not intend to imitate a liquid rocket engine, say, the Space Shuttle Main Engine, where pure hydrogen and pure oxygen are originally compressed and stored in the liquid phase and are afterwards released and vaporized due to pressure difference [2]. Yes, we do hope that our current research will lead to better understanding of a liquid-fuel-liquid-oxidizer combustion mechanism, but, to make it theoretically derivable as well as experimentally controllable, we, instead, establish our model through a strict extension of Versaevel's model, so that the governing Navier-Stokes Equations can be largely simplified because of the isobaric condition and that the flame temperature can be easily controlled by changing the original mass fractions of the reactants (the fuel and oxidizer) within the non-reacting, background gases. After the extension, our model is identical to Versaevel's except that both the fuel and oxidizer are originally in liquid droplets, and hence we call ours the "double-spray" model.

Chapter One employs all of Versaevel's assumptions, which lead to our governing equations in Chapter Two. It is worth noting that these assumptions treat, at any given horizontal location (i.e. the x-coordinate), the gas flow as homogeneous and stationary relative to the reactants' droplets, and these droplets as uniform-sized, uniformly vaporized, in a vaporization mechanism macroscopically described and derived by F. A. Williams via the "d² law" [3], which constitutes the vaporization terms for both the fuel and oxidizer in the governing equations.

In Chapter Two we shall extend Versaevel's fuel-spray-only model into our

double-spray model by adding the vaporization term for the oxidizer to our governing equations. It is worth noting that this term can hardly be balanced in the overall coupling function (see Section 3.1) by the already introduced quantities; therefore, we introduce a quantity, the mass fraction of the product, denoted as Y_p , which plays a significant role in the coupling functions of Chapter Three, and in determining the location of the fast-chemistry flame front in Chapter Four.

Now we are able to investigate the key features of our model in Chapter Three by starting with the assumptions that both the chemical reaction rate and vaporization rates (for the fuel and oxidizer) are infinitely large, which implies that both the chemical reaction and the vaporization of sprays will occur at infinitesimally thin fronts. We denote this most special case as "fast vaporization and fast chemistry." The fast-rate assumptions enable us to manipulate and transform the comprehensive differential equations into algebraic expressions, which henceforth allow us to examine certain key factors theoretically and to obtain numerical solutions through a two-parameter algorithm which repeats merely algebraic calculations, as sketched in Section 3.4. It is also worth noting that, when we numerically locate the oxidizer's vaporization front at it own origin, all the algebraic formulas derived in our double-spray model will reduce to those in the fuel-spray-only model.

In Chapter Four we continue our analysis from the previous chapter by allowing the vaporization rates of sprays to be finite, which is more realistic. The two vaporization fronts for the fuel and oxidizer in Chapter Three are now released into two

broader regions, denoted as the "vaporization zones." We denote this case as "finite-rate vaporization and fast chemistry." The associated solution to the governing equations may be numerically acquired through a two-parameter algorithm which repeats integration over the two vaporization zones, as sketched in Section 4.2.

To accomplish the most realistic case in Chapter Five, we continue the analysis from the previous chapter by setting the chemical reaction rate to be finite, hence stretching the flame front onto a broad domain known as the flame zone. We denote this case as "finite-rate vaporization and finite-rate chemistry." The associated solution to the governing equations may be numerically acquired through an eight-parameter algorithm (containing two more parameters than that for the fuel-spray-only model) which repeats an overall integration throughout the entire flow field, and which is thoroughly sketched in Section 5.1.

Next, we proceed to demonstrate our double-spray model by selecting liquid hydrogen as the fuel and liquid oxygen as the oxidizer, and we employ certain reference for their thermodynamic properties [4,5]. Since the liquid phase of hydrogen under one atmosphere requires an ambient temperature as low as 20.38 Kelvin, we tend to select helium, which has the lowest boiling point in the Universe [6], as the non-reacting, background gas to carry both the fuel and oxidizer liquid phases. However, the subsequent computations show trouble. Basically, to prevent droplets from deterring the momentum of the gas flow, the original mass fraction of each liquid phase must be as low as 15% of the mass of the background gas. But, due to oxygen's large molecular weight compared to

helium's, a low oxygen mass fraction compared to the mass of helium will lead to a even lower molecular fraction which results in low concentration, hence weak chemical reaction, and low flame temperature. Therefore, we finally employ gaseous nitrogen, which has a similar molecular weight and slightly lower boiling temperature than that of oxygen, as the background gas carrying liquid oxygen droplets, and gaseous helium to carry the liquid hydrogen droplets only (see Figure 1). Nevertheless, we shall regard the gas properties such as ρ_g , λ , C_p , and D as constant throughout the flow field, and their values are based upon the mixture of equal numbers of moles of helium and nitrogen.

With our final selection for the reactants and background gases, we input the values of their associated properties into the computing algorithms for the three cases described in Chapters 3, 4, and 5, respectively. The numerical results of these cases, illustrated by diagrams, are placed in the three corresponding sections of Chapter Six.

Finally, for comparison, we transform our model into the fuel-spray-only model by employing the same reactants and background gases from Chapter 5 but slightly raising the ambient temperature on the oxidizer side so that the oxidizer is originally gaseous; consequently, we transform that fuel-spray-only model into the purely gaseous model by slightly raising the ambient temperature on the fuel side so that the fuel is originally gaseous, too. We compare the numerical results obtained in Chapter 5 to those of the two models here in Chapter Seven, which gives us a comprehensive understanding of counterflow spray flame problems.

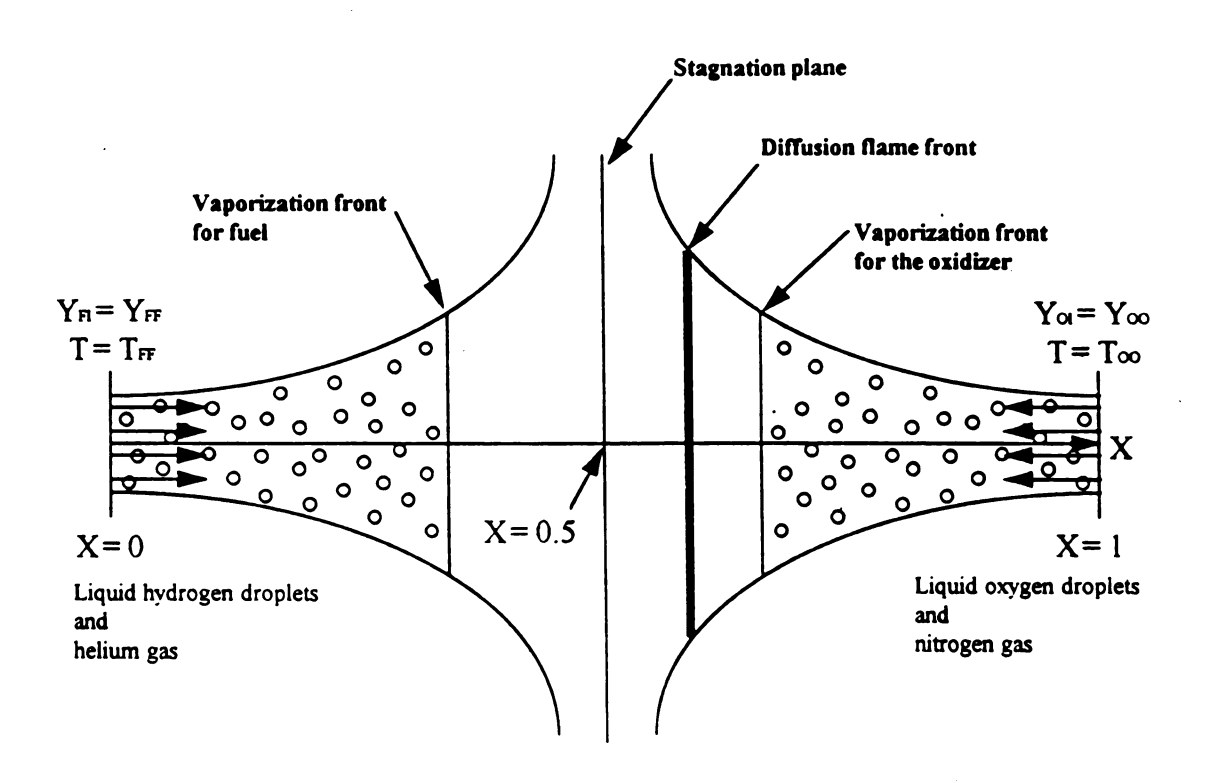


Figure 1. A Representation of the Tentative Double-Spray Model

CHAPTER ONE

MAIN ASSUMPTIONS

In this chapter, the six main assumptions made in this thesis are described in detail:

- 1. Both the fuel and oxidizer droplets are so scarce that the mixture density is equal to the gas density ρ_g , and all gas properties are constituted of those of the background gases only.
- 2. The density, thermal conductivity, and specific heat of the gas, denoted by ρ_g , λ , and C_p respectively, are constant. The diffusion coefficients of gaseous species (say, i), denoted by D_i , are equal to a constant value D. The gas phase Lewis number is unity.
- 3. Time rates of vaporized mass per unit volume per second for the fuel and oxidizer droplets, respectively, are as follows:

$$\dot{w}_{\rm Fv} = 4 \pi r_{\rm F} n_{\rm F} \frac{\lambda}{C_{\rm p}} ln \left[1 + \frac{C_{\rm p}}{L_{\rm F}} (T - T_{\rm F}l) \cdot u(T - T_{\rm F}l) \right],$$

$$w_{Ov} = 4 \pi r_{O} n_{O} \frac{\lambda}{C_{p}} ln \left[1 + \frac{C_{p}}{L_{O}} (T - T_{Ol}) \cdot u(T - T_{Ol}) \right],$$

where
$$u(t) \equiv \begin{cases} 0, t < 0, \\ 1, t \ge 0. \end{cases}$$

4. The axial velocity is proportional in magnitude and opposite in direction to the axial coordinate, which is expressed as:

$$v = -K x.$$

5. The time rate of fuel mass consumption per unit volume is expressed as:

$$\dot{w_c} = B \rho_g Y_{Fg}^p Y_{Og}^q exp\left(-\frac{T_a}{T}\right).$$

6. The product is in the gaseous phase only.

CHAPTER TWO

GENERAL FORMULATION

In this chapter, the governing equations are first written, then nondimensionalized. These equations, subject to various simplifications and alterations, are solved in Chapters 3, 4, and 5.

2-1. Governing Equations

The equations for conservation of energy [(1)], gaseous species [(2), (3), (4)] and liquid species [(5), (6)] are:

$$\rho_g \, v \, \frac{dT}{dx} = \rho_g \, v \, \frac{d^2T}{dx^2} + \frac{Q}{C_p} \, \dot{w}_c - \frac{L_F}{C_p} \, \dot{w}_{Fv} - \frac{L_O}{C_p} \, \dot{w}_{Ov}, \qquad (1)$$

$$\rho_g \, v \, \frac{dY_{Fg}}{dx} = \rho_g \, D \, \frac{d^2 Y_{Fg}}{dx^2} - \dot{w_c} + \dot{w_{Fv}},$$
 (2)

$$\rho_g \, v \, \frac{dY_{Og}}{dx} = \rho_g \, D \, \frac{d^2 Y_{Og}}{dx^2} - v \, \dot{w_c} + \dot{w_{Ov}},$$
(3)

$$\rho_g v \frac{dY_P}{dx} = \rho_g D \frac{d^2 Y_P}{dx^2} + (1 + v) \dot{w_c},$$
 (4)

$$\rho_g \, v \, \frac{dY_{Fl}}{dx} = - \stackrel{\cdot}{w}_{Fv} \,, \tag{5}$$

$$\rho_g \, v \, \frac{dY_{Ol}}{dx} = - \stackrel{\cdot}{w}_{Ov} \,. \tag{6}$$

These equations are subject to the relations:

$$Y_{Fl} = \frac{4}{3} \pi r_F n_F \frac{\rho_{Fl}}{\rho_g} ,$$

$$Y_{Ol} = \frac{4}{3} \pi r_O n_O \frac{\rho_{Ol}}{\rho_g} ,$$

and the boundary conditions:

at
$$x = -\infty$$
: $T = T_{FF}$, $Y_{Fg} = 0$, $Y_{Og} = 0$, $Y_{P} = 0$, $Y_{Ol} = 0$, $Y_{Fl} = Y_{FF} = \frac{4}{3} \pi r_{FF} n_F \frac{\rho_{Fl}}{\rho_g}$; at $x = +\infty$: $T = T_{OO}$, $Y_{Fg} = 0$, $Y_{Og} = 0$, $Y_{P} = 0$, $Y_{Fl} = 0$, $Y_{Ol} = Y_{OO} = \frac{4}{3} \pi r_{OO} n_O \frac{\rho_{Ol}}{\rho_g}$.

4



2-2. Nondimensionalization

In order to nondimensionalize these equations, we introduce:

$$\tilde{x} \equiv \sqrt{\frac{K}{D}} x$$
, $X \equiv \frac{1}{2} \left[erf\left(\frac{\tilde{x}}{\sqrt{2}}\right) + 1 \right]$, $\tilde{T} \equiv \frac{C_p T}{Q Y_{FF}}$, $\tilde{Y}_{Fg} \equiv \frac{Y_{Fg}}{Y_{FF}}$,

$$\tilde{Y}_{Og} \equiv \frac{Y_{Og}}{v Y_{FF}}, \quad \tilde{Y}_{P} \equiv \frac{Y_{P}}{(1+v) Y_{FF}}, \quad \tilde{Y}_{Fl} \equiv \frac{Y_{Fl}}{Y_{FF}}, \quad \tilde{Y}_{Ol} \equiv \frac{Y_{Ol}}{v Y_{FF}},$$

and then Equations (1) to (6) become, respectively:

$$\frac{d^{2}\tilde{T}}{dX^{2}} \left(\frac{dX}{d\tilde{x}}\right)^{2} = -D_{c} \tilde{Y}_{Fg}^{p} \tilde{Y}_{Og}^{q} exp\left(-\frac{\tilde{T}_{a}}{\tilde{T}}\right)
+ \frac{L_{F}}{Q} D_{Fv} \tilde{r}_{F} ln\left[1 + \frac{Q Y_{FF}}{L_{F}} (\tilde{T} - \tilde{T}_{Fl}) \cdot u(\tilde{T} - \tilde{T}_{Fl})\right]
+ \frac{1}{\phi} \frac{v L_{O}}{Q} D_{Ov} \tilde{r}_{O} ln\left[1 + \frac{Q Y_{FF}}{L_{O}} (\tilde{T} - \tilde{T}_{Ol}) \cdot u(\tilde{T} - \tilde{T}_{Ol})\right], \quad (7)$$

$$\frac{d^{2}\tilde{Y}_{Fg}}{dX^{2}} \left(\frac{dX}{d\tilde{x}}\right)^{2} = D_{c} \tilde{Y}_{Fg}^{p} \tilde{Y}_{Og}^{q} exp\left(-\frac{\tilde{T}_{a}}{\tilde{T}}\right)$$

$$-D_{Fv} \tilde{r}_{F} ln\left[1 + \frac{Q Y_{FF}}{L_{F}} (\tilde{T} - \tilde{T}_{Fl}) \cdot u(\tilde{T} - \tilde{T}_{Fl})\right], \tag{8}$$



$$\frac{d^{2}\tilde{Y}_{Og}}{dX^{2}} \left(\frac{dX}{d\tilde{x}}\right)^{2} = D_{c} \tilde{Y}_{Fg}^{p} \tilde{Y}_{Og}^{q} exp\left(-\frac{\tilde{T}_{a}}{\tilde{T}}\right)$$

$$-\frac{1}{\phi} D_{Ov} \tilde{r}_{O} ln\left[1 + \frac{Q Y_{FF}}{L_{O}} (\tilde{T} - \tilde{T}_{Ol}) \cdot u(\tilde{T} - \tilde{T}_{Ol})\right], \tag{9}$$

$$\frac{d^2 \tilde{\mathbf{Y}}_{P}}{d\mathbf{X}^2} \left(\frac{d\mathbf{X}}{d\tilde{\mathbf{x}}} \right)^2 = -\mathbf{D}_{c} \tilde{\mathbf{Y}}_{Fg}^{p} \tilde{\mathbf{Y}}_{Og}^{q} exp \left(-\frac{\tilde{\mathbf{T}}_{a}}{\tilde{\mathbf{T}}} \right), \tag{10}$$

$$\frac{d\tilde{\mathbf{Y}}_{Fl}}{d\mathbf{X}} \left(\frac{d\mathbf{X}}{d\tilde{x}} \right) (-\tilde{x}) = -\mathbf{D}_{Fv} \tilde{\mathbf{r}}_{F} \ln \left[1 + \frac{\mathbf{Q} \mathbf{Y}_{FF}}{\mathbf{L}_{F}} (\tilde{\mathbf{T}} - \tilde{\mathbf{T}}_{Fl}) \cdot u(\tilde{\mathbf{T}} - \tilde{\mathbf{T}}_{Fl}) \right], \tag{11}$$

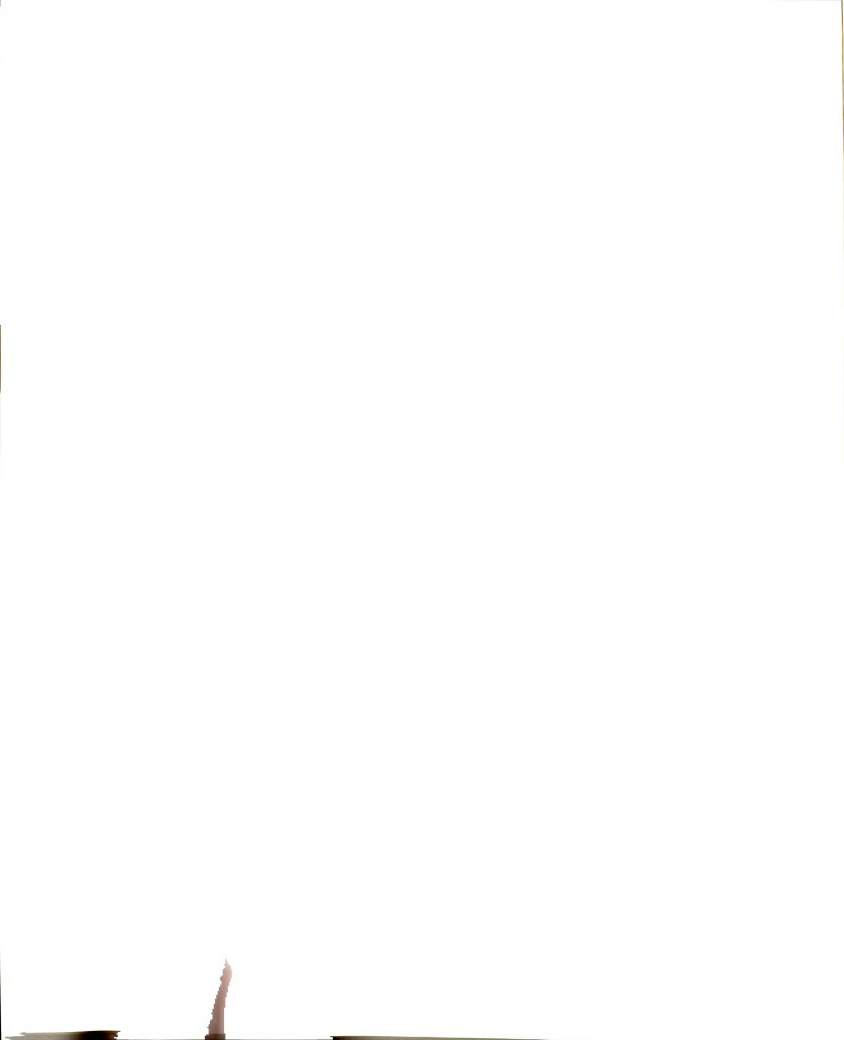
$$\frac{d\tilde{Y}_{Ol}}{dX} \left(\frac{dX}{d\tilde{x}} \right) \tilde{x} = \frac{1}{\phi} D_{Ov} \tilde{r}_{O} ln \left[1 + \frac{Q Y_{FF}}{L_{O}} (\tilde{T} - \tilde{T}_{Ol}) \cdot u(\tilde{T} - \tilde{T}_{Ol}) \right], \qquad (12)$$

subject to the boundary conditions:

at X= 0:
$$\tilde{T} = \tilde{T}_{FF}$$
, $\tilde{Y}_{Fg} = 0$, $\tilde{Y}_{Og} = 0$, $\tilde{Y}_{P} = 0$, $\tilde{Y}_{Fl} = 1$, $\tilde{Y}_{Ol} = 0$, at X= 1: $\tilde{T} = \tilde{T}_{OO}$, $\tilde{Y}_{Fg} = 0$, $\tilde{Y}_{Og} = 0$, $\tilde{Y}_{P} = 0$, $\tilde{Y}_{Fl} = 0$, $\tilde{Y}_{Ol} = \frac{1}{\phi}$,

where

$$\phi \equiv \frac{v Y_{FF}}{Y_{OO}} \ ,$$



$$D_c \equiv \frac{B \ v^q \ Y_{FF}^{\ p+q-1}}{K} \ ,$$

$$D_{Fv} \equiv 3 \frac{D}{K} \frac{1}{r_{FF}^2} \frac{\rho_g}{\rho_{Fl}} ,$$

$$D_{Ov} \equiv 3 \frac{D}{K} \frac{1}{r_{OO}^2} \frac{\rho_g}{\rho_{Ol}} ,$$

$$\tilde{r}_{F} \equiv \frac{r_{F}}{r_{FF}} = \tilde{Y}_{Fl}^{\frac{1}{3}},$$

$$\tilde{r}_{\rm O} \equiv \frac{r_{\rm O}}{r_{\rm OO}} = \phi^{\frac{1}{3}} \tilde{\rm Y}_{\rm Ol}^{\frac{1}{3}} ,$$

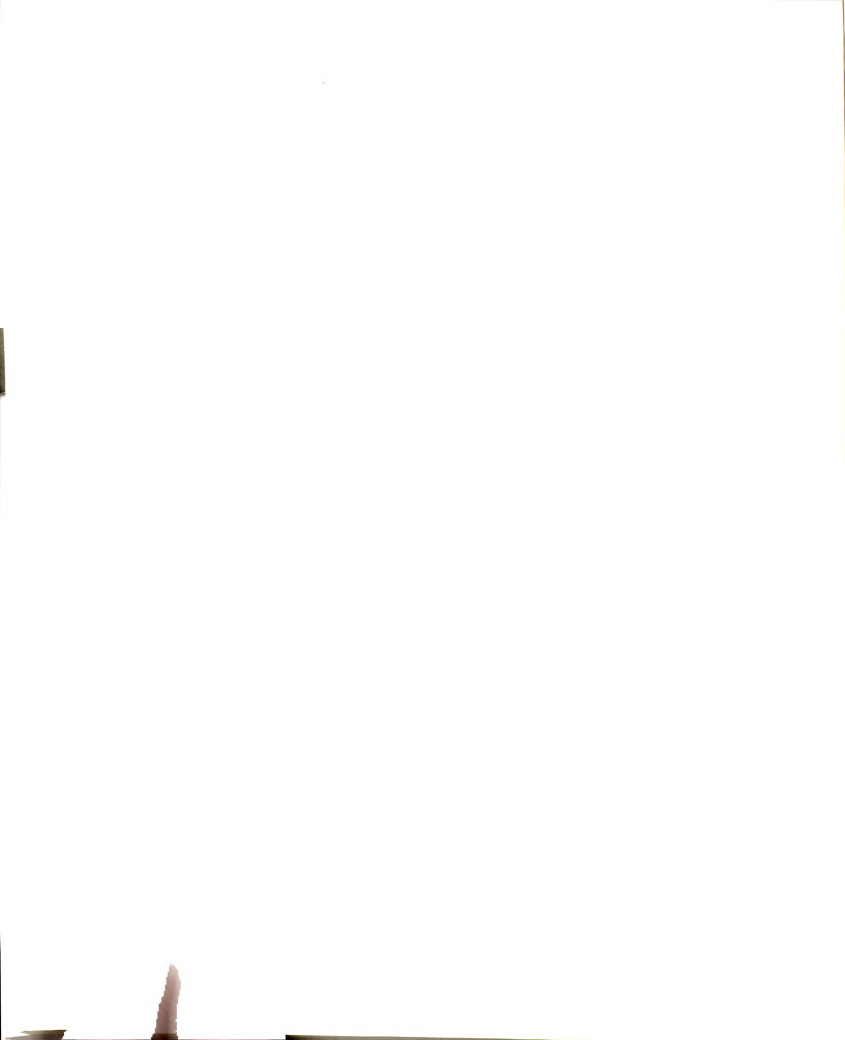
$$\tilde{T}_{Fl} \equiv \frac{C_p T_{Fl}}{Q Y_{FF}} ,$$

$$\tilde{T}_{Ol} \equiv \frac{C_p T_{Ol}}{Q Y_{EF}} ,$$

$$\tilde{T}_{FF} \equiv \frac{C_p T_{FF}}{Q Y_{FF}} ,$$

$$\tilde{T}_{OO} \equiv \frac{C_p \; T_{OO}}{Q \; Y_{FF}} \; . \label{eq:Too}$$

These nondimensional parameters are defined in the Nomenclature.



CHAPTER THREE

FAST VAPORIZATION AND FAST CHEMISTRY

Fast chemistry assumes that the reaction terms in Equations (7) to (10) exists only at an infinitesimally thin flame front, i.e. $X = X_{eq}$, and that the reaction at the flame is complete, i.e.:

$$\tilde{Y}_{Fg} = 0$$
, over $[X_{eq}, 1]$,

$$\tilde{Y}_{Og} = 0$$
, over $[0, X_{eq}]$.

In other words, the fuel and oxidizer cannot coexist.

Fast vaporization assumes that the vaporization terms for the fuel and oxidizer in Equations (7) to (12) exist only at two infinitesimally thin vaporization fronts: $X = X_{Fv}$ at the fuel vaporization front and $X = X_{Ov}$ at the oxidizer vaporization front and that the vaporization at each of the two fronts is complete. Therefore,

$$\mathbf{Y}_{Fl} = \begin{cases} \mathbf{Y}_{FF}, & \text{over } [0, \mathbf{X}_{Fv}], \\ \\ 0, & \text{over } [\mathbf{X}_{Fv}, 1], \end{cases}$$

$$\mathbf{Y}_{Ol} = \begin{cases} 0, & \text{over } [0, \mathbf{X}_{Ov}], \\ \mathbf{Y}_{OO}, & \text{over } [\mathbf{X}_{Ov}, 1]. \end{cases}$$

The relative positions among these three fronts are:

$$0 < X_{Fv} < {0.5 \brace X_{eq}} < X_{Ov} < 1$$
, i.e. $x_{Fv} < {0 \brace x_{eq}} < x_{Ov}$,

where the brackets denote that X_{eq} may be greater than, equal to, or smaller than 0.5 (i.e., x_{eq} may be greater than, equal to, or smaller than zero).

3-1. Formulation by Coupling

By proper combinations of Equations (7) to (10), we create coupling functions whose second derivatives with respect to X are zero and which are thus linear functions of X over certain applicable domains:

Over $[X_{Fv}, 1]$ we have $\tilde{Y}_{Fg} + \tilde{Y}_P = c_1 X + d_1$. The enforcement of boundary conditions at $X = X_{eq}$ and at X = 1 leads to:

$$\tilde{Y}_{Fg} + \tilde{Y}_{P} = \tilde{Y}_{P, eq} \frac{1 - X}{1 - X_{eq}}$$
 (13)

Over $[0, X_{Ov}]$ we have $\tilde{Y}_{Og} + \tilde{Y}_P = c_2 X + d_2$. The enforcement of boundary conditions at X=0 and at $X = X_{eq}$ leads to:

$$\tilde{Y}_{Og} + \tilde{Y}_{P} = \tilde{Y}_{P, eq} \frac{X}{X_{eq}}.$$
(14)

Over $[X_{Fv}, X_{Ov}]$ we combine Equations (13) and (14), and obtain:

$$\tilde{Y}_{Fg} - \tilde{Y}_{Og} = \tilde{Y}_{P, eq} \frac{X_{eq} - X}{X_{eq} (1 - X_{eq})}$$
 (15)

At the vaporization fronts $X = X_{Fv}$ and $X = X_{Ov}$, respectively, Equation (15) becomes:

$$\tilde{Y}_{Fg, Fv} = \tilde{Y}_{P, eq} \frac{X_{eq} - X_{Fv}}{X_{eq} (1 - X_{eq})},$$
(16)

$$\tilde{Y}_{Og, Ov} = \tilde{Y}_{P, eq} \frac{X_{Ov} - X_{eq}}{X_{eq} (1 - X_{eq})}$$
 (17)

Throughout the entire flow field [0, 1], without any fast-chemistry or fast-vaporization assumptions, we always have:

$$\tilde{T} \; + \; \frac{L_F}{Q} \; \tilde{Y}_{Fg} \; + \; \frac{v \; L_O}{Q} \; \tilde{Y}_{Og} \; - \; \left(1 - \frac{L_F}{Q} - \frac{v \; L_O}{Q}\right) \; \tilde{Y}_P \; = \; c_3 \; X + d_3 \; , \label{eq:tau_power}$$

which, with boundary conditions at X = 0 and at X = 1, is rewritten as:

$$\tilde{T} - \tilde{T}_{FF} + \frac{L_F}{Q} \tilde{Y}_{Fg} + \frac{v L_O}{Q} \tilde{Y}_{Og} = (\tilde{T}_{OO} - \tilde{T}_{FF}) X + \left(1 - \frac{L_F}{Q} - \frac{v L_O}{Q}\right) \tilde{Y}_P.$$
(18)

By applying the fast-chemistry assumption and setting $X = X_{eq}$, Equation (18) becomes:

$$\tilde{T}_{eq} = \tilde{T}_{FF} + (\tilde{T}_{OO} - \tilde{T}_{FF}) X_{eq} + \left(1 - \frac{L_F}{Q} - \frac{v L_O}{Q}\right) \tilde{Y}_{P, eq}.$$
 (19)

By applying both fast-chemistry and fast-vaporization assumptions and setting $X = X_{Fv}$ and $X = X_{Ov}$, respectively, Equation (18) becomes:

$$\tilde{T}_{Fl} - \tilde{T}_{FF} + \frac{L_F}{Q} \tilde{Y}_{Fg, Fv} = (\tilde{T}_{OO} - \tilde{T}_{FF}) X_{Fv} + \left(1 - \frac{L_F}{Q} - \frac{v L_O}{Q}\right) \tilde{Y}_{P, Fv},$$
 (20)



$$\tilde{T}_{Ol} - \tilde{T}_{FF} + \frac{v L_O}{Q} \tilde{Y}_{Og, Ov} = (\tilde{T}_{OO} - \tilde{T}_{FF}) X_{Ov} + \left(1 - \frac{L_F}{Q} - \frac{v L_O}{Q}\right) \tilde{Y}_{P, Ov}.$$
(21)

3.2 Formulation by Other Manipulations

According to the fast-chemistry and fast-vaporization assumptions, the chemical reaction term and vaporization terms of Equations (7) to (12) are zero over the entire field excluding the flame front and two vaporization fronts which are infinitesimally thin; in other words, the second derivatives of the mass fractions of fuel, the oxidizer, and the product with respect to X are zero over the segmental domains divided by these three fronts. Therefore, without any coupling and simply by applying conditions at X = 0, $X = X_{Fv}$, $X = X_{eq}$, $X = X_{Ov}$, and X = 1, the mass fractions may be determined as:

$$\tilde{Y}_{Fg} = \begin{cases}
\tilde{Y}_{Fg, Fv} \frac{X}{X_{Fv}}, & \text{over } [0, X_{Fv}], \\
\tilde{Y}_{Fg, Fv} \frac{X_{eq} - X}{X_{eq} - X_{Fv}}, & \text{over } [X_{Fv}, X_{eq}], \\
0, & \text{over } [X_{eq}, 1],
\end{cases} (22)$$

$$\tilde{Y}_{Og} = \begin{cases}
0, & \text{over } [0, X_{eq}], \\
\tilde{Y}_{Og, Ov} \frac{X - X_{eq}}{X_{Ov} - X_{eq}}, & \text{over } [X_{eq}, X_{Ov}], \\
\tilde{Y}_{Og, Ov} \frac{1 - X}{1 - X_{Ov}}, & \text{over } [X_{Ov}, 1],
\end{cases} (23)$$

$$\tilde{Y}_{P} = \begin{cases}
\tilde{Y}_{P, eq} \frac{X}{X_{eq}}, & \text{over } [0, X_{eq}], \\
\tilde{Y}_{P, eq} \frac{1 - X}{1 - X_{eq}}, & \text{over } [X_{eq}, 1].
\end{cases}$$
(24)

The discontinuities of the mass fraction gradients at the fronts $X = X_{eq}$, $X = X_{Fv}$, and $X = X_{Ov}$ may cause unequal diffusion rates for each species across these fronts. This inspires us to investigate how the mass fluxes are balanced. Here we use X_{Fv}^- and X_{Ov}^+ to denote the upstream sides (which contain droplets) of the vaporization fronts for the fuel and oxidizer, respectively, X_{Fv}^+ and X_{Ov}^- the downstream sides of the vaporization fronts, and X_{eq}^- and X_{eq}^+ the two sides of the flame front, facing the fuel and oxidizer mass fluxes, respectively. Also note that $X_{eq}^- = X_{eq}^+ = X_{eq}$, $X_{Fv}^- = X_{Fv}^+ = X_{Fv}$, and $X_{Ov}^- = X_{Ov}^+ = X_{Ov}$; i.e., $x_{eq}^- = x_{eq}^+ = x_{eq}$, $x_{Fv}^- = x_{Fv}^+ = x_{Fv}^-$, and $x_{Ov}^- = x_{Ov}^+ = x_{Ov}^-$.

Under the fast chemistry and fast vaporization assumptions, the mass conservation law describing mass across the two vaporization fronts, $X = X_{Fv}$ and $X = X_{Ov}$, respectively, is stated as:

$$\rho_g Y_{FF} (-K x_{Fv}^-) + \rho_g \tilde{Y}_{Fg, Fv} (-K x_{Fv}^-) - \rho_g D \left(\frac{dY_{Fg}}{dx}\right)_{x = x_{Fv}^-}$$

$$= \rho_g \tilde{Y}_{Fg, Fv} (-K x_{Fv}^+) - \rho_g D \left(\frac{dY_{Fg}}{dx}\right)_{x = x_{Fv}^+},$$
 (25)

$$\rho_{g} \tilde{Y}_{Og,Ov} (-K x_{Ov}^{-}) - \rho_{g} D \left(\frac{dY_{Og}}{dx}\right)_{x = x_{Ov}^{-}}$$

$$= \rho_{g} Y_{OO} (-K x_{Ov}^{+}) + \rho_{g} \tilde{Y}_{Og,Ov} (-K x_{Ov}^{+}) - \rho_{g} D \left(\frac{dY_{Og}}{dx}\right)_{x = x_{Ov}^{+}}.$$

Under the fast chemistry assumption, the mass conservation law describing

mass conservation across the flame front is stated as:

(26)

$$-\rho_{g} D\left(\frac{dY_{Fg}}{dx}\right)_{x = x_{eq}^{-}} + \rho_{g} \tilde{Y}_{P, eq} \left(-K x_{eq}^{-}\right) - \rho_{g} D\left(\frac{dY_{P}}{dx}\right)_{x = x_{eq}^{-}}$$

$$= -\rho_{g} D\left(\frac{dY_{Og}}{dx}\right)_{x = x_{eq}^{+}} + \rho_{g} \tilde{Y}_{P, eq} \left(-K x_{eq}^{+}\right) - \rho_{g} D\left(\frac{dY_{P}}{dx}\right)_{x = x_{eq}^{+}}.$$

$$(27)$$

Since $x_{eq}^- = x_{eq}^+ = x_{eq}$, $x_{Fv}^- = x_{Fv}^+ = x_{Fv}$, and $x_{Ov}^- = x_{Ov}^+ = x_{Ov}$ (or since there are no velocity jumps), all of the gaseous convection terms above are cancelled out, and Equations (25) to (27) henceforth become:

$$\rho_g Y_{FF} (-K x_{Fv}) - \rho_g D \left(\frac{dY_{Fg}}{dx}\right)_{x = x_{Fv}^-} = -\rho_g D \left(\frac{dY_{Fg}}{dx}\right)_{x = x_{Fv}^+},$$
 (28)

$$-\rho_g D\left(\frac{dY_{Og}}{dx}\right)_{x = x_{Ov}^-} = \rho_g Y_{OO} \left(-K x_{Ov}\right) - \rho_g D\left(\frac{dY_{Og}}{dx}\right)_{x = x_{Ov}^+},$$
(29)

$$-\rho_g D\left(\frac{dY_{Fg}}{dx}\right)_{x = x_{eq}^-} - \rho_g D\left(\frac{dY_P}{dx}\right)_{x = x_{eq}^-}$$

$$= -\rho_g D\left(\frac{dY_{Og}}{dx}\right)_{x = x_{eq}^+} - \rho_g D\left(\frac{dY_P}{dx}\right)_{x = x_{eq}^+}.$$
 (30)

Then, in terms of absolute values, equations (28) to (30) may be rewritten as:

$$\rho_{g} Y_{FF} K \cdot |x_{Fv}| = \rho_{g} D \cdot \left[\left| \frac{dY_{Fg}}{dx} \right|_{x = x_{Fv}^{-}} + \left| \frac{dY_{Fg}}{dx} \right|_{x = x_{Fv}^{+}} \right],$$

$$(31)$$

$$\rho_g Y_{OO} K \cdot |x_{Ov}| = \rho_g D \cdot \left[\left| \frac{dY_{Og}}{dx} \right|_{x = x_{Ov}^-} + \left| \frac{dY_{Og}}{dx} \right|_{x = x_{Ov}^+} \right], \tag{32}$$

$$\rho_{g} D \cdot \left[\left| \frac{dY_{Fg}}{dx} \right|_{x = x_{eq}^{-}} + \left| \frac{dY_{Og}}{dx} \right|_{x = x_{eq}^{+}} \right]$$

$$= \rho_{g} D \cdot \left[\left| \frac{dY_{P}}{dx} \right|_{x = x_{eq}^{-}} + \left| \frac{dY_{P}}{dx} \right|_{x = x_{eq}^{+}} \right]. \tag{33}$$

Equations (31) and (32) show that, for either the fuel or oxidizer, the total amount of mass diffusion at the vaporization front is equal to the mass convection of the liquid phase from upstream; moreover, Equation (23) shows that the total amount of mass diffusion of the product at the flame front is equal to the total amount of mass diffusion of the gaseous fuel from the fuel side plus the gaseous oxidizer from the oxidizer side.

In addition, Equations (31) and (32) may be further transformed through nondimensionalization and then be substituted into by the derivative forms of Equations (22) and (23), respectively; accordingly, relations concerning the locations of the vaporization fronts, $\tilde{x}_{\rm Fv}$ and $\tilde{x}_{\rm Ov}$, respectively, are obtained as follows:

$$-\tilde{x}_{Fv} = \frac{1}{\sqrt{2 \pi}} \tilde{Y}_{Fg, Fv} \frac{X_{eq}}{X_{Fv} (X_{eq} - X_{Fv})} exp\left(-\frac{\tilde{x}_{Fv}^{2}}{2}\right), \quad (34)$$

$$\tilde{x}_{Ov} = \frac{1}{\sqrt{2\pi}} \phi \tilde{Y}_{Og,Ov} \frac{1 - X_{eq}}{(X_{Ov} - X_{eq}) (1 - X_{Ov})} exp\left(-\frac{\tilde{x}_{Ov}^2}{2}\right).$$
(35)



3-3. Locations of the Vaporization Fronts

Rearrangement of Equations (34) and (35), respectively, gives the following relations:

$$\sqrt{2 \pi} (-\tilde{x}_{Fv}) X_{Fv} (1 - X_{Fv}) exp\left(\frac{\tilde{x}_{Fv}^2}{2}\right) = \tilde{Y}_{Fg, Fv} \frac{X_{eq} (1 - X_{Fv})}{X_{eq} - X_{Fv}},$$
 (36)

$$\sqrt{2 \pi} \tilde{x}_{Ov} X_{Ov} (1 - X_{Ov}) exp \left(\frac{\tilde{x}_{Ov}^2}{2} \right) = \phi \tilde{Y}_{Og, Ov} \frac{(1 - X_{eq}) X_{Ov}}{X_{Ov} - X_{eq}}.$$
 (37)

Then, we define $F(X) \equiv \sqrt{2 \pi} \cdot |\tilde{x}| \cdot X \cdot (1 - X) \cdot exp\left(\frac{\tilde{x}^2}{2}\right)$, where \tilde{x} is related to X

by the definition $X = \frac{1}{2} \left[erf\left(\frac{\tilde{x}}{\sqrt{2}}\right) + 1 \right]$. Hence Equations (36) and (37), respectively,

become:

$$\tilde{Y}_{Fg, Fv} = F(X_{Fv}) \cdot \frac{X_{eq} - X_{Fv}}{X_{eq} (1 - X_{Fv})},$$
(38)

$$\tilde{Y}_{Og, Ov} = \frac{1}{\phi} \cdot F(X_{Ov}) \cdot \frac{X_{Ov} - X_{eq}}{(1 - X_{eq}) X_{Ov}}$$
 (39)

3-3. Locations of the Vaporization Fronts

Rearrangement of Equations (34) and (35), respectively, gives the following relations:

$$\sqrt{2 \pi} (-\tilde{x}_{Fv}) X_{Fv} (1 - X_{Fv}) exp\left(\frac{\tilde{x}_{Fv}^2}{2}\right) = \tilde{Y}_{Fg, Fv} \frac{X_{eq} (1 - X_{Fv})}{X_{eq} - X_{Fv}},$$
 (36)

$$\sqrt{2 \pi} \tilde{x}_{Ov} X_{Ov} (1 - X_{Ov}) exp \left(\frac{\tilde{x}_{Ov}^{2}}{2} \right) = \phi \tilde{Y}_{Og, Ov} \frac{(1 - X_{eq}) X_{Ov}}{X_{Ov} - X_{eq}}.$$
 (37)

Then, we define $F(X) \equiv \sqrt{2 \pi} \cdot |\tilde{x}| \cdot X \cdot (1 - X) \cdot exp(\frac{\tilde{x}^2}{2})$, where \tilde{x} is related to X

by the definition $X = \frac{1}{2} \left[erf\left(\frac{\tilde{x}}{\sqrt{2}}\right) + 1 \right]$. Hence Equations (36) and (37), respectively,

become:

$$\tilde{Y}_{Fg, Fv} = F(X_{Fv}) \cdot \frac{X_{eq} - X_{Fv}}{X_{eq} (1 - X_{Fv})},$$
 (38)

$$\tilde{Y}_{Og, Ov} = \frac{1}{\phi} \cdot F(X_{Ov}) \cdot \frac{X_{Ov} - X_{eq}}{(1 - X_{eq}) X_{Ov}}.$$
 (39)

_

Next, by combining Equations (16) with (38), (17) with (39), to eliminate $\tilde{Y}_{Fg, Fv}$, $\tilde{Y}_{Og, Ov}$, respectively, we have:

$$\frac{\tilde{Y}_{P, eq}}{1 - X_{eq}} = \frac{F(X_{Fv})}{1 - X_{Fv}}, \qquad (40)$$

$$\frac{\tilde{Y}_{P, eq}}{X_{eq}} = \frac{1}{\phi} \frac{F(X_{Ov})}{X_{Ov}}. \tag{41}$$

Also, by setting $X = X_{Fv}$ and $X = X_{Ov}$, respectively, Equation (24) becomes:

$$\tilde{Y}_{P, Fv} = \tilde{Y}_{P, eq} \frac{X_{Fv}}{X_{eq}}, \qquad (42)$$

$$\tilde{Y}_{P,Ov} = \tilde{Y}_{P,eq} \frac{1 - X_{Ov}}{1 - X_{eq}}$$
 (43)

Now, to determine the locations of the vaporization fronts, i.e., \tilde{x}_{Fv} and \tilde{x}_{Ov} , we substitute Equations (16) and (42) into (20) to replace $\tilde{Y}_{Fg, Fv}$ and $\tilde{Y}_{P, Fv}$, and we substitute Equations (17) and (43) into (21) to replace $\tilde{Y}_{Og, Ov}$ and $\tilde{Y}_{P, Ov}$. Then, within either Equation (20) or (21), there coexist $\frac{\tilde{Y}_{P, eq}}{1 - X_{eq}}$ and $\frac{\tilde{Y}_{P, eq}}{X_{eq}}$, the former of

which can be replaced by $\frac{F(X_{Fv})}{1-X_{Fv}}$ from Equation (40), and the latter of which by

 $\frac{1}{\phi} \frac{F(X_{Ov})}{X_{Ov}}$ from Equation (41). As a result, Equations (20) and (21) become, respectively:

$$X_{Fv} = \frac{1}{1 - \frac{v L_{O}}{Q}} \frac{\phi X_{Ov}}{F(X_{Ov})} \left\{ \tilde{T}_{Fl} - \tilde{T}_{FF} - (\tilde{T}_{OO} - \tilde{T}_{FF}) X_{Fv} + \frac{L_{F}}{Q} F(X_{Fv}) \right\},$$
(44)

$$1 - X_{Ov}$$

$$= \frac{1}{1 - \frac{L_F}{Q}} \frac{1 - X_{Fv}}{F(X_{Fv})} \left\{ \tilde{T}_{Ol} - \tilde{T}_{FF} - (\tilde{T}_{OO} - \tilde{T}_{FF}) X_{Ov} + \frac{1}{\phi} \frac{v L_O}{Q} F(X_{Ov}) \right\}.$$
(45)

Figure 2 shows five functions with respect to X: F(X) over [0, 1], $\frac{F(X)}{1-X}$ and 1-X over [0, 0.5], and $\frac{F(X)}{X}$ and X over [0.5, 1]. Since, as mentioned at the beginning of this chapter, $0 < X_{Fv} < 0.5 < X_{Ov} < 1$, the diagram of Figure 2 informs us that neither the term $\frac{X_{Ov}}{F(X_{Ov})}$ in Equation (44) nor $\frac{1-X_{Fv}}{F(X_{Fv})}$ in Equation (45) is likely to be

zero; therefore, $X_{Fv} \to 0$ only when $\tilde{T}_{Fl} \to \tilde{T}_{FF}$ and $\frac{L_F}{Q} \to 0$, and $X_{Ov} \to 1$ only when $\tilde{T}_{Ol} \to \tilde{T}_{OO}$ and $\frac{L_O}{Q} \to 0$; that is to say, $X_{Fv} = 0$ only when the fuel is originally gaseous, and $X_{Ov} = 1$ only when the oxidizer is originally gaseous, both of which are consistent with physical reality.

3-4. Location of the Flame Front

Equations (40) and (41) give:

$$\begin{cases} X_{eq} + \frac{1 - X_{Fv}}{F(X_{Fv})} & \tilde{Y}_{P, eq} = 1 \\ X_{eq} + \frac{\phi X_{Ov}}{F(X_{Ov})} & \tilde{Y}_{P, eq} = 0 \end{cases}$$

Then, by solving the simultaneous equations above, we are able to determine the location of the flame front, X_{eq} , and the rescaled mass fraction of the product at the flame front, $\tilde{Y}_{P, eq}$, as follows:

$$X_{eq} = \frac{\frac{\phi X_{Ov}}{F(X_{Ov})}}{\frac{1 - X_{Fv}}{F(X_{Fv})} + \frac{\phi X_{Ov}}{F(X_{Ov})}} = \frac{\phi}{\frac{1 - X_{Fv}}{F(X_{Fv})} \frac{F(X_{Ov})}{X_{Ov}} + \phi},$$
 (46)



$$\tilde{Y}_{P, eq} = \frac{1}{\frac{1 - X_{Fv}}{F(X_{Fv})} + \frac{\phi X_{Ov}}{F(X_{Ov})}}$$
 (47)

From Equation (46) we observe that the variation in either X_{Fv} or X_{Ov} may influence the value of X_{eq} , and hence may shift the flame front either toward the fuel side or toward the oxidizer side. For convenience of discussion, here we introduce some new indices which are used in this section only:

Og: refers to the fuel-spray-only model, in which the oxidizer is originally gaseous, i.e. $X_{Oy} = 1$;

Fg: refers to the model that the fuel is originally gaseous, i.e. $X_{Fv} = 0$;

OFg: refers to the purely-gaseous model, where both $X_{Ov} = 1$ and $X_{Fv} = 0$.

Note that OFg is a special situation of either Og or Fg, and all these three models are special situations of our generalized "double-spray" model. Then we may express the location of the flame front in each of the four models. First, we recall Equation (46):

$$X_{eq} = \frac{\phi}{\frac{1 - X_{Fv}}{F(X_{Fv})} \frac{F(X_{Ov})}{X_{Ov}} + \phi},$$

which generally refers to the double-spray model and, when applied to models Og, Fg, and OFg, respectively, reduces to:

$$X_{\text{eq, O}g} = \frac{\phi}{\frac{1 - X_{\text{Fv}}}{F(X_{\text{Fv}})} + \phi},$$

$$X_{eq, Fg} = \frac{\phi}{\frac{F(X_{Ov})}{X_{Ov}} + \phi},$$

$$X_{eq, OFg} = \frac{\phi}{1+\phi}$$
.

For comparison, let the value in the global equivalence ratio ϕ be fixed throughout these four models. Then, look at X_{Fv} and X_{Ov} . Although Equations (44) and (45) indicate that the variation in the value of X_{Ov} may influence that of X_{Fv} , and viceversa, the influences may be negligible since, numerically speaking, X_{Ov} is usually close



(but not equal) to 1, and X_{Fv} usually close (but not equal) to zero, so that the values in X_{Fv} and in X_{Ov} throughout the four expressions above may be considered as fixed, which enables us to make the following comparison:

$$0 < X_{\rm eq,\,Og} < \left\{ \begin{array}{c} X_{\rm eq} \\ X_{\rm eq,\,OFg} \end{array} \right\} < X_{\rm eq,\,Fg} < 1 \; , \label{eq:Xeq,ofg}$$
 (the oxidizer side)

where X_{eq} may be greater than, equal to, or smaller than $X_{eq, OFg}$. The inequality relation above may be interpreted in a few ways, and here we take what we are most interested in:

$$X_{\rm eq,~Og} < X_{\rm eq}$$
 : means that the existence of the oxidizer spray (Fuel spray only) (Double spray)

shifts the flame toward the oxidizer side;

$$X_{eq, Og}$$
 < $X_{eq, OFg}$: means that the existence of the fuel spray shifts (Fuel spray only) (Purely gaseous)

the flame toward the fuel side.

To sum up: The flame moves toward the side where droplets originate.



3.5 Procedure to Determine the Profile

The entire fast-vaporization-fast-chemistry profile is linear with the physical coordinate X and can thus be explicitly determined by determining the locations of the vaporization and flame fronts $(X_{Fv}, X_{Ov}, \text{ and } X_{eq})$, the former two of which may be found through mutual iterations into Equations (44) and (45), and the latter by substituting the final values of the former two into Equation (46). The procedure is sketched below:

1. Setting up:

Starting values: $X_{Fv,i}$, $X_{Fv,j}$; $X_{Ov,i}$, $X_{Ov,j}$.

Iteration parameters: $\sigma_1^{(old)}$, σ_1 , $\sigma_1^{(new)}$ (for X_{Fv}); $\sigma_2^{(old)}$, σ_2 , $\sigma_2^{(new)}$ (for X_{Ov}).

Evaluation variables: $\eta_1^{(old)}$, η_1 ; $\eta_2^{(old)}$, η_2 .

Equation (45)
$$\Rightarrow \frac{F(X_{Fv})}{1 - X_{Fv}} = f_1(X_{Ov})$$
. (f₁: function)

Equation (44)
$$\Rightarrow \frac{F(X_{Ov})}{X_{Ov}} = f_2(X_{Fv})$$
. (f₂: function)

Preliminary inputs: Y_{OO}, Y_{FF}.

2. Algorithm for finding X_{Fv} and X_{Ov} :

I. Set:
$$\sigma_2 = X_{Ov, i}$$
.

II. i. Set:
$$\sigma_1 = X_{Fv,i}$$
.

ii. Set:
$$\eta_1 = \frac{F(\sigma_1)}{1 - \sigma_1} - f_1(\sigma_2)$$
.

iii. Set:
$$\sigma_1^{(old)} = \sigma_1$$
, $\eta_1^{(old)} = \eta_1$, $\sigma_1 = X_{Fv,j}$. Repeat (ii).

iv. Do:

a. Set:
$$\sigma_1^{(\text{new})} = \sigma_1 - (\sigma_1 - \sigma_1^{(\text{old})}) \cdot \frac{\eta_1}{\eta_1 - \eta_1^{(\text{old})}}$$
. (Newton's)

b. Set:
$$\sigma_1^{(\text{old})} = \sigma_1$$
, $\eta_1^{(\text{old})} = \eta_1$, $\sigma_1 = \sigma_1^{(\text{new})}$. Repeat (ii).

Until
$$\eta_1 < 10^{-6}$$
.

v. Set:
$$\eta_2 = \frac{F(\sigma_2)}{\sigma_2} - f_2(\sigma_1)$$
.

III. Set:
$$\sigma_2^{\text{(old)}} = \sigma_2$$
, $\eta_2^{\text{(old)}} = \eta_2$, $\sigma_2 = X_{Ov,j}$. Repeat (II).

IV. Do:

i. Set:
$$\sigma_2^{(\text{new})} = \sigma_2 - (\sigma_2 - \sigma_2^{(\text{old})}) \cdot \frac{\eta_2}{\eta_2 - \eta_2^{(\text{old})}}$$
. (Newton's)

ii. Set:
$$\sigma_2^{(old)} = \sigma_2$$
, $\eta_2^{(old)} = \eta_2$, $\sigma_2 = \sigma_2^{(new)}$. Repeat (II).

Until
$$\eta_2 < 10^{-6}$$
.

V. Final values:
$$X_{Fv} = \sigma_1$$
; $X_{Ov} = \sigma_2$.

3. The profile:

Once the final values of X_{Fv} and X_{Ov} are obtained, the profiles of all the



key variables can be subsequently determined by recalling equations from the previous sections:

$$X_{\text{eq}} = \frac{\frac{\phi}{1 - X_{\text{Fv}}} \frac{\phi}{F(X_{\text{Ov}})}}{\frac{F(X_{\text{Ov}})}{X_{\text{Ov}}} + \phi},$$
 (46)

$$\tilde{Y}_{P, eq} = \frac{1}{\frac{1 - X_{Fv}}{F(X_{Fv})} + \frac{\phi X_{Ov}}{F(X_{Ov})}},$$
(47)

$$\tilde{Y}_{Fg, Fv} = \tilde{Y}_{P, eq} \frac{X_{eq} - X_{Fv}}{X_{eq} (1 - X_{eq})},$$
(16)

$$\tilde{Y}_{Og, Ov} = \tilde{Y}_{P, eq} \frac{X_{Ov} - X_{eq}}{X_{eq} (1 - X_{eq})},$$
(17)

$$\tilde{T}_{eq} = \tilde{T}_{FF} + (\tilde{T}_{OO} - \tilde{T}_{FF}) X_{eq} + \left(1 - \frac{L_F}{O} - \frac{v L_O}{O}\right) \tilde{Y}_{P, eq},$$
 (19)

$$\tilde{Y}_{Fg} = \begin{cases}
\tilde{Y}_{Fg, Fv} \frac{X}{X_{Fv}}, & \text{over } [0, X_{Fv}], \\
\tilde{Y}_{Fg, Fv} \frac{X_{eq} - X}{X_{eq} - X_{Fv}}, & \text{over } [X_{Fv}, X_{eq}], \\
0, & \text{over } [X_{eq}, 1],
\end{cases}$$
(22)

$$\tilde{Y}_{Og} = \begin{cases}
0, & \text{over } [0, X_{eq}], \\
\tilde{Y}_{Og, Ov} \frac{X - X_{eq}}{X_{Ov} - X_{eq}}, & \text{over } [X_{eq}, X_{Ov}], \\
\tilde{Y}_{Og, Ov} \frac{1 - X}{1 - X_{Ov}}, & \text{over } [X_{Ov}, 1],
\end{cases} (23)$$



$$\tilde{Y}_{P} = \begin{cases}
\tilde{Y}_{P, eq} \frac{X}{X_{eq}}, & \text{over } [0, X_{eq}], \\
\tilde{Y}_{P, eq} \frac{1 - X}{1 - X_{eq}}, & \text{over } [X_{eq}, 1],
\end{cases}$$
(24)

$$\tilde{T} = \begin{cases} \tilde{T}_{FF} + (\tilde{T}_{Fl} - \tilde{T}_{FF}) \frac{X}{X_{Fv}}, & \text{over } [0, X_{Fv}], \\ \tilde{T}_{Fl} + (\tilde{T}_{eq} - \tilde{T}_{Fl}) \frac{X - X_{Fv}}{X_{eq} - X_{Fv}}, & \text{over } [X_{Fv}, X_{eq}], \\ \tilde{T}_{Ol} + (\tilde{T}_{eq} - \tilde{T}_{Ol}) \frac{X_{Ov} - X}{X_{Ov} - X_{eq}}, & \text{over } [X_{eq}, X_{Ov}], \\ \tilde{T}_{OO} + (\tilde{T}_{Ol} - \tilde{T}_{OO}) \frac{1 - X}{1 - X_{Ov}}, & \text{over } [X_{Ov}, 1], \end{cases}$$

$$\tilde{Y}_{Fl} = u(X_{Fv} - X)$$
, over [0, 1],

$$\tilde{Y}_{Ol} = \frac{1}{\phi} u(X - X_{Ov})$$
, over [0, 1],

where
$$u(t) \equiv \begin{cases} 0, t < 0, \\ 1, t \ge 0. \end{cases}$$



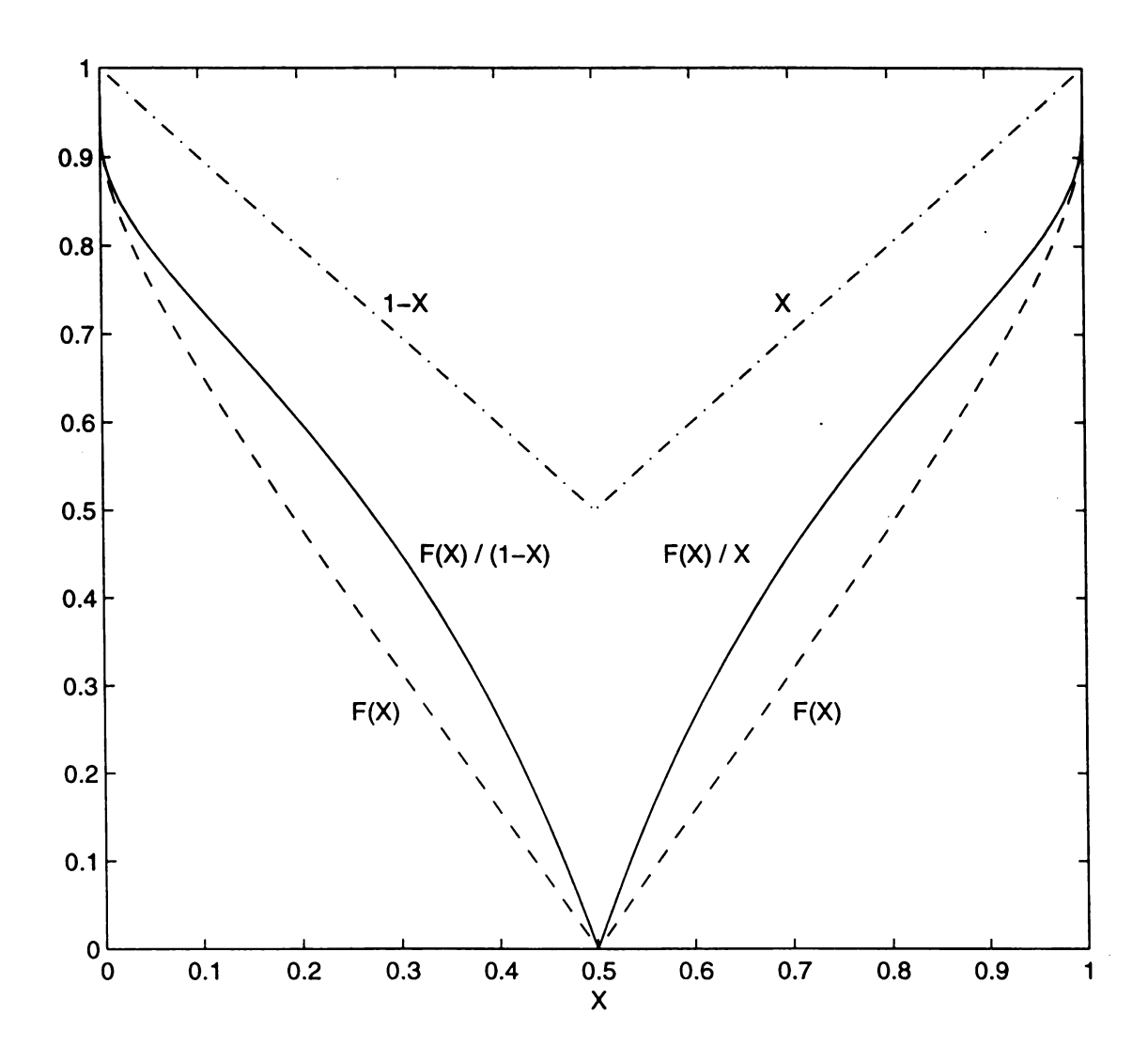


Figure 2. Five functions versus X: $\frac{F(X)}{1-X}$ and 1-X over [0, 0.5], $\frac{F(X)}{X}$ and X over [0.5, 1], and F(X) over [0, 1].

CHAPTER FOUR

FINITE-RATE VAPORIZATION AND FAST CHEMISTRY

An obvious distinction between fast vaporization and finite-rate one is that the former features $X_{Fv}^- = X_{Fv}^+ = X_{Fv}$ and $X_{Ov}^- = X_{Ov}^+ = X_{Ov}$, and the latter $X_{Fv}^- \neq X_{Fv}^+$ and $X_{Ov}^+ \neq X_{Ov}^-$. For finite-rate vaporization, intervals $[X_{Fv}^-, X_{Fv}^+]$ and $[X_{Ov}^-, X_{Ov}^+]$ are the so-called vaporization zones, and we have:

$$\tilde{Y}_{Fl} = \begin{cases} 1, & \text{over } [0, X_{Fv}^{-}], \\ 1 + \int \frac{X}{X_{Fv}^{-}} \left(\frac{d\tilde{Y}_{Fl}}{dt}\right) dt, & \text{for } X \in [X_{Fv}^{-}, X_{Fv}^{+}], \\ 0, & \text{over } [X_{Fv}^{+}, 1], \end{cases}$$

$$\tilde{Y}_{Ol} = \begin{cases} 0, & \text{over } [0, X_{Ov}^{-}], \\ \frac{1}{\phi} + \int \frac{X}{X_{Ov}^{+}} \left(\frac{d\tilde{Y}_{Ol}}{dt} \right) dt, & \text{for } X \in [X_{Ov}^{-}, X_{Ov}^{+}], \\ \frac{1}{\phi}, & \text{over } [X_{Ov}^{+}, 1], \end{cases}$$

$$\text{where } \begin{cases} X_{Fv}^{-} : \text{beginning of vaporization,} \\ X_{Fv}^{+} : \text{end of vaporization,} \end{cases} \text{ and } \begin{cases} X_{Ov}^{+} : \text{beginning of vaporization.} \\ X_{Ov}^{-} : \text{end of vaporization.} \end{cases}$$

For expressional convenience in the following sections, we define:

$$\begin{split} \tilde{T}_{Fv+} &\equiv \tilde{T}(X = X_{Fv}^{+}) \,, \; \tilde{Y}_{P,\,Fv+} \equiv \tilde{Y}_{P}(X = X_{Fv}^{+}) \,, \; \tilde{Y}_{Fg,\,Fv+} \equiv \tilde{Y}_{Fg}(X = X_{Fv}^{+}) \,, \\ \\ \tilde{T}_{Ov-} &\equiv \tilde{T}(X = X_{Ov}^{-}) \,, \; \tilde{Y}_{P,\,Ov-} \equiv \tilde{Y}_{P}(X = X_{Ov}^{-}) \,, \; \tilde{Y}_{Og,\,Ov-} \equiv \tilde{Y}_{Og}(X = X_{Ov}^{-}) \,. \end{split}$$

4.1 Preliminary Relations

By eliminating the chemical reaction term from the Governing Equations (7) to (10), we are able to derive the following coupling functions:

 $\tilde{T} + \tilde{Y}_{Fg} = c_F X + d_F$, over $[X_{Fv}^+, X_{Ov}^-]$. Applying the boundary conditions, we have:

$$\begin{cases} \text{at } X = X_{Fv}^{+}, & c_{F} X_{Fv}^{+} + d_{F} = \tilde{T}_{Fv+} + \tilde{Y}_{Fg, Fv+}, \\ \text{at } X = X_{Ov}^{-}, & c_{F} X_{Ov}^{-} + d_{F} = \tilde{T}_{Ov-}, \end{cases}$$

$$\Rightarrow c_{F} = \frac{\tilde{T}_{Ov-} - \tilde{T}_{Fv+} - \tilde{Y}_{Fg, Fv+}}{X_{Ov}^{-} - X_{Fv}^{+}}. \tag{48}$$



Similarly, $\tilde{T} + \tilde{Y}_{Og} = c_O X + d_O$, over $[X_{Fv}^+, X_{Ov}^-]$. With the boundary conditions we have:

$$\begin{cases} \text{at } X = X_{Fv}^{+}, & c_{O} X_{Fv}^{+} + d_{O} = \tilde{T}_{Fv+}, \\ \text{at } X = X_{Ov}^{-}, & c_{O} X_{Ov}^{-} + d_{O} = \tilde{T}_{Ov-} + \tilde{Y}_{Og,Ov-}, \end{cases}$$

$$\Rightarrow c_{O} = \frac{\tilde{T}_{Ov} + \tilde{Y}_{Og,Ov} - \tilde{T}_{Fv+}}{X_{Ov}^{-} - X_{Fv}^{+}}.$$
 (49)

These two coupling functions, $\tilde{T} + \tilde{Y}_{Fg}$ and $\tilde{T} + \tilde{Y}_{Og}$, can be reduced respectively by applying the following relations:

$$\tilde{Y}_{Fg} = 0$$
, over $[X_{eq}, 1]$, $\Rightarrow \tilde{T} = c_F X + d_F$, over $[X_{eq}, X_{Ov}]$, (50)

$$\tilde{Y}_{Og} = 0$$
, over $[0, X_{eq}]$, \Rightarrow $\tilde{T} = c_O X + d_O$, over $[X_{Fv}^+, X_{eq}]$, (51)

of which the derivative forms lead to the following relations, respectively:

$$c_{F} = \frac{d\tilde{T}}{dX} \left| X \in [X_{cq}, X_{Ov}^{-}] \right| = \frac{d\tilde{T}}{dX} \left| X = X_{Ov}^{-} \right|.$$
 (52)

$$c_{O} = \frac{d\tilde{T}}{dX} \left| X \in [X_{Fv}^{+}, X_{eo}] \right| = \frac{d\tilde{T}}{dX} \left| X = X_{Fv}^{+} \right|.$$
 (53)



Finally, we apply the boundary conditions of equation (50) and of equation (51), respectively, and obtain:

$$\begin{cases} \text{at } X = X_{eq} , \quad \tilde{T}_{eq} = c_F X_{eq} + d_F , \\ \text{at } X = X_{Ov}^- , \quad \tilde{T}_{Ov-} = c_F X_{Ov}^- + d_F , \end{cases} \Rightarrow \tilde{T}_{eq} = \tilde{T}_{Ov-} - c_F (X_{Ov}^- - X_{eq}^-) , \quad (54)$$

$$\begin{cases} \text{at } X = X_{Fv}^{+}, \quad \tilde{T}_{Fv+} = c_{O} X_{Fv}^{+} + d_{O}, \\ \text{at } X = \tilde{T}_{eq}, \quad \tilde{T}_{eq} = c_{O} X_{eq} + d_{O}, \end{cases} \Rightarrow \tilde{T}_{eq} = \tilde{T}_{Fv+} + c_{O} (X_{eq} - X_{Fv}^{+}), \quad (55)$$

the two of which imply:

$$X_{eq} = \frac{\tilde{T}_{Ov-} + c_O X_{Fv}^+ - \tilde{T}_{Fv+} - c_F X_{Ov}^-}{c_O - c_F}, \qquad (56)$$

$$= \frac{\tilde{T}_{Ov-} + X_{Fv}^{+} \cdot \frac{d\tilde{T}}{dX} \left| X = X_{Fv}^{+} - \tilde{T}_{Fv+} - X_{Ov}^{-} \cdot \frac{d\tilde{T}}{dX} \right| X = X_{Ov}^{-}}{\frac{d\tilde{T}}{dX} \left| X = X_{Fv}^{+} - \frac{d\tilde{T}}{dX} \right| X = X_{Ov}^{-}},$$

4.2 Procedure to Determine the Profile

1. Setting up:

Starting values: $X_{Fv, i}^-$, $X_{Fv, j}^-$; $X_{Ov, i}^+$, $X_{Ov, j}^+$.

Iteration parameters: $\sigma_1^{(old)}$, σ_1 , $\sigma_1^{(new)}$ (for X_{Fv}^-); $\sigma_2^{(old)}$, σ_2 , $\sigma_2^{(new)}$ (for X_{Ov}^+).

Evaluation variables: $\eta_1^{(old)}$, η_1 ; $\eta_2^{(old)}$, η_2 .

Dependent variables of σ_1 only: $X_{Fv}^{}$, $c_O^{},\,\tilde{T}_{Fv+}$.

Dependent variables of $\sigma_2^{}$ only: X_{Ov}^{-} , $c_F^{}$, $\tilde{T}_{Ov-}^{}$.

Dependent variables of (σ_1, σ_2) : $X_{eq}, \tilde{T}_{eq}, \tilde{Y}_{P, eq}; \tilde{Y}_{P, Fv+}, \tilde{Y}_{P, Ov-};$

$$\tilde{Y}_{Fg, Fv+}, \tilde{Y}_{Og, Ov-}$$

Governing differential equations:

on the fuel side:

$$\frac{d^2\tilde{T}}{dX^2} \left(\frac{dX}{d\tilde{x}}\right)^2 = \frac{L_F}{Q} D_{Fv} \tilde{r}_F ln \left[1 + \frac{Q Y_{FF}}{L_F} (\tilde{T} - \tilde{T}_{Fl}) \cdot u(\tilde{T} - \tilde{T}_{Fl})\right],$$

$$\frac{d\tilde{\mathbf{Y}}_{Fl}}{d\mathbf{X}} \left(\frac{d\mathbf{X}}{d\tilde{x}} \right) (-\tilde{x}) = -\mathbf{D}_{Fv} \tilde{\mathbf{r}}_{F} \ln \left[1 + \frac{\mathbf{Q} \mathbf{Y}_{FF}}{\mathbf{L}_{F}} (\tilde{\mathbf{T}} - \tilde{\mathbf{T}}_{Fl}) \cdot u(\tilde{\mathbf{T}} - \tilde{\mathbf{T}}_{Fl}) \right]$$

on the oxidizer side:

$$\frac{d^2\tilde{T}}{dX^2} \left(\frac{dX}{d\tilde{x}}\right)^2 =$$

$$\frac{1}{\phi} \frac{v L_{O}}{Q} D_{Ov} \tilde{r}_{O} ln \left[1 + \frac{Q Y_{FF}}{L_{O}} (\tilde{T} - \tilde{T}_{Ol}) \cdot u(\tilde{T} - \tilde{T}_{Ol}) \right],$$

$$\frac{d\tilde{Y}_{Ol}}{dX} \left(\frac{dX}{d\tilde{x}} \right) \tilde{x} = \frac{1}{\phi} D_{Ov} \tilde{r}_{O} ln \left[1 + \frac{Q Y_{FF}}{L_{O}} (\tilde{T} - \tilde{T}_{Ol}) \cdot u(\tilde{T} - \tilde{T}_{Ol}) \right]$$

Preliminary inputs: Y_{OO} , Y_{FF} , D_{Ov} , D_{Fv} .



2. Algorithm for finding X_{Fv}^- and X_{Ov}^+ :

I. Set:
$$\sigma_2 = X_{Ov,i}^+$$
.

II. i. Find
$$X_{Ov}^-$$
, so that: $\frac{1}{\phi} + \int \frac{X_{Ov}^-}{\sigma_2} \left(\frac{d\tilde{Y}_{Ol}}{dX}\right) dX = 0$. (Kutta's)

ii. Applying equation (52) and the definition for \tilde{T}_{Ov-} , set:

$$c_{F} = \frac{d\tilde{T}}{dX} \left| X = X_{Ov}^{-} = \frac{\tilde{T}_{OO} - \tilde{T}_{Ol}}{1 - \sigma_{2}} + \int \frac{X_{Ov}^{-}}{\sigma_{2}} \left(\frac{d^{2}\tilde{T}}{dX^{2}} \right) dX, \quad (Kutta's)$$

$$\tilde{T}_{Ov-} \equiv \tilde{T}(X = X_{Ov}^{-}) = \tilde{T}_{Ol} + \int \frac{X_{Ov}^{-}}{\sigma_2} \left(\frac{d\tilde{T}}{dX}\right) dX$$
 (Kutta's)

III. i. Set:
$$\sigma_1 = X_{Fv,i}$$

ii. a. Find
$$X_{Fv}^+$$
, so that: $1 + \int \frac{X_{Fv}^+}{\sigma_1} \left(\frac{d\tilde{Y}_{Fl}}{dX}\right) dX = 0$. (Kutta's)

b. Applying equation (53) and the definition for \tilde{T}_{Fv+} , set:

$$c_{O} = \frac{d\tilde{T}}{dX} \left| X = X_{Fv}^{+} \right| = \frac{\tilde{T}_{Fl} - \tilde{T}_{FF}}{\sigma_{1}} + \int \frac{X_{Fv}^{+}}{\sigma_{1}} \left(\frac{d^{2}\tilde{T}}{dX^{2}} \right) dX, \qquad (Kutta's)$$

$$\tilde{T}_{Fv+} \equiv \tilde{T}(X = X_{Fv}^{+}) = \tilde{T}_{Fl} + \int \frac{X_{Fv}^{+}}{\sigma_{1}} \left(\frac{d\tilde{T}}{dX}\right) dX .$$
 (Kutta's)

c. Applying equations (56), (55), (19), (24), and (18), set:

$$X_{eq} = \frac{\tilde{T}_{Ov-} + c_O X_{Fv}^+ - \tilde{T}_{Fv+} - c_F X_{Ov}^-}{c_O - c_F},$$

$$\tilde{T}_{eq} = \tilde{T}_{Fv+} + c_O (X_{eq} - X_{Fv}^+)$$
,

$$\tilde{Y}_{P, eq} = \frac{\tilde{T}_{eq} - \tilde{T}_{FF} - (\tilde{T}_{OO} - \tilde{T}_{FF})X_{eq}}{1 - \frac{L_F}{Q} - \frac{v L_O}{Q}},$$

$$\tilde{Y}_{P, Fv+} = \tilde{Y}_{P, eq} \frac{X_{Fv}^{+}}{X_{eq}}, \qquad \tilde{Y}_{P, Ov-} = \tilde{Y}_{P, eq} \frac{1 - X_{Ov}^{-}}{1 - X_{eq}},$$

$$\tilde{Y}_{Fg, Fv+} =$$

$$\frac{Q}{L_{F}} \left\{ \tilde{T}_{FF} - \tilde{T}_{Fv+} + (\tilde{T}_{OO} - \tilde{T}_{FF}) X_{Fv}^{+} + \left(1 - \frac{L_{F}}{Q} - \frac{v L_{O}}{Q}\right) \tilde{Y}_{P, Fv+} \right\},\,$$

$$\tilde{Y}_{Og, Ov-} =$$

$$\frac{Q}{v \; L_{O}} \left\{ \tilde{T}_{FF} - \tilde{T}_{Ov-} + (\tilde{T}_{OO} - \tilde{T}_{FF}) X_{Ov}^{-} + \left(1 - \frac{L_{F}}{Q} - \frac{v \; L_{O}}{Q}\right) \tilde{Y}_{P, \; Ov-} \right\}.$$

d. Applying (49), set:
$$\eta_1 = c_O - \frac{\tilde{T}_{Ov-} + \tilde{Y}_{Og,Ov-} - \tilde{T}_{Fv+}}{X_{Ov}^- - X_{Fv}^+}$$
.

iii. Set:
$$\sigma_1^{(old)} = \sigma_1$$
, $\eta_1^{(old)} = \eta_1$, $\sigma_1 = X_{Fv,j}$. Repeat (ii).

iv. Do:

a. Set:
$$\sigma_1^{(\text{new})} = \sigma_1 - (\sigma_1 - \sigma_1^{(\text{old})}) \cdot \frac{\eta_1}{\eta_1 - \eta_1^{(\text{old})}}$$
. (Newton's)

b. Set:
$$\sigma_1^{(\text{old})} = \sigma_1$$
, $\eta_1^{(\text{old})} = \eta_1$, $\sigma_1 = \sigma_1^{(\text{new})}$. Repeat (ii).

Until
$$\eta_1 < 10^{-6}$$
.

IV. Applying equation (48), set:
$$\eta_2 = c_F - \frac{\tilde{T}_{Ov} - \tilde{T}_{Fv} - \tilde{Y}_{Fg, Fv}}{X_{Ov}^- - X_{Fv}^+}$$
.

V. Set:
$$\sigma_2^{\text{(old)}} = \sigma_2$$
, $\eta_2^{\text{(old)}} = \eta_2$, $\sigma_2 = X_{Ov,j}$. Repeat (II) to (IV).

VI. Do:

i. Set:
$$\sigma_2^{(\text{new})} = \sigma_2 - (\sigma_2 - \sigma_2^{(\text{old})}) \cdot \frac{\eta_2}{\eta_2 - \eta_2^{(\text{old})}}$$
. (Newton's)

ii. Set:
$$\sigma_2^{(old)}=\sigma_2$$
, $\eta_2^{(old)}=\eta_2$, $\sigma_2=\sigma_2^{(new)}$. Repeat (II) to (IV). Until $\eta_2<10^{-6}$.

VII. Final values: $X_{Fv}^- = \sigma_1$; $X_{Ov}^+ = \sigma_2$.

3. The profile:

$$\tilde{T}_{FF} + (\tilde{T}_{Fl} - \tilde{T}_{FF}) \frac{X}{X_{Fv}^{-}}, \quad \text{over } [0, X_{Fv}^{-}],$$

$$\tilde{T}_{Fl} + \int \frac{X}{X_{Fv}^{-}} \left(\frac{d\tilde{T}}{dt} \right) dt, \quad \text{for } X \in [X_{Fv}^{-}, X_{Fv}^{+}],$$

$$\tilde{T}_{Fv+} + (\tilde{T}_{eq} - \tilde{T}_{Fv+}) \frac{X - X_{Fv}^{+}}{X_{eq} - X_{Fv}^{+}}, \quad \text{over } [X_{Fv}^{+}, X_{eq}],$$

$$\tilde{T}_{Ov-} + (\tilde{T}_{eq} - \tilde{T}_{Ov-}) \frac{X_{Ov}^{-} - X}{X_{Ov}^{-} - X_{eq}}, \quad \text{over } [X_{eq}^{-}, X_{Ov}^{-}],$$

$$\tilde{T}_{Ol} + \int \frac{X}{X_{Ov}^{+}} \left(\frac{d\tilde{T}}{dt} \right) dt, \quad \text{for } X \in [X_{Ov}^{-}, X_{Ov}^{+}],$$

$$\tilde{T}_{OO} + (\tilde{T}_{Ol} - \tilde{T}_{OO}) \frac{1 - X}{1 - X_{Ov}^{+}}, \quad \text{over } [X_{Ov}^{+}, 1],$$



$$\tilde{Y}_{P} = \begin{cases}
\tilde{Y}_{P, eq} \frac{X}{X_{eq}}, & \text{over } [0, X_{eq}], \\
\tilde{Y}_{P, eq} \frac{1 - X}{1 - X_{eq}}, & \text{over } [X_{eq}, 1],
\end{cases}$$
(24)

then, derived from equation (18), there are:

$$\tilde{Y}_{Fg} = \begin{cases} \frac{Q}{L_F} \left\{ \tilde{T}_{FF} - \tilde{T} + (\tilde{T}_{OO} - \tilde{T}_{FF})X + \left(1 - \frac{L_F}{Q} - \frac{v L_O}{Q}\right) \tilde{Y}_P \right\}, & \text{over } [0, X_{eq}], \\ \\ 0, & \text{over } [X_{eq}, 1], \end{cases}$$

$$\tilde{Y}_{Og} = \begin{cases} 0, & \text{over } [0, X_{eq}], \\ \\ \frac{Q}{\nu L_O} \left\{ \tilde{T}_{FF} - \tilde{T} + (\tilde{T}_{OO} - \tilde{T}_{FF})X + \left(1 - \frac{L_F}{Q} - \frac{\nu L_O}{Q}\right) \tilde{Y}_P \right\}, & \text{over } [X_{eq}, 1]. \end{cases}$$

Finally, recalling from the beginning of this chapter, we have the following:

$$\tilde{Y}_{Fl} = \begin{cases} 1, & \text{over } [0, X_{Fv}^{-}], \\ 1 + \int \frac{X}{X_{Fv}^{-}} \left(\frac{d\tilde{Y}_{Fl}}{dt}\right) dt, & \text{for } X \in [X_{Fv}^{-}, X_{Fv}^{+}], \\ 0, & \text{over } [X_{Fv}^{+}, 1], \end{cases}$$

$$\tilde{Y}_{Ol} = \begin{cases} 0, & \text{over } [0, X_{Ov}^{-}], \\ \frac{1}{\phi} + \int \frac{X}{X_{Ov}^{+}} \left(\frac{d\tilde{Y}_{Ol}}{dt}\right) dt, & \text{for } X \in [X_{Ov}^{-}, X_{Ov}^{+}], \\ \frac{1}{\phi}, & \text{over } [X_{Ov}^{+}, 1]. \end{cases}$$



CHAPTER FIVE

FINITE-RATE VAPORIZATION AND FINITE-RATE CHEMISTRY

In this chapter the reaction rate is no longer infinitely large and the reaction can not be completed merely at an infinitesimally thin interface. Therefore, integration over the broad flame zone as well as the overall domain [0,1] is required, and all the governing Equations (7) to (12) must be taken into account. Then, the whole computation process is sketched as follows:

5.1 Procedure to Determine the Profile

1. Setting up:

Starting values:

$$\begin{split} & \left(\frac{d\tilde{\Gamma}}{dX} \bigg|_{X=0} \right)_{i}, \left(\frac{d\tilde{\Gamma}}{dX} \bigg|_{X=0} \right)_{j}; \left(\frac{d\tilde{\Gamma}}{dX} \bigg|_{X=1} \right)_{i}, \left(\frac{d\tilde{\Gamma}}{dX} \bigg|_{X=1} \right)_{j}; \\ & \left(\frac{d\tilde{Y}_{Fg}}{dX} \bigg|_{X=0} \right)_{i}, \left(\frac{d\tilde{Y}_{Fg}}{dX} \bigg|_{X=0} \right)_{j}; \left(\frac{d\tilde{Y}_{Fg}}{dX} \bigg|_{X=1} \right)_{i}, \left(\frac{d\tilde{Y}_{Fg}}{dX} \bigg|_{X=1} \right)_{j}; \\ & \left(\frac{d\tilde{Y}_{Og}}{dX} \bigg|_{X=0} \right)_{i}, \left(\frac{d\tilde{Y}_{Og}}{dX} \bigg|_{X=0} \right)_{j}; \left(\frac{d\tilde{Y}_{Og}}{dX} \bigg|_{X=1} \right)_{i}, \left(\frac{d\tilde{Y}_{Og}}{dX} \bigg|_{X=1} \right)_{j}; \end{split}$$

$$\tilde{Y}_{Fg}(X = X_{eq})_i$$
 , $\tilde{Y}_{Fg}(X = X_{eq})_j$; K_i , K_j .

Iteration parameters:

$$\begin{split} &\sigma_{1}^{(\text{old})},\,\sigma_{1},\,\sigma_{1}^{(\text{new})}\,\,(\text{for }\frac{d\tilde{T}}{dX}\bigg|_{X=0});\,\sigma_{2}^{(\text{old})},\,\sigma_{2},\,\sigma_{2}^{(\text{new})}\,\,(\text{for }\frac{d\tilde{T}}{dX}\bigg|_{X=1});\\ &\sigma_{3}^{(\text{old})},\,\sigma_{3},\,\sigma_{3}^{(\text{new})}\,\,(\text{for }\frac{d\tilde{Y}_{Fg}}{dX}\bigg|_{X=0});\,\sigma_{4}^{(\text{old})},\,\sigma_{4},\,\sigma_{4}^{(\text{new})}\,\,(\text{for }\frac{d\tilde{Y}_{Fg}}{dX}\bigg|_{X=1});\\ &\sigma_{5}^{(\text{old})},\,\sigma_{5},\,\sigma_{5}^{(\text{new})}\,\,(\text{for }\frac{d\tilde{Y}_{Og}}{dX}\bigg|_{X=0});\,\sigma_{6}^{(\text{old})},\,\sigma_{6},\,\sigma_{6}^{(\text{new})}\,\,(\text{for }\frac{d\tilde{Y}_{Og}}{dX}\bigg|_{X=1});\\ &\sigma_{7}^{(\text{old})},\,\sigma_{7},\,\sigma_{7}^{(\text{new})}\,\,(\text{for }\tilde{Y}_{Fg}(X=X_{eq}));\,\sigma_{8}^{(\text{old})},\,\sigma_{8},\,\sigma_{8}^{(\text{new})}\,\,(\text{for }K). \end{split}$$

Evaluation variables:

$$\begin{split} &\eta_1^{(old)},\,\eta_1\,;\,\eta_2^{(old)},\,\eta_2\,;\,\eta_3^{(old)},\,\eta_3\,;\,\eta_4^{(old)},\,\eta_4\,;\\ &\eta_5^{(old)},\,\eta_5\,;\,\eta_6^{(old)},\,\eta_6\,;\,\eta_7^{(old)},\,\eta_7\,;\,\eta_8^{(old)},\,\eta_8\,. \end{split}$$

Dependent variables of σ_8 only: D_C , D_{Ov} , D_{Fv} , X_{eq} .

Dependent variables of $(\sigma_1, \sigma_3, \sigma_5, \sigma_8)$:

$$\frac{d\tilde{\Upsilon}}{dX} \left| X = X_{eq}^{-}, \frac{d\tilde{\Upsilon}_{Fg}}{dX} \right| X = X_{eq}^{-}, \frac{d\tilde{\Upsilon}_{Og}}{dX} \left| X = X_{eq}^{-}, \tilde{\Upsilon}_{Og}(X = X_{eq}^{-}).$$

Dependent variables of (σ_2 , σ_4 , σ_6 , σ_8):

$$\left. \frac{d\tilde{\Upsilon}}{dX} \right| X = X_{\rm eq}^+ , \left. \frac{d\tilde{\Upsilon}_{Fg}}{dX} \right| X = X_{\rm eq}^+ , \left. \frac{d\tilde{\Upsilon}_{Og}}{dX} \right| X = X_{\rm eq}^+ .$$

Preliminary inputs: Y_{OO} , Y_{FF} , r_{OO} , r_{FF} , \tilde{T}_f .

2. Algorithm for determining the iteration parameters:

I. Set:
$$\sigma_8 = K_i$$
.

$$II. i. Set: \begin{cases} D_c = \frac{B \, v^q \, Y_{FF}^{\, p+q-1}}{\sigma_8} \, . \\ \\ D_{Ov} = 3 \, \frac{D}{\sigma_8} \, \frac{1}{r_{OO}^2} \frac{\rho_g}{\rho_{Ol}} \, . \\ \\ D_{Fv} = 3 \, \frac{D}{\sigma_8} \, \frac{1}{r_{FF}^2} \frac{\rho_g}{\rho_{Fl}} \, . \end{cases}$$

ii. Applying the algorithm in Section 4.2, find X_{eq} .

III. i. Set:
$$\sigma_7 = \tilde{Y}_{Fg}(X = X_{eq})_i$$
.

ii. Set:
$$\sigma_5 = \left(\frac{\tilde{dY}_{Og}}{dX}\middle|_{X=0}\right)_i$$
.

iii. a. Set:
$$\sigma_1 = \left(\frac{d\tilde{T}}{dX}\Big|_{X=0}\right)_i$$
.

b. Set:
$$\sigma_3 = \left(\frac{d\tilde{Y}_{Fg}}{dX}\Big|_{X=0}\right)_i$$
.

c. Set:
$$\eta_3 = \int \frac{X_{eq}}{0} \left(\frac{d\tilde{Y}_{Fg}}{dX} \right) dX - \sigma_7$$
. (Kutta's)

d. Set:
$$\sigma_3^{\text{(old)}} = \sigma_3$$
, $\eta_3^{\text{(old)}} = \eta_3$, $\sigma_3 = \left(\frac{d\tilde{Y}_{Fg}}{dX} \middle|_{X=0}\right)_j$.

Repeat (c).

e. Do:

Set:
$$\sigma_3^{(\text{new})} = \sigma_3 - (\sigma_3 - \sigma_3^{(\text{old})}) \cdot \frac{\eta_3}{\eta_3 - \eta_3^{(\text{old})}}$$
. (Newton's)

Set:
$$\sigma_3^{(old)} = \sigma_3$$
, $\eta_3^{(old)} = \eta_3$, $\sigma_3 = \sigma_3^{(new)}$.

Repeat (c).

Until $\eta_3 < 10^{-5}$.

f. Set:
$$\eta_1 = \tilde{T}_{FF} + \int \frac{X_{eq}}{0} \left(\frac{d\tilde{T}}{dX} \right) dX - \tilde{T}_f$$
. (Kutta's)

h. Set:
$$\sigma_1^{\text{(old)}} = \sigma_1$$
, $\eta_1^{\text{(old)}} = \eta_1$, $\sigma_1 = \left(\frac{d\tilde{T}}{dX} \middle|_{X=0}\right)_i$.

Repeat from (b) to (f).

i. Do:

Set:
$$\sigma_1^{(\text{new})} = \sigma_1 - (\sigma_1 - \sigma_1^{(\text{old})}) \cdot \frac{\eta_1}{\eta_1 - \eta_1^{(\text{old})}}$$
. (Newton's)

Set:
$$\sigma_1^{(old)} = \sigma_1$$
, $\eta_1^{(old)} = \eta_1$, $\sigma_1 = \sigma_1^{(new)}$

Repeat from (b) to (f).

Until $\eta_1 < 10^{-5}$.

$$\begin{split} \text{j.} \qquad & \text{Set:} \\ \left| \begin{array}{c} \frac{d\tilde{\mathbf{T}}}{d\mathbf{X}} \right|_{\mathbf{X} = \mathbf{X}_{eq}^{-}} = \sigma_{1} + \int \overset{\mathbf{X}_{eq}}{0} \left(\frac{d^{2}\tilde{\mathbf{T}}}{d\mathbf{X}^{2}} \right) d\mathbf{X} \; . \\ \\ \frac{d\tilde{\mathbf{Y}}_{Fg}}{d\mathbf{X}} \right|_{\mathbf{X} = \mathbf{X}_{eq}^{-}} = \sigma_{3} + \int \overset{\mathbf{X}_{eq}}{0} \left(\frac{d^{2}\tilde{\mathbf{Y}}_{Fg}}{d\mathbf{X}^{2}} \right) d\mathbf{X} \; . \\ \\ \frac{d\tilde{\mathbf{Y}}_{Og}}{d\mathbf{X}} \right|_{\mathbf{X} = \mathbf{X}_{eq}^{-}} = \sigma_{5} + \int \overset{\mathbf{X}_{eq}}{0} \left(\frac{d^{2}\tilde{\mathbf{Y}}_{Og}}{d\mathbf{X}^{2}} \right) d\mathbf{X} \; . \\ \\ \tilde{\mathbf{Y}}_{Og}(\mathbf{X} = \mathbf{X}_{eq}^{-}) = \int \overset{\mathbf{X}_{eq}}{0} \left(\frac{d\tilde{\mathbf{Y}}_{Og}}{d\mathbf{X}} \right) d\mathbf{X} \; . \end{split}$$

(Kutta's)

iv. a. Set:
$$\sigma_2 = \left(\frac{d\tilde{T}}{dX}\Big|_{X=1}\right)_i$$
.

b. Set:
$$\sigma_4 = \left(\frac{\tilde{dY}_{Fg}}{dX}\Big|_{X=1}\right)_i$$
.

c. Set:
$$\sigma_6 = \left(\frac{d\tilde{Y}_{Og}}{dX} \middle|_{X=1}\right)_i$$
.

d. Set:
$$\eta_6 = \int_{1}^{X_{eq}} \left(\frac{d\tilde{Y}_{Og}}{dX}\right) dX - \tilde{Y}_{Og}(X = X_{eq}^-)$$
. (Kutta's)

e. Set:
$$\sigma_6^{\text{(old)}} = \sigma_6$$
, $\eta_6^{\text{(old)}} = \eta_6$, $\sigma_6 = \left(\frac{d\tilde{Y}_{Og}}{dX} \middle|_{X=1}\right)_j$.

Repeat (d).

f. Do:

Set:
$$\sigma_6^{(\text{new})} = \sigma_6 - (\sigma_6 - \sigma_6^{(\text{old})}) \cdot \frac{\eta_6}{\eta_6 - \eta_6^{(\text{old})}}$$
. (Newton's)

Set:
$$\sigma_6^{(old)} = \sigma_6$$
, $\eta_6^{(old)} = \eta_6$, $\sigma_6 = \sigma_6^{(new)}$.

Repeat (d).

 $Until \quad \eta_6 < 10^{-5} \, .$

g. Set:
$$\eta_4 = \int_{-1}^{X_{eq}} \left(\frac{d\tilde{Y}_{Fg}}{dX} \right) dX - \sigma_7$$
. (Kutta's)

h. Set:
$$\sigma_4^{(\text{old})} = \sigma_4$$
, $\eta_4^{(\text{old})} = \eta_4$, $\sigma_4 = \left(\frac{d\tilde{Y}_{Fg}}{dX} \middle|_{X=1}\right)_j$.

Repeat from (c) to (g).

i. Do:



Set:
$$\sigma_4^{(\text{new})} = \sigma_4 - (\sigma_4 - \sigma_4^{(\text{old})}) \cdot \frac{\eta_4}{\eta_4 - \eta_4^{(\text{old})}}$$
. (Newton's)

Set:
$$\sigma_4^{(old)} = \sigma_4$$
, $\eta_4^{(old)} = \eta_4$, $\sigma_4 = \sigma_4^{(new)}$.

Repeat from (c) to (g).

Until $\eta_4 < 10^{-5}$.

j. Set:
$$\eta_2 = \tilde{T}_{OO} + \int_{1}^{X_{eq}} \left(\frac{d\tilde{T}}{dX}\right) dX - \tilde{T}_f$$
. (Kutta's)

k. Set:
$$\sigma_2^{\text{(old)}} = \sigma_2$$
, $\eta_2^{\text{(old)}} = \eta_2$, $\sigma_2 = \left(\frac{d\tilde{T}}{dX} \middle|_{X=1}\right)_j$.

Repeat from (b) to (j).

l. Do:

Set:
$$\sigma_2^{(\text{new})} = \sigma_2 - (\sigma_2 - \sigma_2^{(\text{old})}) \cdot \frac{\eta_2}{\eta_2 - \eta_2^{(\text{old})}}$$
. (Newton's)

Set:
$$\sigma_2^{(old)} = \sigma_2$$
, $\eta_2^{(old)} = \eta_2$, $\sigma_2 = \sigma_2^{(new)}$.

Repeat from (b) to (j).

 $Until \quad \eta_2 < 10^{-5} \, .$

m. Set:
$$\begin{cases} \frac{d\tilde{\Gamma}}{dX} \Big|_{X = X_{eq}^{+}} = \sigma_{2} + \int \frac{X_{eq}}{1} \left(\frac{d^{2}\tilde{\Gamma}}{dX^{2}} \right) dX. \\ \frac{d\tilde{Y}_{Fg}}{dX} \Big|_{X = X_{eq}^{+}} = \sigma_{4} + \int \frac{X_{eq}}{1} \left(\frac{d^{2}\tilde{Y}_{Fg}}{dX^{2}} \right) dX. \\ \frac{d\tilde{Y}_{Og}}{dX} \Big|_{X = X_{eq}^{+}} = \sigma_{6} + \int \frac{X_{eq}}{1} \left(\frac{d^{2}\tilde{Y}_{Og}}{dX^{2}} \right) dX. \end{cases}$$
(Kutta's)



v. Set:
$$\eta_5 = \frac{d\tilde{Y}_{Og}}{dX} \left| X = X_{eq}^+ - \frac{d\tilde{Y}_{Og}}{dX} \right| X = X_{eq}^-$$
.

vi. Set:
$$\sigma_5^{\text{(old)}} = \sigma_5$$
, $\eta_5^{\text{(old)}} = \eta_5$, $\sigma_5 = \left(\frac{d\tilde{Y}_{Og}}{dX} \middle|_{X=0}\right)_j$.

Repeat from (iii) to (v).

vii. Do:

Set:
$$\sigma_5^{(\text{new})} = \sigma_5 - (\sigma_5 - \sigma_5^{(\text{old})}) \cdot \frac{\eta_5}{\eta_5 - \eta_5^{(\text{old})}}$$
. (Newton's)

Set:
$$\sigma_5^{(old)} = \sigma_5$$
, $\eta_5^{(old)} = \eta_5$, $\sigma_5 = \sigma_5^{(new)}$.

Repeat from (iii) to (v).

Until $\eta_5 < 10^{-4}$.

viii. Set:
$$\eta_7 = \frac{d\tilde{Y}_{Fg}}{dX} \left| X = X_{eq}^+ - \frac{d\tilde{Y}_{Fg}}{dX} \right| X = X_{eq}^-$$
.

ix. Set:
$$\sigma_7^{(old)} = \sigma_7$$
, $\eta_7^{(old)} = \eta_7$, $\sigma_7 = \tilde{Y}_{Fg}(X = X_{eq})_j$.

Repeat from (ii) to (viii).

x. Do:

Set:
$$\sigma_7^{\text{(new)}} = \sigma_7 - (\sigma_7 - \sigma_7^{\text{(old)}}) \cdot \frac{\eta_7}{\eta_7 - \eta_7^{\text{(old)}}}$$
. (Newton's)

Set:
$$\sigma_7^{(old)} = \sigma_7$$
, $\eta_7^{(old)} = \eta_7$, $\sigma_7 = \sigma_7^{(new)}$.

Repeat from (ii) to (viii).

Until $\eta_7 < 10^{-4}$.



IV. Set:
$$\eta_8 = \frac{d\tilde{T}}{dX} \Big|_{X = X_{eq}^+} - \frac{d\tilde{T}}{dX} \Big|_{X = X_{eq}^-}$$
.

V. Set:
$$\sigma_8^{(old)} = \sigma_8$$
, $\eta_8^{(old)} = \eta_8$, $\sigma_8 = K_j$.

Repeat from (II) to (IV).

VI. Do:

Set:
$$\sigma_8^{(\text{new})} = \sigma_8 - (\sigma_8 - \sigma_8^{(\text{old})}) \cdot \frac{\eta_8}{\eta_8 - \eta_8^{(\text{old})}}$$
. (Newton's)

$$\text{Set:} \quad \sigma_8^{(old)} \, = \, \sigma_8 \, , \, \eta_8^{(old)} \, = \, \eta_8 \, , \, \sigma_8 \, = \, \sigma_8^{(new)} \, .$$

Repeat from (II) to (IV).

Until
$$\eta_8 < 10^{-4}$$
.

VII. Final values:

$$\frac{d\tilde{\Gamma}}{dX}\bigg|_{X=0} = \sigma_1, \frac{d\tilde{\Gamma}}{dX}\bigg|_{X=1} = \sigma_2, \frac{d\tilde{Y}_{Fg}}{dX}\bigg|_{X=0} = \sigma_3, \frac{d\tilde{Y}_{Fg}}{dX}\bigg|_{X=1} = \sigma_4,$$

$$\frac{d\tilde{Y}_{Og}}{dX}\Big|_{X=0} = \sigma_5, \frac{d\tilde{Y}_{Og}}{dX}\Big|_{X=1} = \sigma_6, \tilde{Y}_{Fg}(X = X_{eq}) = \sigma_7, K = \sigma_8.$$

3. The profile:

$$\tilde{\mathbf{T}} = \begin{cases} \int \frac{\mathbf{X}}{0} \left(\frac{d\tilde{\mathbf{T}}}{dt} \right) dt , & \text{for } \mathbf{X} \in [0, \mathbf{X}_{eq}] , \\ \int \frac{\mathbf{X}}{1} \left(\frac{d\tilde{\mathbf{T}}}{dt} \right) dt , & \text{for } \mathbf{X} \in [\mathbf{X}_{eq}, 1] , \end{cases}$$



$$\tilde{\mathbf{Y}}_{Fg} = \begin{cases} \int \frac{\mathbf{X}}{0} \left(\frac{d\tilde{\mathbf{Y}}_{Fg}}{dt} \right) dt , & \text{for } \mathbf{X} \in [0, \mathbf{X}_{eq}], \\ \int \frac{\mathbf{X}}{1} \left(\frac{d\tilde{\mathbf{Y}}_{Fg}}{dt} \right) dt , & \text{for } \mathbf{X} \in [\mathbf{X}_{eq}, 1], \end{cases}$$

$$\tilde{\mathbf{Y}}_{\mathrm{O}g} = \begin{cases} \int \frac{\mathbf{X}}{0} \left(\frac{d\tilde{\mathbf{Y}}_{\mathrm{O}g}}{dt} \right) dt , & \text{for } \mathbf{X} \in [0, \mathbf{X}_{\mathrm{eq}}] , \\ \int \frac{\mathbf{X}}{1} \left(\frac{d\tilde{\mathbf{Y}}_{\mathrm{O}g}}{dt} \right) dt , & \text{for } \mathbf{X} \in [\mathbf{X}_{\mathrm{eq}}, 1] . \end{cases}$$

Then, Equation (18) gives:

$$\tilde{Y}_{P} = \frac{\tilde{T} - \tilde{T}_{FF} + \frac{L_{F}}{Q} \tilde{Y}_{Fg} + \frac{v L_{O}}{Q} \tilde{Y}_{Og} - (\tilde{T}_{OO} - \tilde{T}_{FF}) X_{eq}}{1 - \frac{L_{F}}{Q} - \frac{v L_{O}}{Q}}, \text{ over } [0,1].$$

Finally,

$$\tilde{\mathbf{Y}}_{Fl} = \begin{cases} 1 + \int \frac{\mathbf{X}}{0} \left(\frac{d\tilde{\mathbf{Y}}_{Fl}}{dt} \right) dt, & \text{for } \mathbf{X} \in [0, \mathbf{X}_{Fv}^+], \\ 0, & \text{over } [\mathbf{X}_{Fv}^+, 1], \end{cases}$$

where
$$1 + \int_{0}^{X_{Fv}^{+}} \left(\frac{d\tilde{Y}_{Fl}}{dX}\right) dX = 0$$
,



$$\tilde{\mathbf{Y}}_{Ol} = \begin{cases} 0, & \text{over } [0, \mathbf{X}_{Ov}^{-}], \\ \frac{1}{\phi} + \int_{1}^{X} \left(\frac{d\tilde{\mathbf{Y}}_{Ol}}{dt}\right) dt, & \text{for } \mathbf{X} \in [\mathbf{X}_{Ov}^{-}, 1], \end{cases}$$

where
$$\frac{1}{\phi} + \int \frac{X_{Ov}^{-}}{1} \left(\frac{d\tilde{Y}_{Ol}}{dX} \right) dX = 0$$
.

CHAPTER SIX

NUMERICAL RESULTS OF THE DOUBLE-SPRAY MODEL

The boiling points under one atmosphere for hydrogen (our fuel) and oxygen (our oxidizer), respectively, are:

$$T_{Fl} = 20.38 \text{ K}$$
, and $T_{Ol} = 90.18 \text{ K}$.

To keep each reactant in liquid phase at its own origin under one atmosphere, we pick the values for the ambient temperatures as:

$$T_{FF} = 15 \text{ K}$$
, and $T_{OO} = 85 \text{ K}$.

In addition, we look at the chemical reaction: $H_2 + \frac{1}{2}O_2 \rightarrow H_2O$, where the stoichiometric ratio is: V = 8, and, according to Strahle [7], the indices p and q in the chemical reaction term, $D_c \tilde{Y}_{Fg}^{\ p} \tilde{Y}_{Og}^{\ q} \exp\left(-\frac{\tilde{T}_a}{\tilde{T}}\right)$, in Equations (7) to (10), are determined as: p=1.5, and q=0.5.



Then, our computations ensue, and their subsequent results are plotted onto diagrams. Now we are going to present and explain these diagrams which consist of the three cases corresponding to our theoretical analysis in Chapter 3, 4, and 5, respectively:

6.1 Fast Vaporization and Fast Chemistry

Figure 3 features the entire profile, which is linear with X. The dotted lines indicate the locations of the vaporization and flame fronts, where the inflection points exist. Figure 4 is an image of Figure 3 by transforming the horizontal axis from coordinate X into \tilde{x} , a nondimensionalized but much realistic coordinate directly proportional to the exact spacial coordinate x.

From Figures 5 and 6 we observe that, the higher Y_{FF} (i.e. the higher global equivalence ratio ϕ , since Y_{OO} is fixed), then the farther the flame front is pushed away from the fuel side, as well as the higher the flame temperature is raised (due to the fuel-richer chemical reaction), both of which are consistent with physical reality.

Figures 7 and 8 feature six combinations of (Y_{OO}, Y_{FF}) which construct two different values for the global equivalence ratios ϕ (0.8 and 3.2) versus three different values of Y_{OO} (0.15, 0.1, and 0.05). Amazingly, the location of the flame front, indicated by dotted lines, remains almost the same with the same value of the global equivalent ratio, despite the variety of Y_{OO} ; in other words, the global equivalent ratio is the key

parameter controlling the location of the flame front. In addition, we notice that the flame temperature shifts tremendously with the variety of Y_{OO} rather than with that of the global equivalent ratio. Therefore, in order to create a flame temperature high enough to keep the product of the reaction, i.e. water, from condensing, we decide to pick up a sufficiently high value, 0.15, for Y_{OO} throughout the rest of our report.

6.2 Finite-Rate Vaporization and Fast Chemistry

In Chapter 3 and in Section 6.1, fast vaporization assumes that the vaporization Damköhler numbers of fuel and the oxidizer, denoted D_{Fv} and D_{Ov} respectively, are infinitely large, and the entire profile may be addressed without involving any specific value for Damköhler numbers. Finite-rate vaporization in this section as well as in Chapter 4, in contrast, requires inputs of specific values for both D_{Fv} and D_{Ov} . Instead of arbitrarily generating a variety of values for D_{Fv} versus a variety of values for D_{Ov} , we try to make our investigations simple and efficient by seeking the correlation, if any, between these two numbers, prior to our numerical work.

Quoting Equation (2.9) from "Atomization and Sprays," by Lefebvre [8], we have:

maximum stable droplet size:
$$D_{max} = \frac{8 \sigma}{C_D \rho_A U_{R}^2}$$
,



where σ is the surface tension of the droplet, C_D the drag coefficient, ρ_A and U_R the density and relative velocity of the surrounding air, respectively. With the relation above, we may estimate the ratio of the original droplet size on the oxidizer side to that on the fuel side, by assuming the drag coefficient and flow velocity to be identical on both sides, and by quoting data for surface tensions of liquid oxygen and liquid hydrogen [5] and data for densities of gaseous nitrogen and helium [4]:

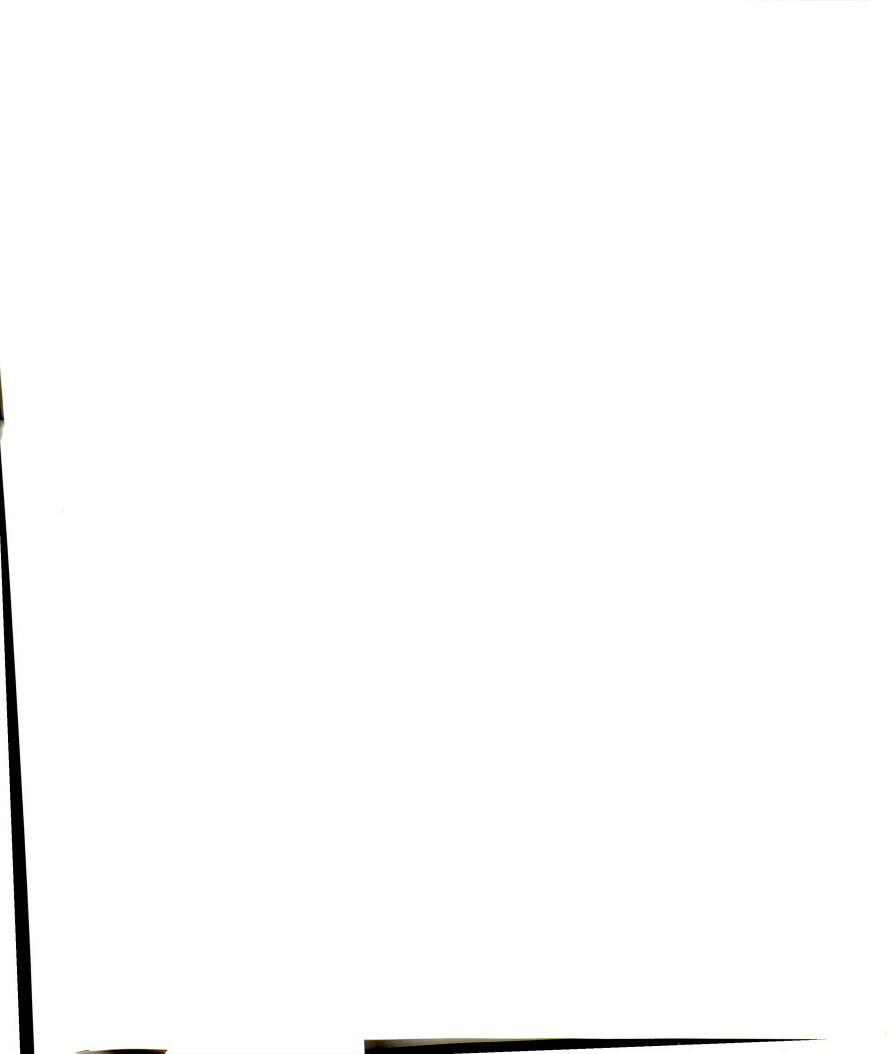
$$\frac{r_{OO}}{r_{FF}} \approx \frac{\left(\frac{\sigma}{\rho_A}\right)_{\text{oxidizer side}}}{\left(\frac{\sigma}{\rho_A}\right)_{\text{fuel side}}} \approx 4.83.$$

Then, by applying the mathematical definitions of these two Damköhler numbers, as expressed on Page 12, and by quoting data for densities of liquid oxygen and liquid hydrogen [4], we obtain a rough yet usable relation between the vaporization Damköhler numbers:

$$\frac{D_{Fv}}{D_{Ov}} = \frac{r_{OO}^2}{r_{FF}^2} \frac{\rho_{Ol}}{\rho_{Fl}} \approx 380.4 ,$$

which, in our belief, is realistic. Therefore, in this section and next one, when we pick up a value for D_{Ov} , we automatically set the value of D_{Fv} to be 380.4 times D_{Ov} .

· 2



Figures 9 and 10 feature a typical finite-rate-vaporization-fast-chemistry profile, with dotted lines showing the ranges of two vaporization zones and the location of the fast-chemistry flame front. We shall keep in mind that the input value of the vaporization Damköhler number for fuel is 380 times that for the oxidizer. As the physical definition shows, a larger vaporization Damköhler number means a larger mechanical-time-to-vaporization-time ratio, i.e. faster vaporization with respect to a time frame attached to a specific group of moving droplets, i.e. the droplets vanish completely while travelling for a shorter distance; that is to say, a larger vaporization Damköhler number should physically lead to a thinner vaporization zone, and vice-versa. Our numerical result, as plotted on Figures 9 and 10, shows the fuel vaporization zone obviously thinner than the oxidizer's, which implies that our calculations are trustable.

Figures 11 and 12 present different profiles with the inverse of D_{Ov} ranging from 0.0001 to 1.0, i.e. D_{Ov} ranging from 10000 to 1 and D_{Fv} decreasing accordingly. The results show that, as the two vaporization Damköhler numbers decrease, both the oxidizer and fuel vaporization zones stretch toward the flame front, which is consistent to our physical predictions. The oxidizer vaporization zone may ultimately coincide with the flame front, which is demonstrated later in Figure 15. It is worth noticing that, while both vaporization zones stretch toward the flame front, the flame front itself shifts toward the oxidizer side instead of toward the fuel side, implying that the oxidizer in our model, whose droplet size is estimated at 4.83 times the fuel's, has a dominant influence rather than fuel does.

Figure 13 is corresponding to figure 11. The end of oxidizer vaporization zone and the flame front meet at $1/D_{Ov} = 1.06$ (i.e. $D_{Ov} = 0.943$), beyond which are indicated by the dashed lines to represent the unrealistic, merely numerical result. The unreality can be demonstrated by following exactly the same derivation procedure for Equation (15) except over $[X_{Fv}^+, X_{Ov}^-]$, which implies:

$$\tilde{Y}_{Og, Ov-} = \tilde{Y}_{P, eq} \frac{X_{Ov}^{-} - X_{eq}}{X_{eq} (1 - X_{eq})}$$

where the value of $\tilde{Y}_{Og,\,Ov-}$ turns negative whenever $X_{Ov}^{-} < X_{eq}$.

If we replace the input value, 0.03, of Y_{FF} in Figure 13 with a variety of values, the X-versus-1/ D_{Ov} and T-versus-1/ D_{Ov} curve patterns will remain similar, but the 1/ D_{Ov} value at which $X_{Ov}^- = X_{eq}$ may differ, as shown in Figure 14. This figure features $Y_{FF} = 0.015, 0.03, 0.045,$ and 0.06 (i.e., the global equivalence ratio = 0.8, 1.6, 2.4, and 3.2, respectively), whose corresponding maximum values of 1/ D_{Ov} that can exist in reality are: 1.37, 1.06, 0.91, 0.83, respectively, at which $X_{Ov}^- = X_{eq} = 0.577, 0.682,$ 0.746, 0.787, respectively.



6.3 Finite-Rate Vaporization and Finite-Rate Chemistry

1. T_f versus K

The computation procedure in Section 5.1 requires the input of \tilde{T}_f , which is obtained through the following definition:

$$\tilde{T}_f \equiv \frac{C_p T_f}{Q Y_{Fi}} ,$$

where T_f is our presumed value for the temperature measured at the location of the fast-chemistry flame front, X_{eq} , which is determined through the algorithm in Section 4.2. Each input value of T_f leads to a solution set which includes the strain rate K; hence, by inputting a variety of T_f values, we may create a T_f -versus-K curve, for any fixed (Y_{OO} , Y_{FF} , r_{OO}) combination. Figure 15 presents six such curves corresponding to six input combinations which represent three different original droplet diameters of oxygen being 1 μ m, 10 μ m, and 20 μ m (i.e., the original droplet diameters of hydrogen being 0.21 μ m, 2.1 μ m, and 4.1 μ m, respectively) versus two different Y_{FF} values being 0.025 and 0.035 (i.e., the global equivalence ratios being 1.33 and 1.87, respectively). The diagram informs that, as the fuel becomes richer, the effect of droplet size becomes more distinctive.

Figure 16 is a rearrangement of Figure 15 by dividing the curves representing three different droplet sizes into three separate diagrams and by inputting Y_{FF} values



between 0.025 and 0.035. The significance of these three diagrams is explained as follows: First, each of the diagrams constructs a good data base for relations among T_f , K, the global equivalence ratio, and droplet size, any of which, if given the other two quantities, can be easily anticipated by interpolation of the diagrams. Second, the higher the global equivalence ratio, the higher upper limit of strain rate there exists to maintain the flame from extinction. Third, given the same global equivalence ratio, the smaller droplet size will allow a higher upper limit of strain rate to maintain the flame from extinction. The second and the third will be discussed later.

2. The Profile (T, \tilde{Y}_{Fg} , \tilde{Y}_{Og} , \tilde{Y}_{P} , \tilde{Y}_{Fl} , \tilde{Y}_{Ol} versus X, \tilde{x}) at Extinction

The largest value of strain rate on each T_f -versus-K curves, beyond which the flame can no longer exist, is exactly where extinction occurs. Figures 17 to 28 present the temperature and mass fraction profiles (T, \tilde{Y}_{Fg} , \tilde{Y}_{Og} , \tilde{Y}_P , \tilde{Y}_{Fl} , \tilde{Y}_{Ol} versus X, \tilde{x}) corresponding to the largest values of strain rate ever obtained on each of the selected T_f -versus-K curves featuring the original droplet diameter of oxygen at 1 μ m, 10 μ m, and 20 μ m (i.e. the original droplet diameter of hydrogen at 0.21 μ m, 2.1 μ m, and 4.1 μ m, respectively), with $Y_{FF}=0.035$ and 0.025 (i.e., the global equivalence ratio $\phi=1.87$ and 1.33, respectively). The dotted lines indicate the location of the fast-chemistry flame front, X_{eq} or \tilde{x}_{eq} . From these twelve figures, we may observe qualitatively that either a higher global equivalence ratio or a smaller droplet size will lead to a sharper temperature profile



at the flame area, which implies faster chemistry.

Moreover, in every diagram from Figures 17 to 28, we are happy to observe that the \tilde{Y}_{Fg} and \tilde{Y}_{Og} profiles intersect with each other at roughly the location of the fast-chemistry flame front, which may be analyzed by the following derivation:

$$\begin{split} \tilde{Y}_{Fg}(X = X_{eq}) &\approx \tilde{Y}_{Og}(X = X_{eq}) \;, \\ \\ &\Rightarrow \quad \frac{Y_{Fg}(X = X_{eq})}{Y_{Fi}} \approx \frac{Y_{Og}(X = X_{eq})}{\nu \; Y_{Fi}} \;, \\ \\ \Rightarrow \quad \frac{Y_{Og}(X = X_{eq})}{Y_{Eg}(X = X_{eq})} \approx \nu \;, \end{split}$$

which means that the location of the fast-chemistry flame front, X_{eq} , is roughly when the stoichiometric ratio ν occurs!

3. The Global Equivalence Ratio versus K_{ext} and $T_{max, ext}$

We denote the strain rate at extinction as K_{ext} and the highest flame temperature on the profile corresponding to K_{ext} as $T_{max, ext}$, both of which are associated with a global equivalence ratio and a droplet size, as presented earlier in Figures 15 and 16. In Figure 29 we present, with the original droplet diameter of oxygen at 1 μ m, 10 μ m,



and 20 μ m (and the original droplet diameter of hydrogen at 0.21 μ m, 2.1 μ m, and 4.1 μ m, respectively), the global equivalence ratio ϕ versus K_{ext} and ϕ versus $T_{max, ext}$. From this figure we observe the following:

- The curves of the global equivalence ratio versus $K_{\rm ext}$ are concave downward and those versus $T_{\rm max,\, ext}$ concave upward, but both converge as the global equivalence ratio reduces toward zero and both diverge as that increases, which indicates that the variety in the droplet size has a significant effect upon extinction when the global equivalence ratio is large (i.e., when the chemical reaction strong), but that it makes little difference when the chemical reaction is weak.
- (2) The strain rate at extinction approaches zero just as the global equivalence ratio does, which implies that even a slow fluid velocity can extinguish the flame if the chemical reaction is weak.
- (3) The curves demonstrate that either raising the global equivalence ratio or reducing the droplet size will increase $T_{max, ext}$ and, we believe, will more or less increase the overall flame temperature.

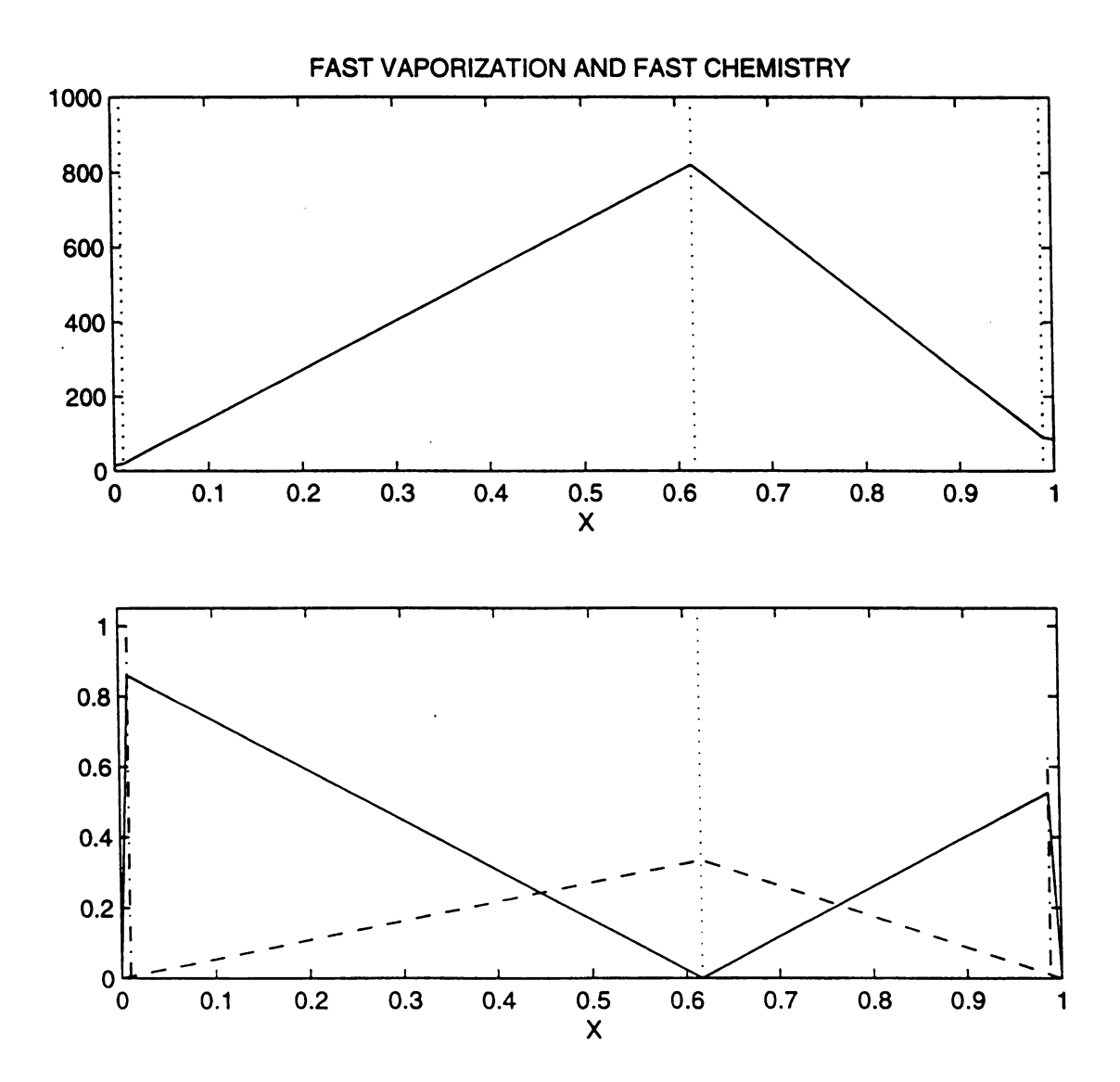


Figure 3. A result of **fast vaporization and fast chemistry** in X-coordinate, with $Y_{OO} = 0.15$, $Y_{FF} = 0.03$ (i.e., $\phi = 1.6$). Upper diagram: T [K]. Lower diagram: \tilde{Y}_{Fg} , \tilde{Y}_{Og} (_), \tilde{Y}_{Fl} , \tilde{Y}_{Ol} (-.), \tilde{Y}_{P} (--).

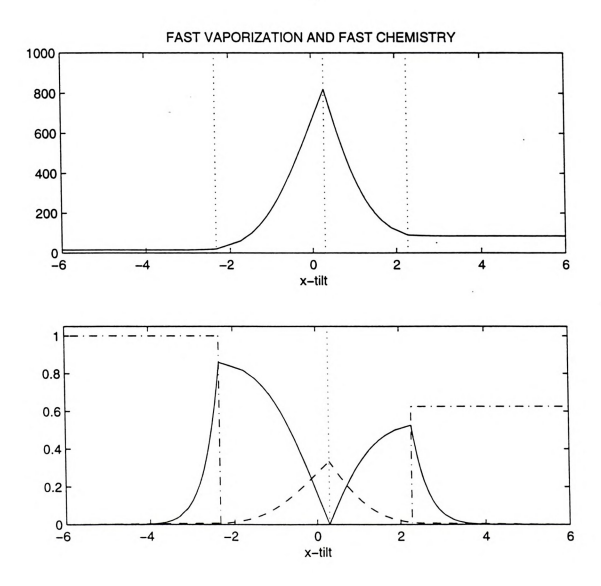


Figure 4. A result of **fast vaporization and fast chemistry** in \bar{x} -coordinate, with $Y_{OO}=0.15$, $Y_{FF}=0.03$ (i.e., $\varphi=1.6$). Upper diagram: T [K]. Lower diagram: \bar{Y}_{Fg} , \bar{Y}_{Og} (_), \bar{Y}_{Fl} , \bar{Y}_{Ol} (--), \bar{Y}_{P} (--).

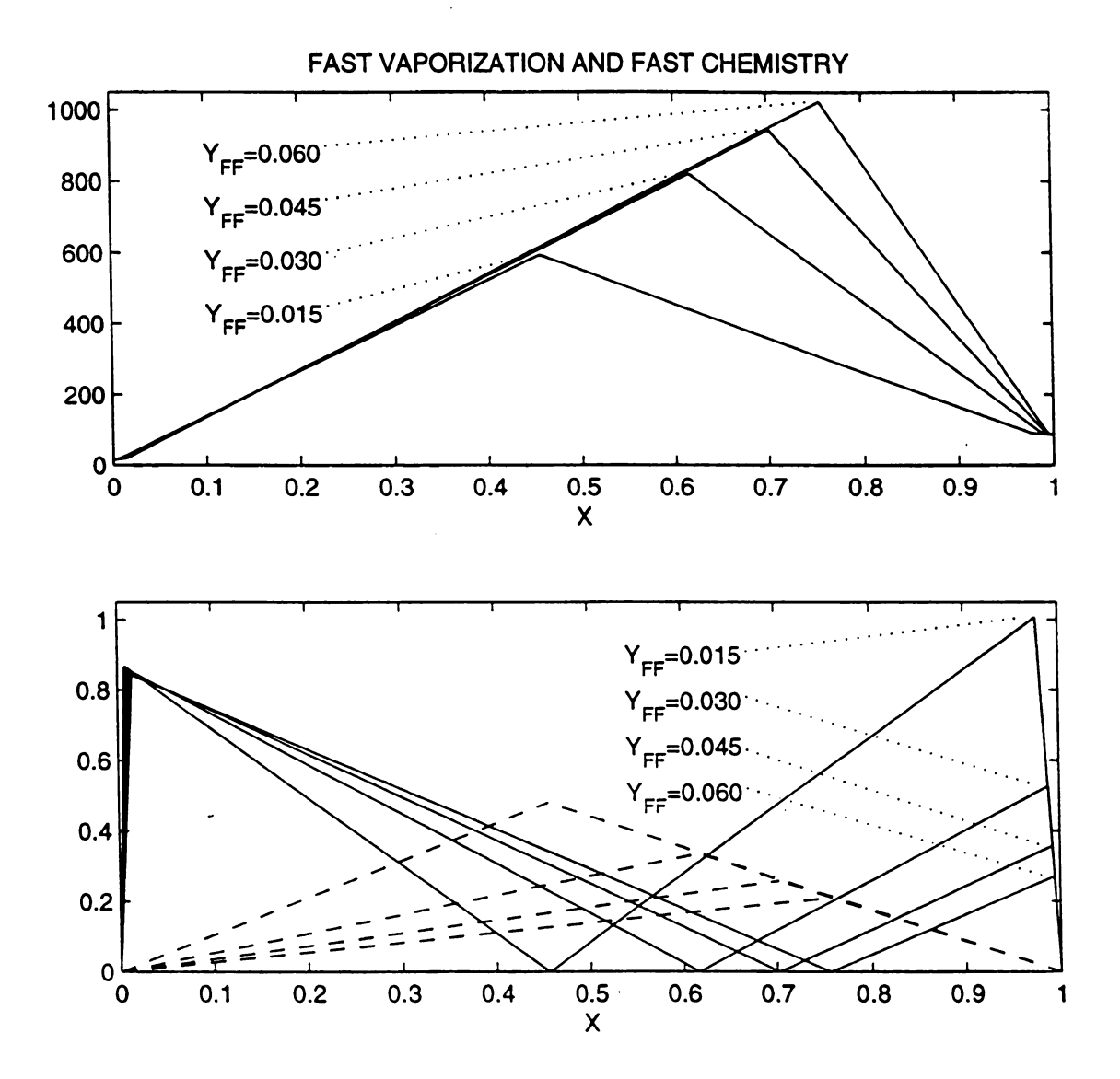


Figure 5. Results of **fast vaporization and fast chemistry** in X-coordinate, with $Y_{OO}=0.15$, $Y_{FF}=0.015$, 0.03, 0.045, 0.06 (i.e., $\phi=0.8$, 1.6, 2.4, 3.2, respectively). Upper diagram: T[K]. Lower diagram: \tilde{Y}_{Fg} , \tilde{Y}_{Og} (_), \tilde{Y}_{P} (--).

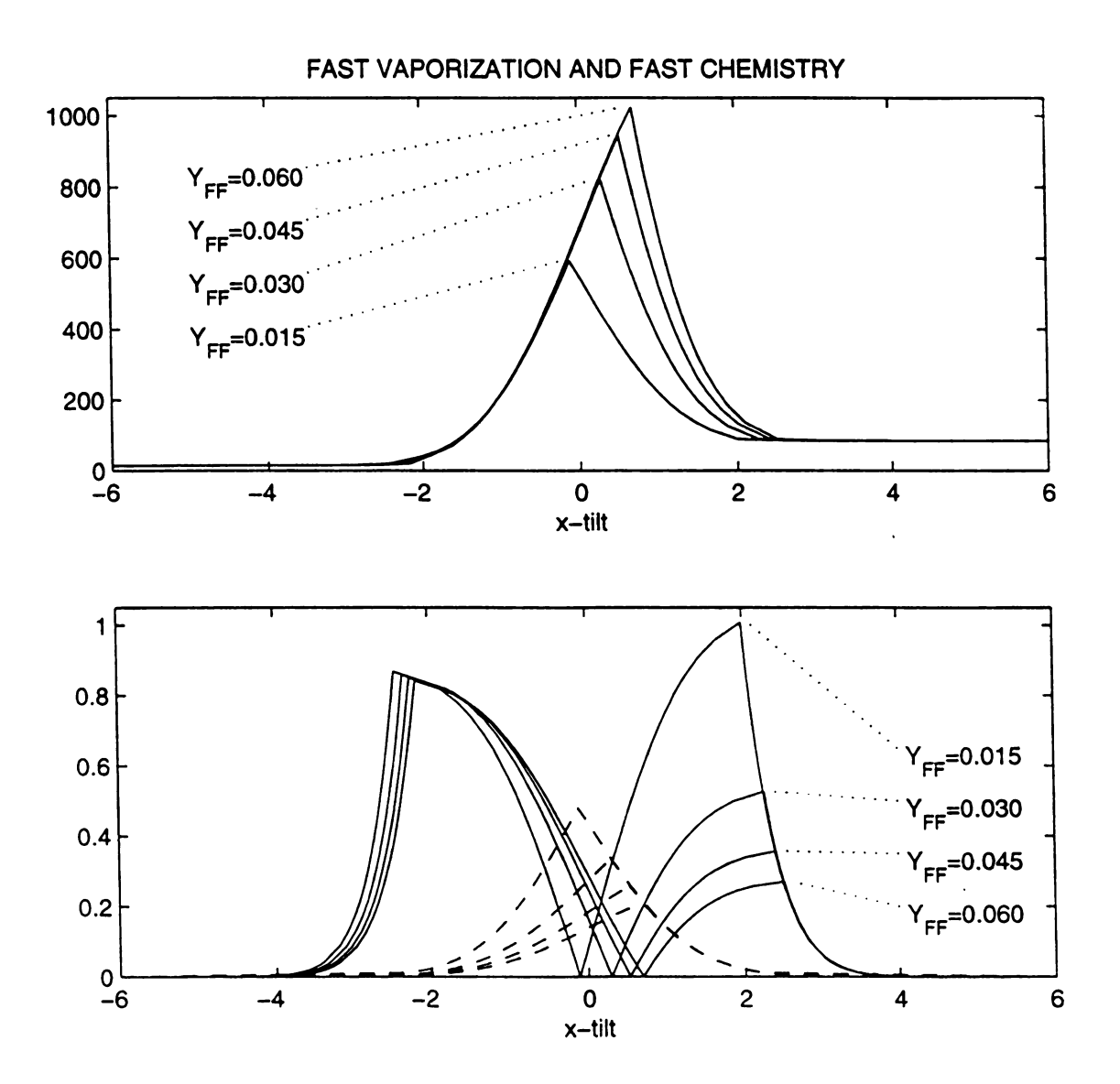


Figure 6. Results of fast vaporization and fast chemistry in \tilde{x} -coordinate, with $Y_{OO}=0.15$, $Y_{FF}=0.015$, 0.03, 0.045, 0.06 (i.e., $\phi=0.8$, 1.6, 2.4, 3.2, respectively). Upper diagram: T[K]. Lower diagram: \tilde{Y}_{Fg} , \tilde{Y}_{Og} (_), \tilde{Y}_{P} (--).



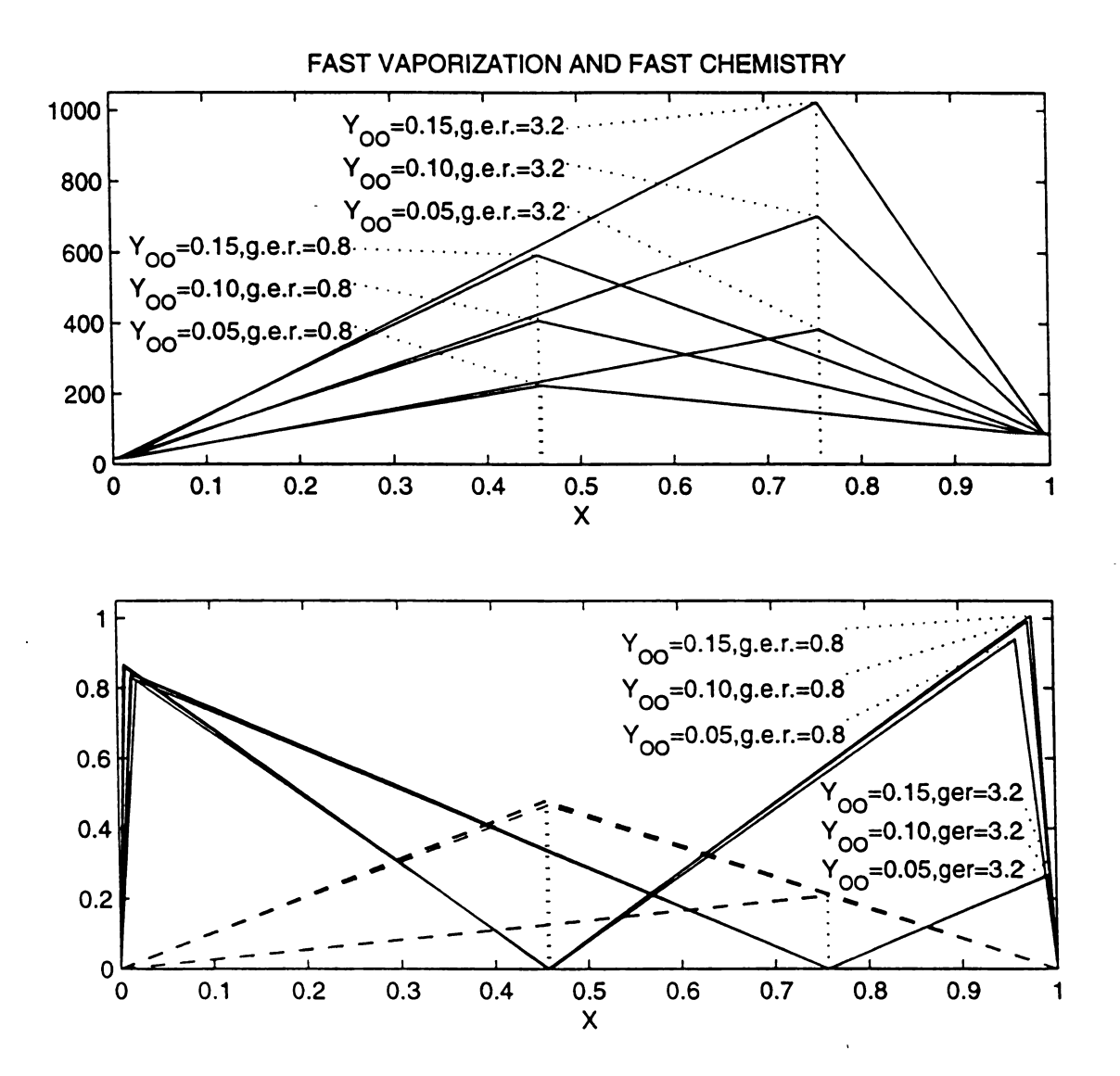
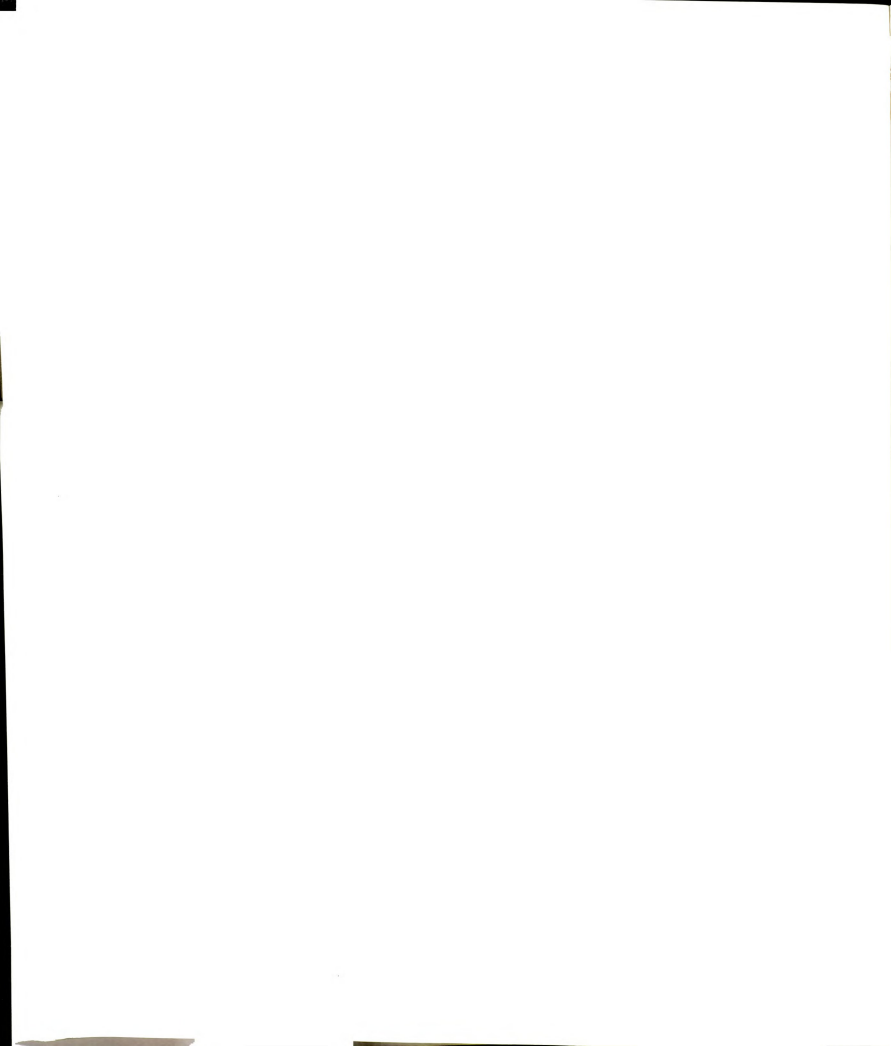


Figure 7. Results of **fast vaporization and fast chemistry** in X-coordinate, with 6 sets of inputs: $Y_{OO} = 0.15$, $Y_{FF} = 0.015$ and 0.06 (i.e., $\phi = 0.8$ and 3.2); $Y_{OO} = 0.1$, $Y_{FF} = 0.01$ and 0.04 ($\phi = 0.8$ and 3.2); $Y_{OO} = 0.05$, $Y_{FF} = 0.005$ and 0.02 ($\phi = 0.8$ and 3.2). Upper diagram: T [K]. Lower diagram: \tilde{Y}_{Fg} , \tilde{Y}_{Og} (_), \tilde{Y}_{P} (--).



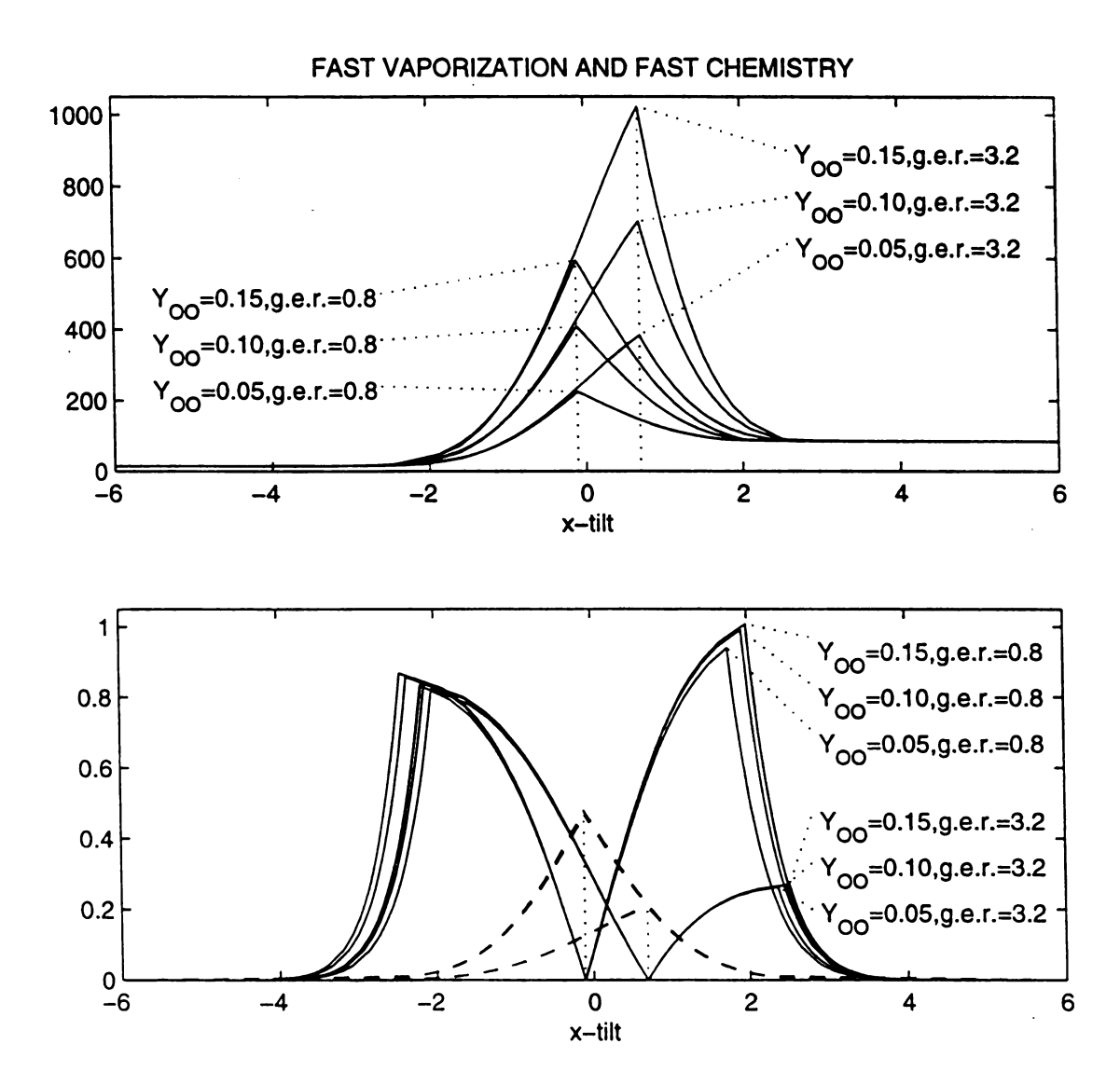


Figure 8. Results of **fast vaporization and fast chemistry** in \tilde{x} -coordinate, with 6 sets of inputs: $Y_{OO} = 0.15$, $Y_{FF} = 0.015$ and 0.06 (i.e., $\phi = 0.8$ and 3.2); $Y_{OO} = 0.1$, $Y_{FF} = 0.01$ and 0.04 ($\phi = 0.8$ and 3.2); $Y_{OO} = 0.05$, $Y_{FF} = 0.005$ and 0.02 ($\phi = 0.8$ and 3.2). Upper diagram: T [K]. Lower diagram: \tilde{Y}_{Fg} , \tilde{Y}_{Og} (_), \tilde{Y}_{P} (--).



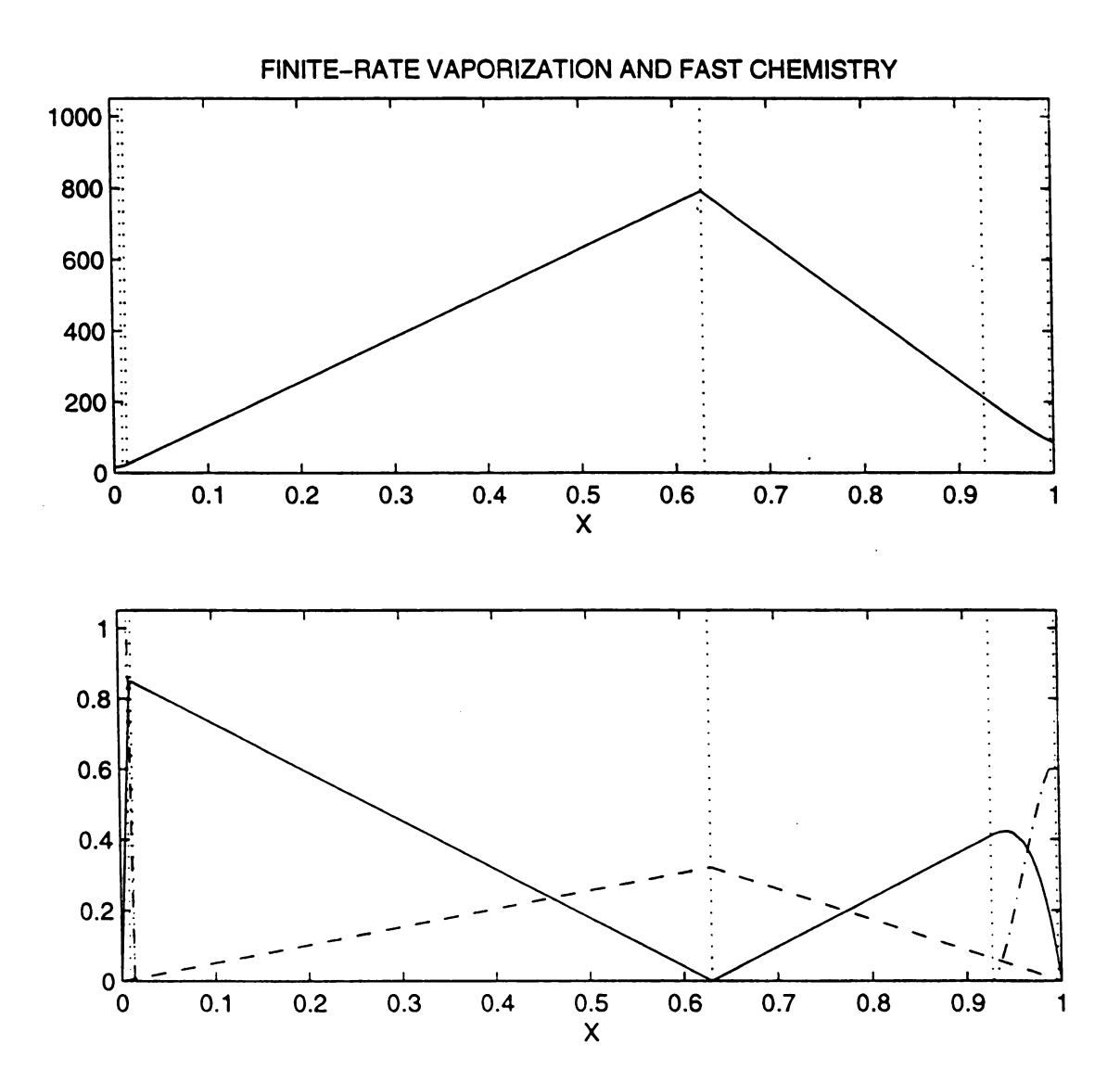


Figure 9. A result of finite-rate vaporization and fast chemistry in X-coordinate, with $Y_{OO} = 0.15$, $Y_{FF} = 0.03$, $1/D_{Ov} = 0.1$. Upper diagram: \tilde{Y}_{Fg} , \tilde{Y}_{Og} (_), \tilde{Y}_{Fl} , \tilde{Y}_{Ol} (-.), \tilde{Y}_{P} (--).

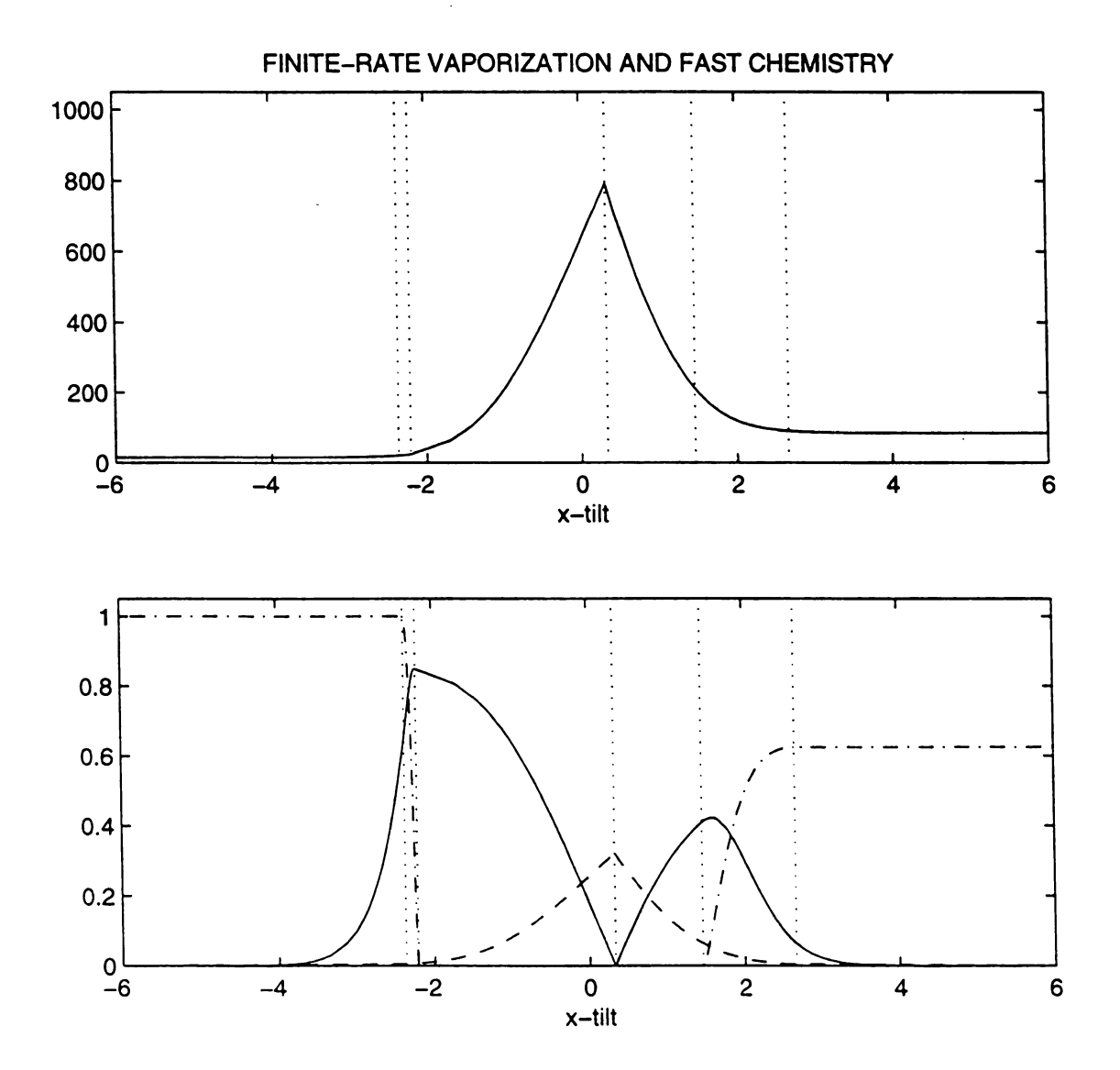


Figure 10. A result of finite-rate vaporization and fast chemistry in \tilde{x} -coordinate, with $Y_{QO} = 0.15$, $Y_{FF} = 0.03$, $1/D_{Ov} = 0.1$. Upper diagram: T[K]. Lower diagram: \tilde{Y}_{Fg} , \tilde{Y}_{Og} (_), \tilde{Y}_{Fl} , \tilde{Y}_{Ol} (-.), \tilde{Y}_{P} (--).



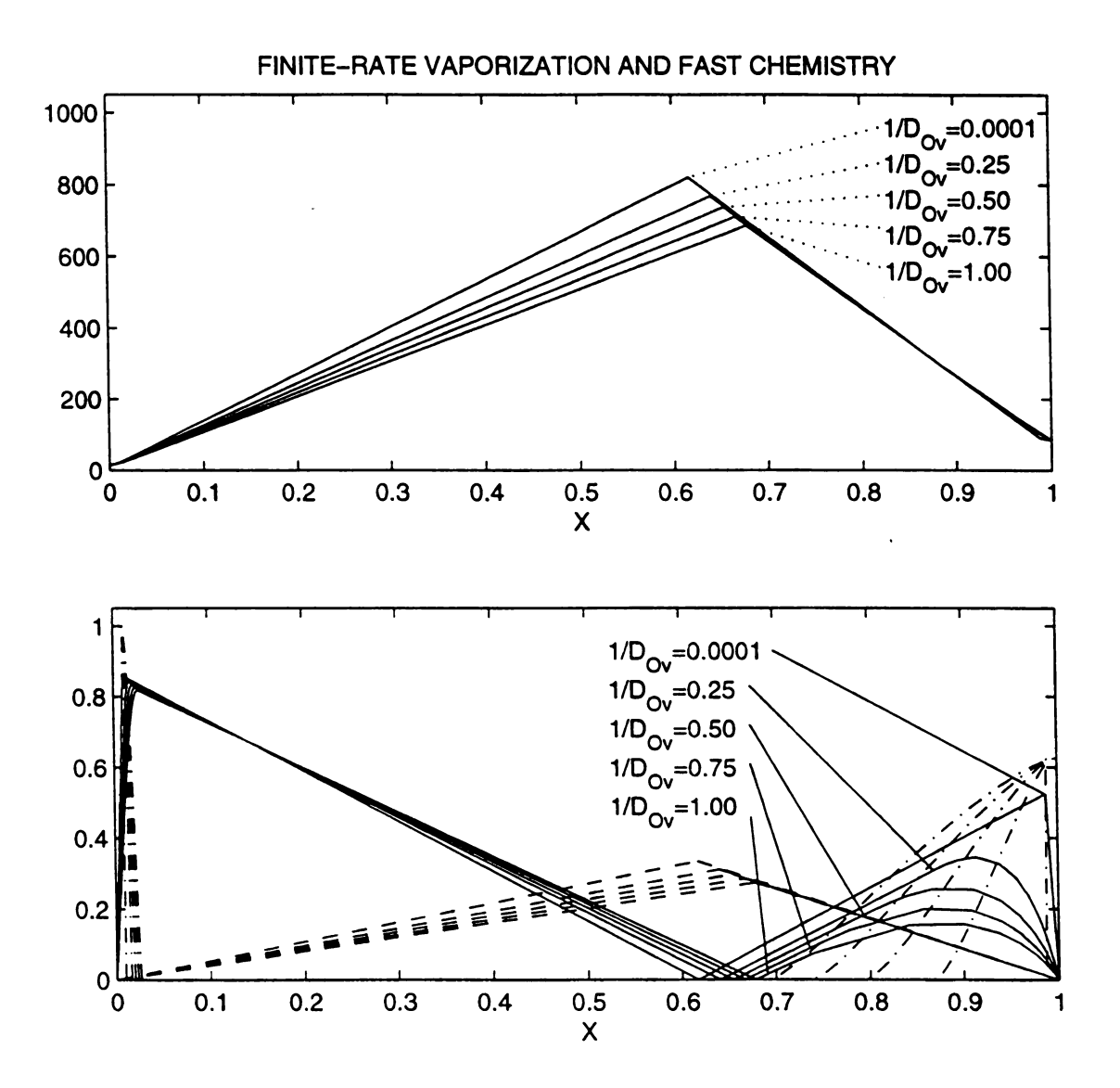


Figure 11. Results of finite-rate vaporization and fast chemistry in X-coordinate, with $Y_{OO} = 0.15$, $Y_{FF} = 0.03$, $1/D_{Ov} = 0.0001$, 0.25, 0.5, 0.75, 1.0. Upper diagram: T [K]. Lower diagram: \tilde{Y}_{Fg} , \tilde{Y}_{Og} (_), \tilde{Y}_{Fl} , \tilde{Y}_{Ol} (-.), \tilde{Y}_{P} (--).



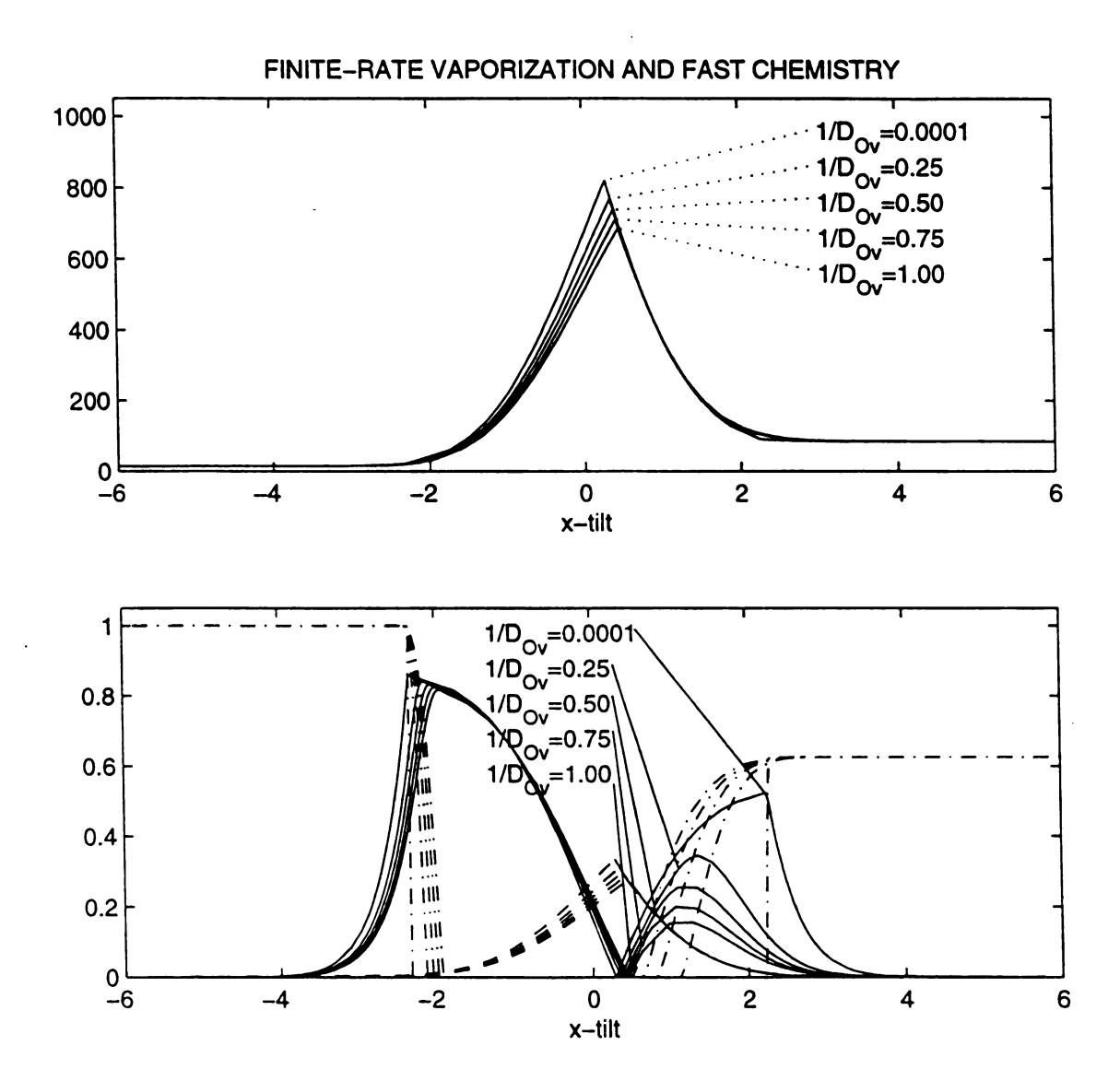


Figure 12. Results of finite-rate vaporization and fast chemistry in \tilde{x} -coordinate, with $Y_{OO} = 0.15$, $Y_{FF} = 0.03$, $1/D_{Ov} = 0.0001$, 0.25, 0.5, 0.75, 1.0. Upper diagram: T [K]. Lower diagram: \tilde{Y}_{Fg} , \tilde{Y}_{Og} (_), \tilde{Y}_{Fl} , \tilde{Y}_{Ol} (-.), \tilde{Y}_{P} (--).

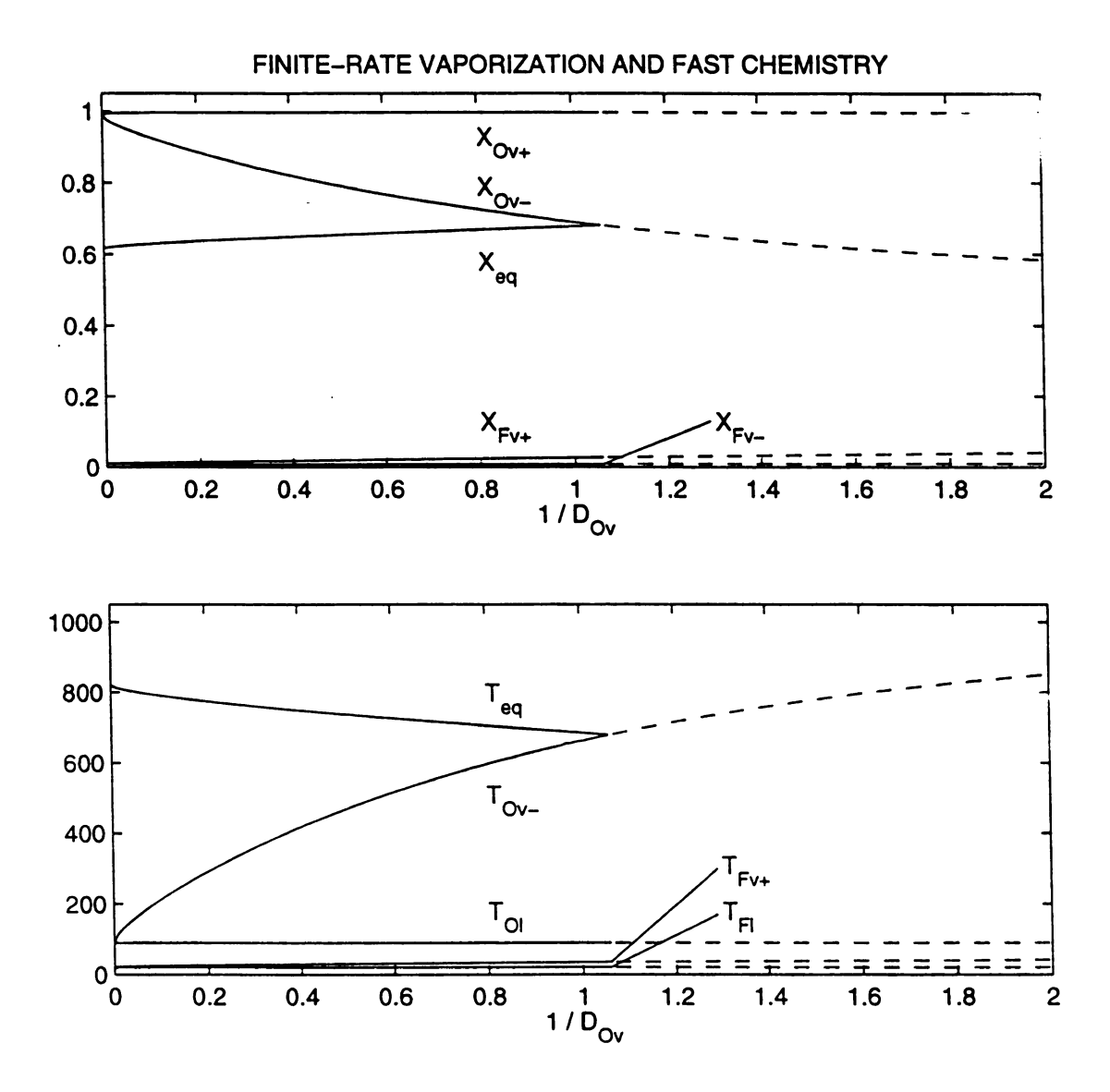


Figure 13. Results of **finite-rate vaporization and fast chemistry** shown as X-locations and temperatures versus a broad range of $1/D_{Ov}$, with $Y_{OO} = 0.15, Y_{FF} = 0.03. \text{ Upper diagram: } X_{Fv}^-, X_{Fv}^+, X_{eq}, \\ X_{Ov}^-, X_{Ov}^+ \text{ . Lower diagram: } T_{Fl}, T_{Fv+}, T_{Ol}, T_{Ov-}, T_{eq} \text{ [K].}$

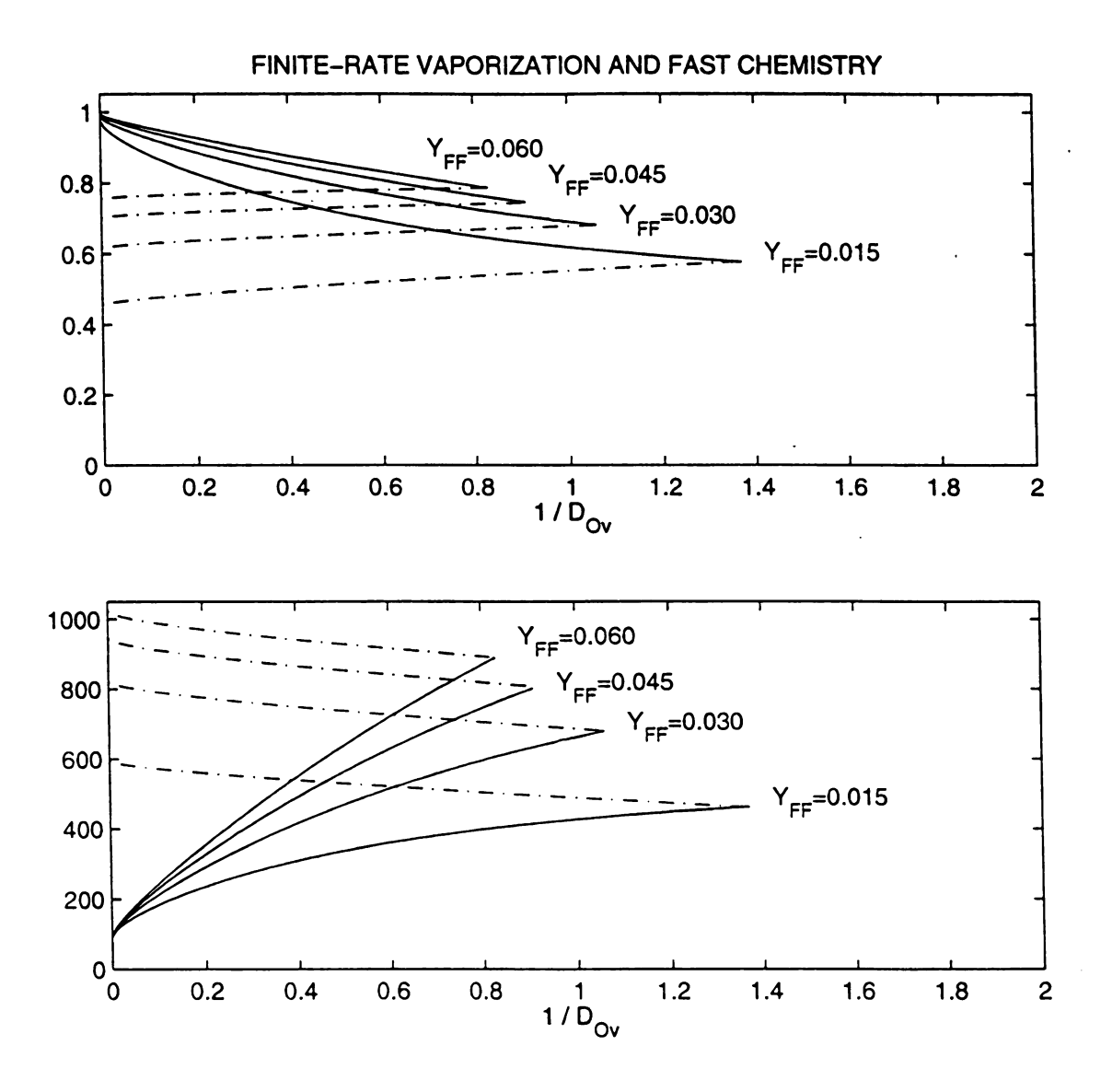


Figure 14. Results of finite-rate vaporization and fast chemistry shown as X-locations and temperatures versus a broad range of $1/D_{Ov}$, with $Y_{OO}=0.15$, $Y_{FF}=0.015$, 0.03, 0.045, 0.06. Upper diagram: X_{Ov}^{-} (_), X_{eq} (-.). Lower diagram: T_{Ov-} (_), T_{eq} (-.) [K].



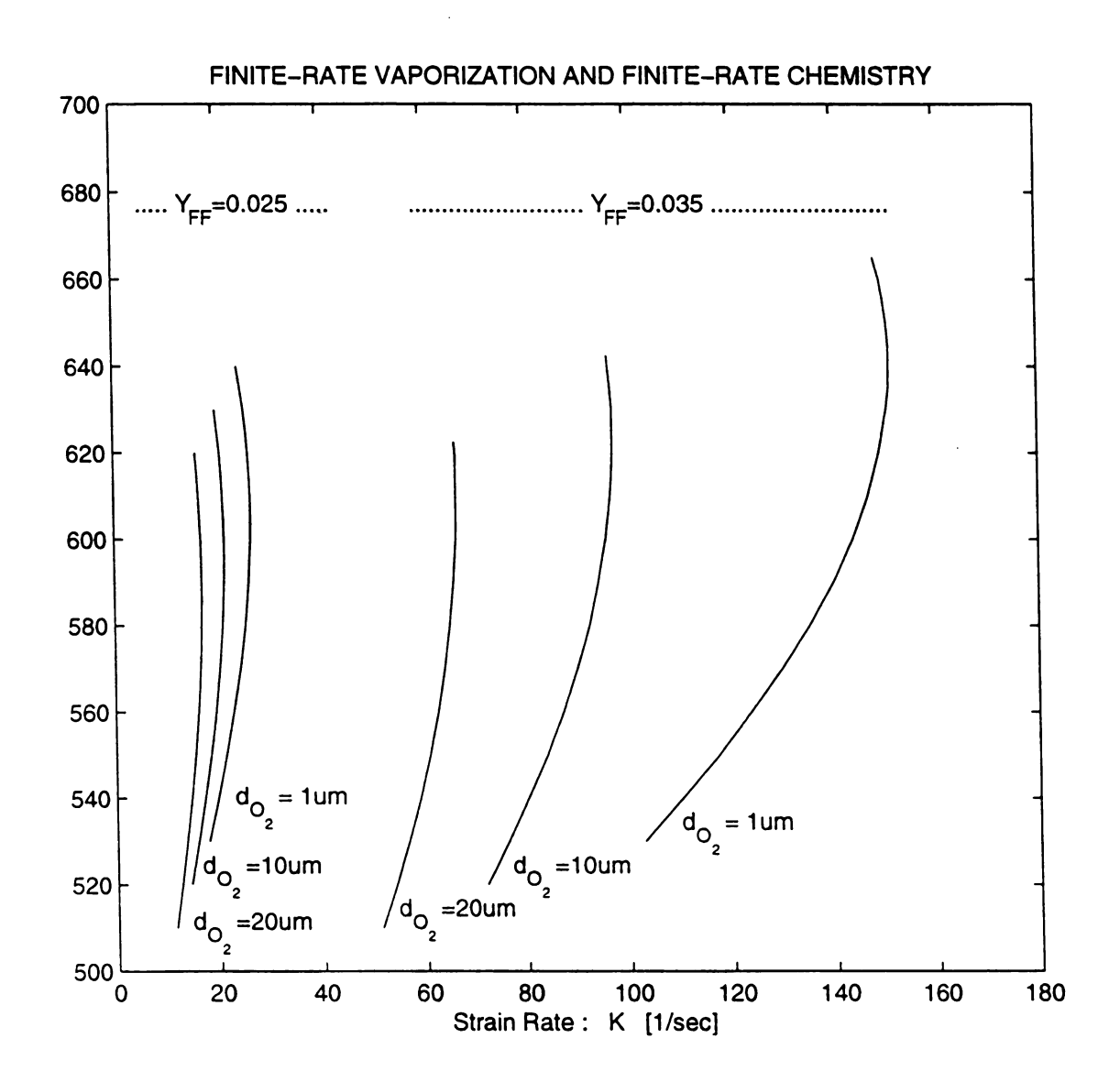


Figure 15. Results of **finite-rate vaporization and finite-rate chemistry** shown as temperature at the fast-chemistry flame front, T_f [K], versus strain rate, K [1/sec], with $Y_{OO}=0.15$, $Y_{FF}=0.025$, 0.035, and the original diameter of $O_2=1~\mu$ m, $10~\mu$ m, $20~\mu$ m.



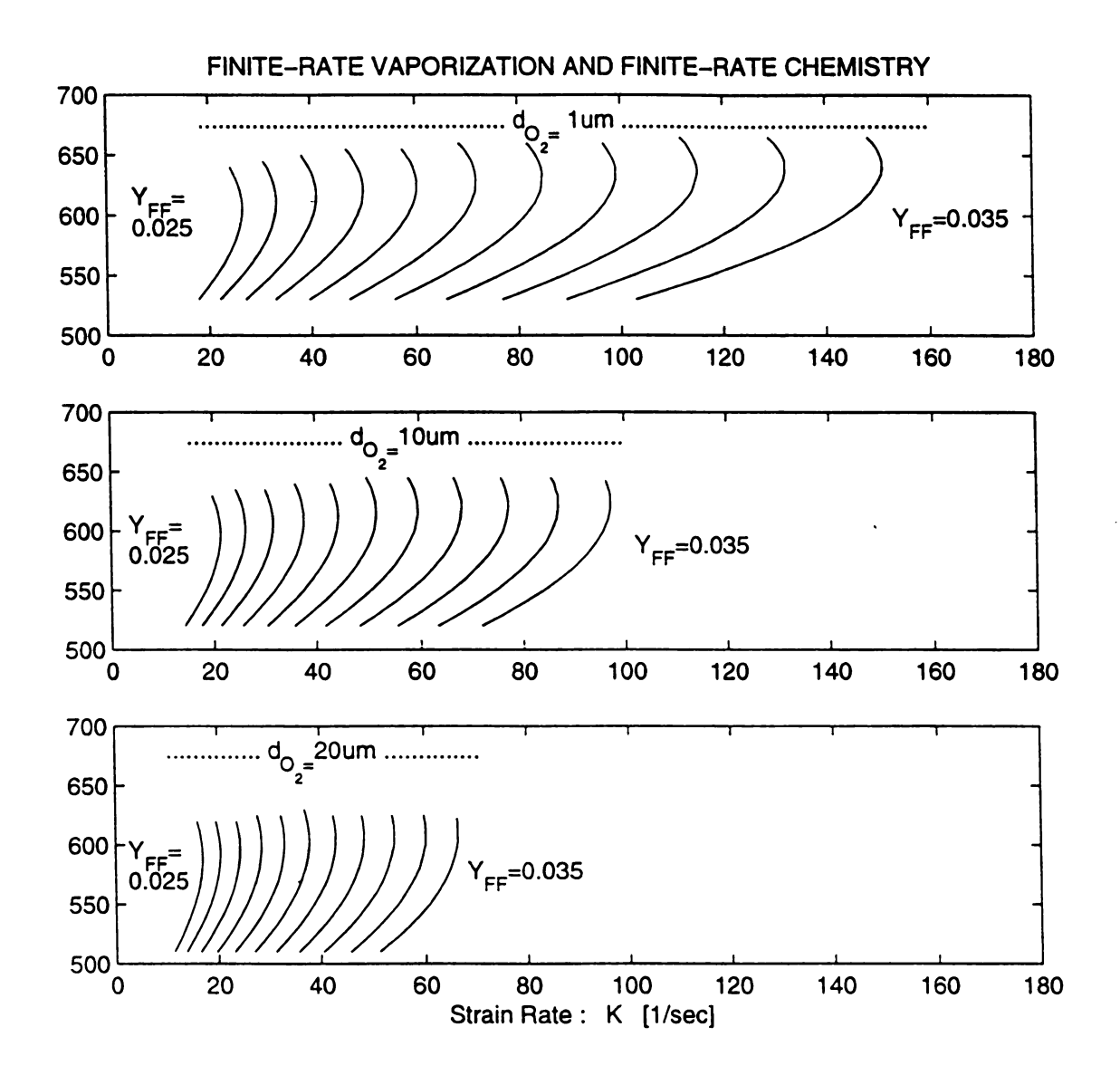


Figure 16. Results of **finite-rate vaporization and finite-rate chemistry** shown as temperature at the fast-chemistry flame front, T_f [K], versus strain rate, K [1/sec], with $Y_{OO}=0.15$, $Y_{FF}=0.025$, 0.026, 0.027, 0.028, 0.029, 0.03, 0.031, 0.032, 0.033, 0.034, 0.035, and the original diameter of $O_2=1~\mu$ m, $10~\mu$ m, $20~\mu$ m.

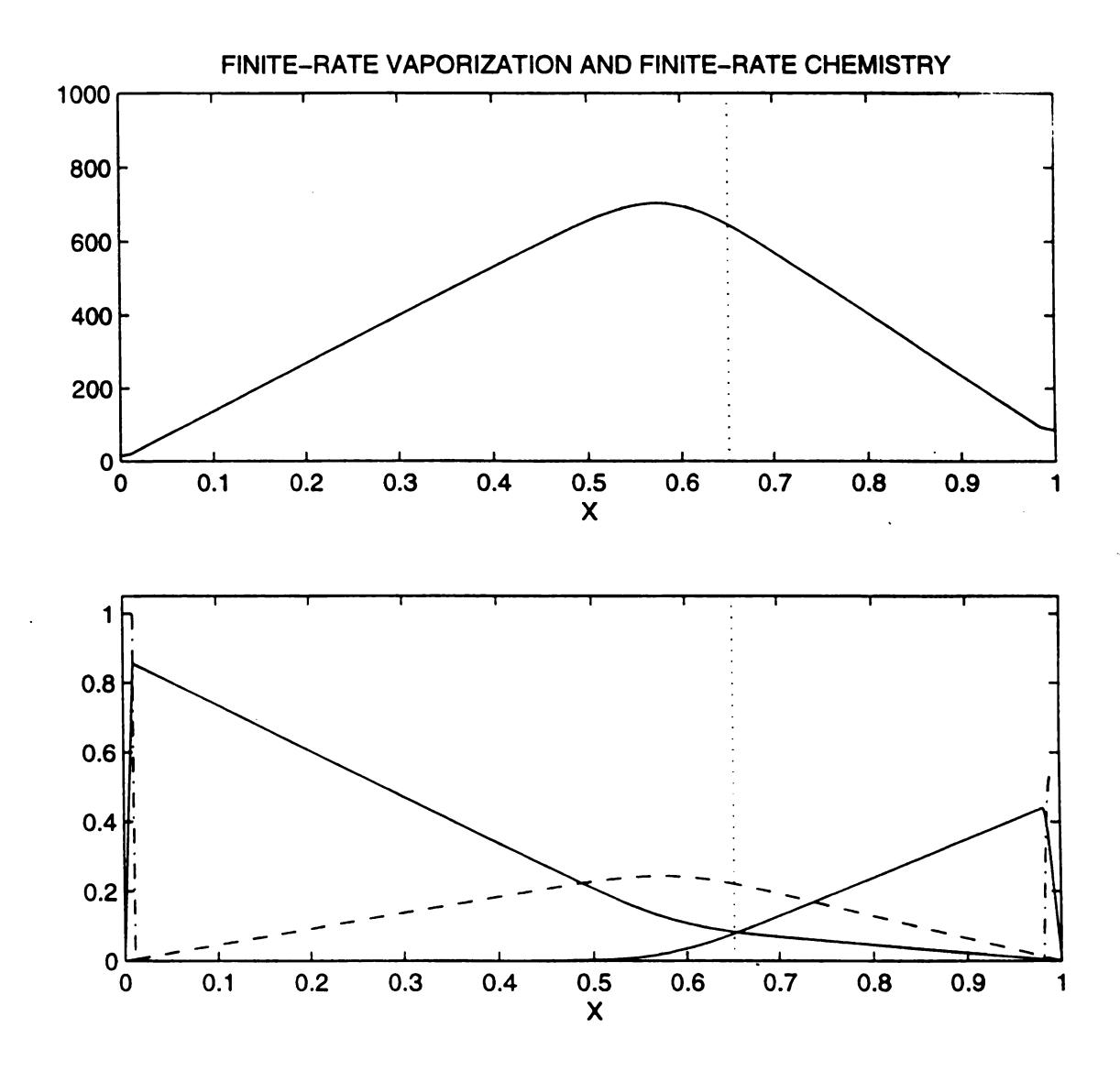


Figure 17. A result of finite-rate vaporization and finite-rate chemistry at extinction in X-coordinate, with $Y_{OO} = 0.15$, $Y_{FF} = 0.035$, K=150.88 /sec, and the original diameter of $O_2 = 1.0 \mu$ m. Upper diagram: T [K]. Lower diagram: \tilde{Y}_{Fg} , \tilde{Y}_{Og} (_), \tilde{Y}_{Fl} , \tilde{Y}_{Ol} (-.), \tilde{Y}_{P} (--).

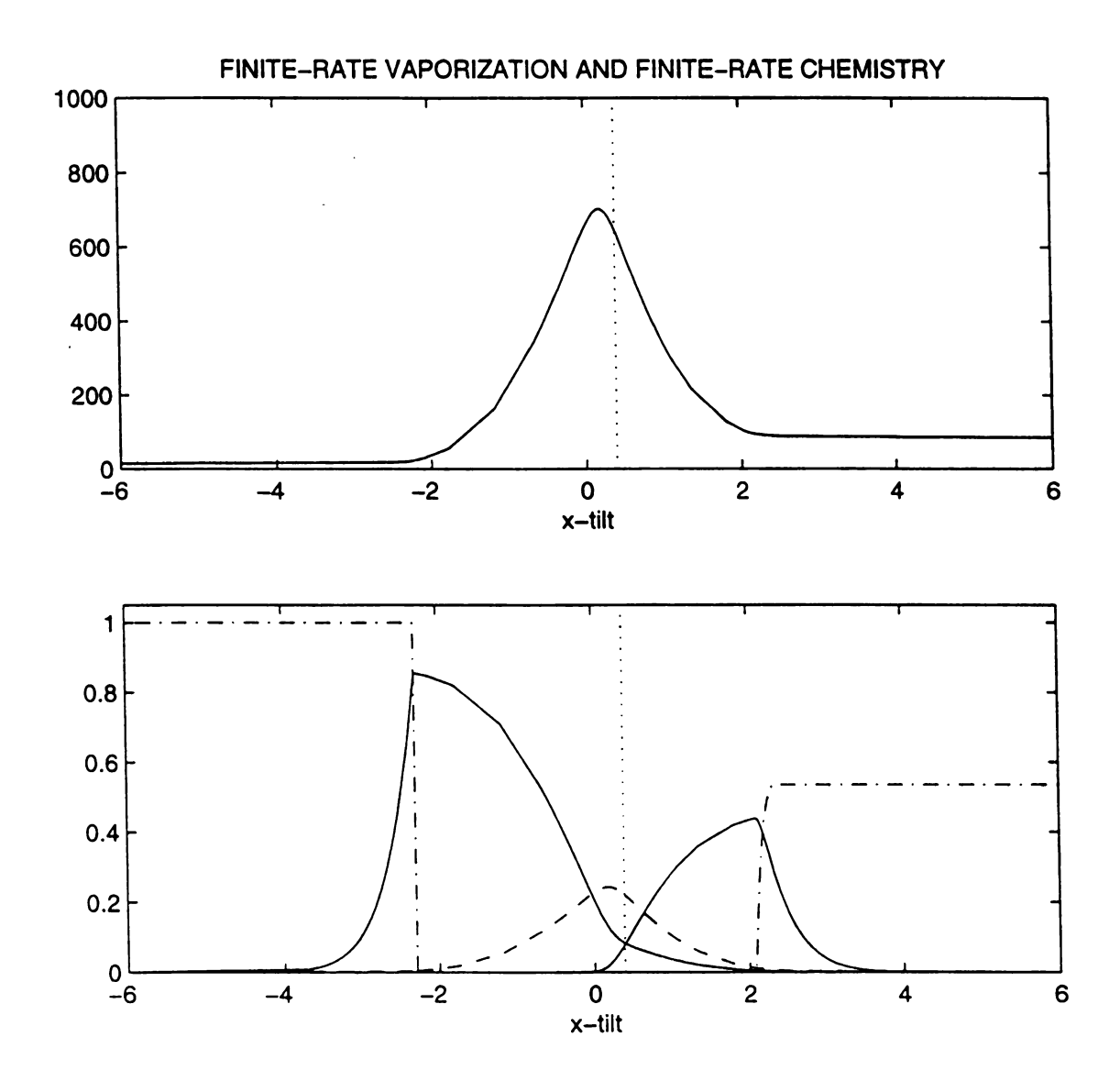


Figure 18. A result of finite-rate vaporization and finite-rate chemistry at extinction in \tilde{x} -coordinate, with $Y_{OO} = 0.15$, $Y_{FF} = 0.035$, K=150.88 /sec, and the original diameter of $O_2 = 1.0 \mu$ m. Upper diagram: T [K]. Lower diagram: \tilde{Y}_{Fg} , \tilde{Y}_{Og} (_), \tilde{Y}_{Fl} , \tilde{Y}_{Ol} (-.), \tilde{Y}_{P} (--).

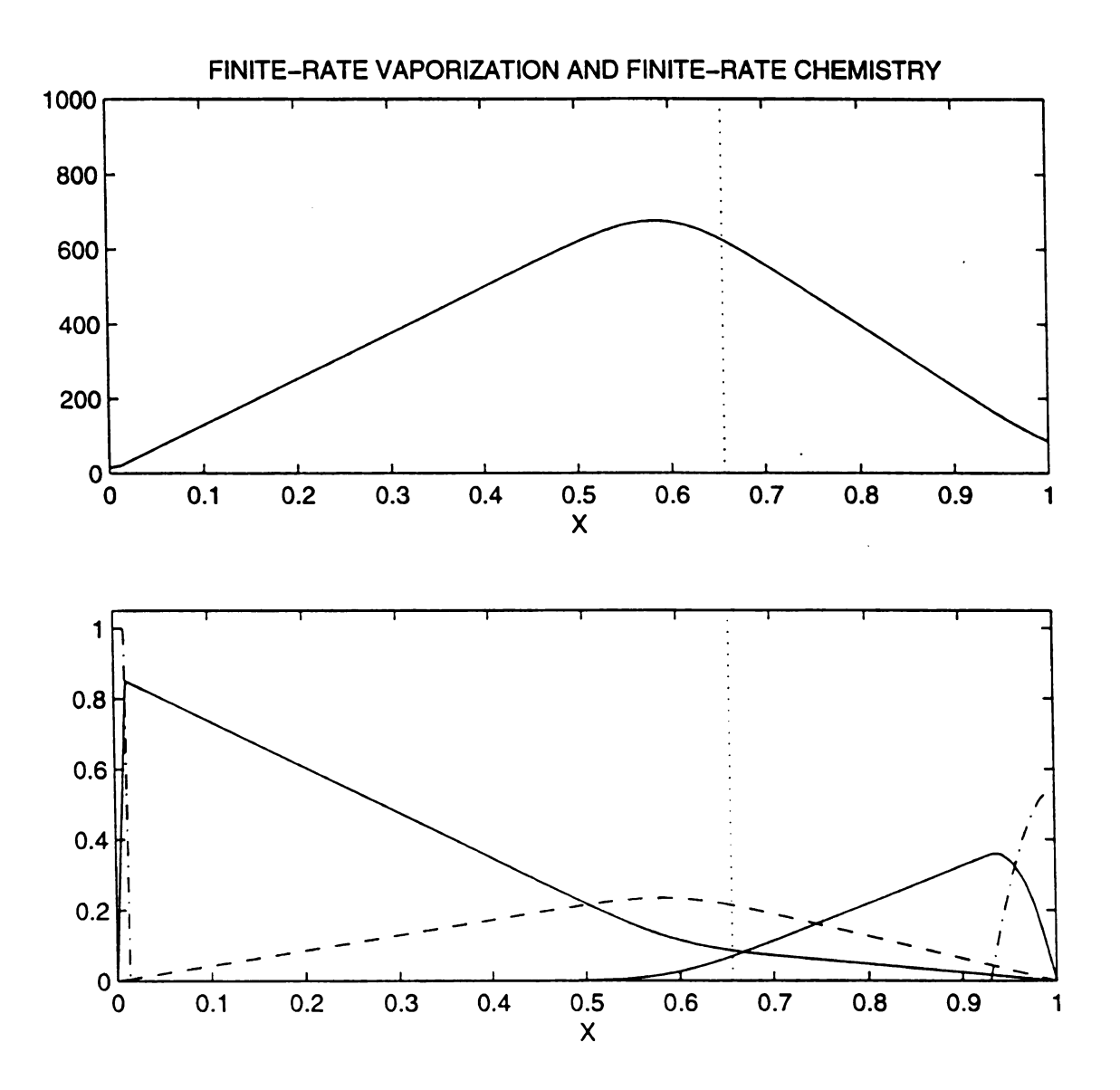


Figure 19. A result of finite-rate vaporization and finite-rate chemistry at extinction in X-coordinate, with $Y_{OO}=0.15$, $Y_{FF}=0.035$, K=97.27 /sec, and the original diameter of $O_2=10~\mu$ m. Upper diagram: T [K]. Lower diagram: \tilde{Y}_{Fg} , \tilde{Y}_{Og} (_), \tilde{Y}_{Fl} , \tilde{Y}_{Ol} (-.), \tilde{Y}_{P} (--).

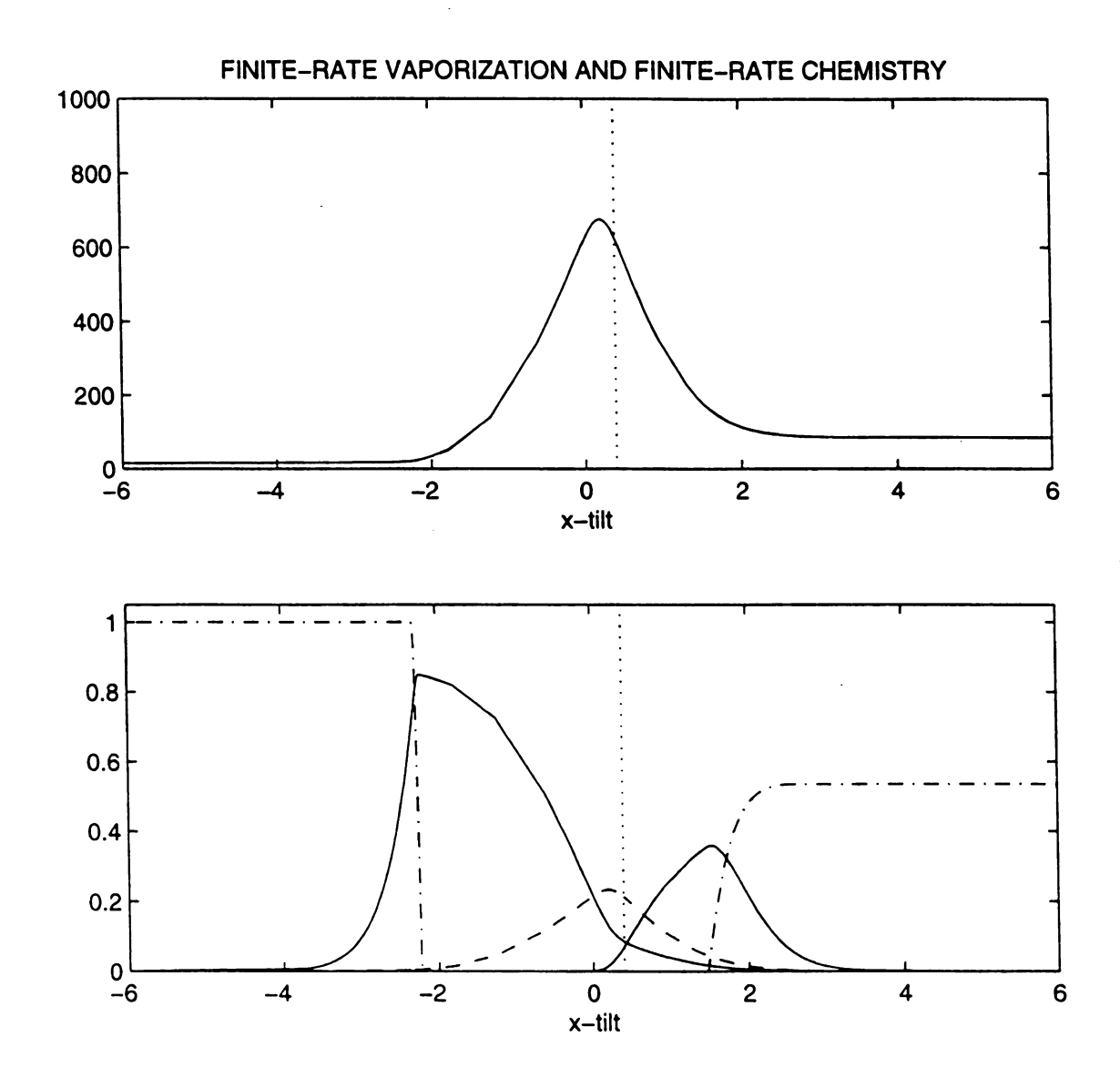


Figure 20. A result of finite-rate vaporization and finite-rate chemistry at extinction in \tilde{x} -coordinate, with $Y_{OO} = 0.15$, $Y_{FF} = 0.035$, K=97.27 /sec, and the original diameter of $O_2 = 10 \,\mu$ m. Upper diagram: T [K]. Lower diagram: \tilde{Y}_{Fg} , \tilde{Y}_{Og} (_), \tilde{Y}_{Fl} , \tilde{Y}_{Ol} (-.), \tilde{Y}_{P} (--).

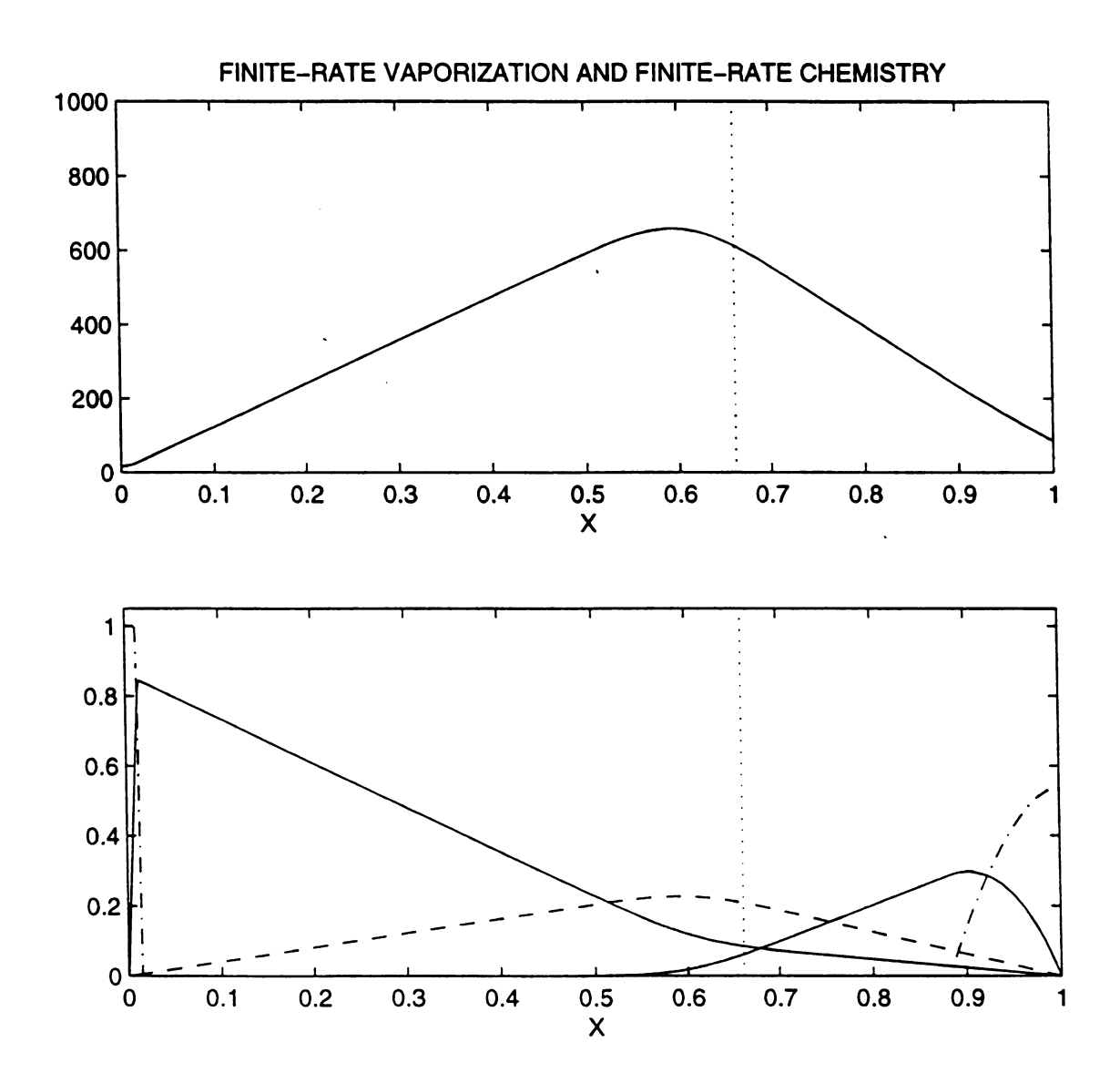


Figure 21. A result of finite-rate vaporization and finite-rate chemistry at extinction in X-coordinate, with $Y_{OO} = 0.15$, $Y_{FF} = 0.035$, K=66.53 /sec, and the original diameter of $O_2 = 20 \mu$ m. Upper diagram: T [K]. Lower diagram: \tilde{Y}_{Fg} , \tilde{Y}_{Og} (_), \tilde{Y}_{Fl} , \tilde{Y}_{Ol} (-.), \tilde{Y}_{P} (--).



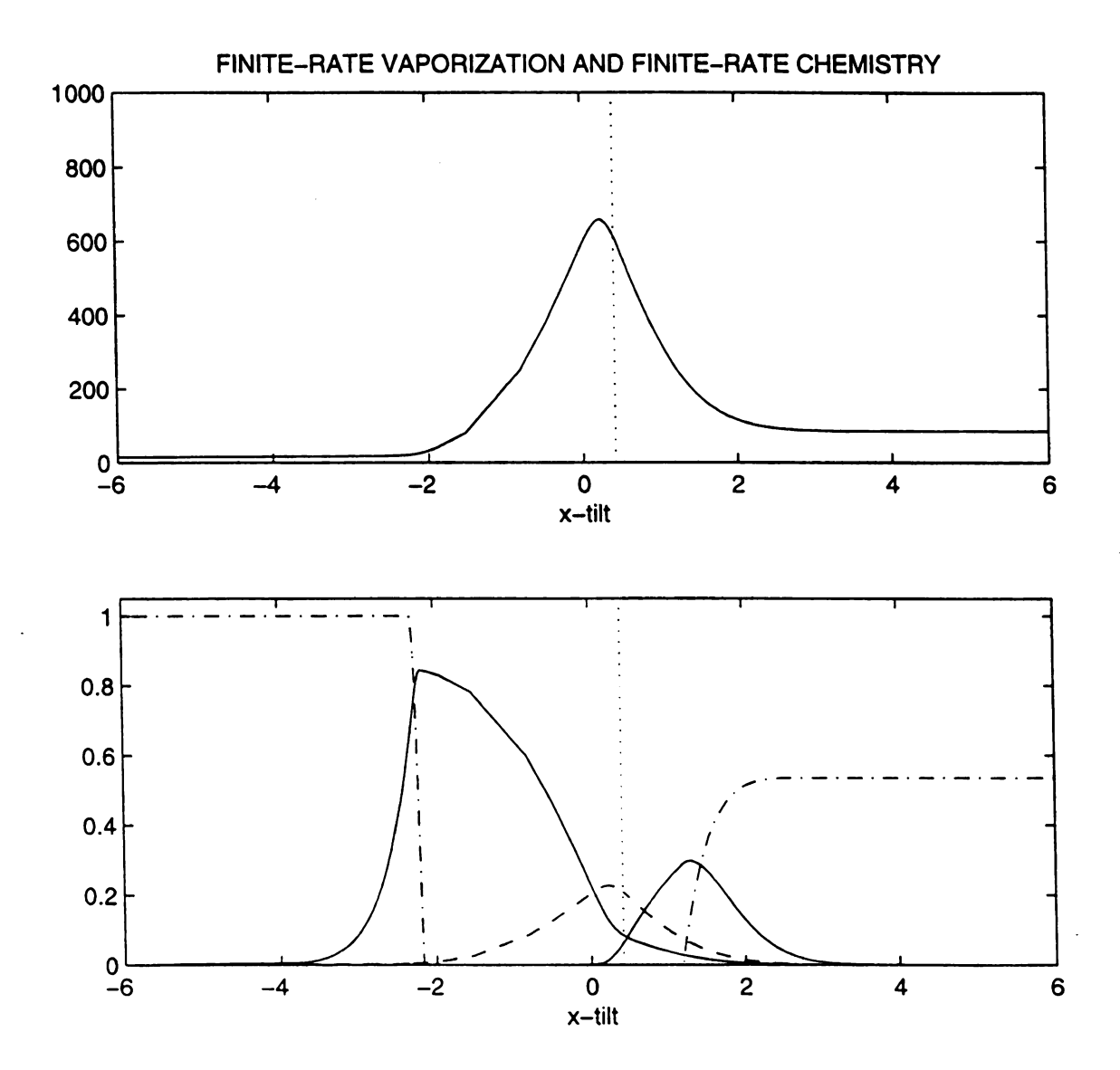


Figure 22. A result of finite-rate vaporization and finite-rate chemistry at extinction in \tilde{x} -coordinate, with $Y_{OO} = 0.15$, $Y_{FF} = 0.035$, K=66.53 /sec, and the original diameter of $O_2 = 20 \mu$ m. Upper diagram: T [K]. Lower diagram: \tilde{Y}_{Fg} , \tilde{Y}_{Og} (_), \tilde{Y}_{Fl} , \tilde{Y}_{Ol} (-.), \tilde{Y}_{P} (--).

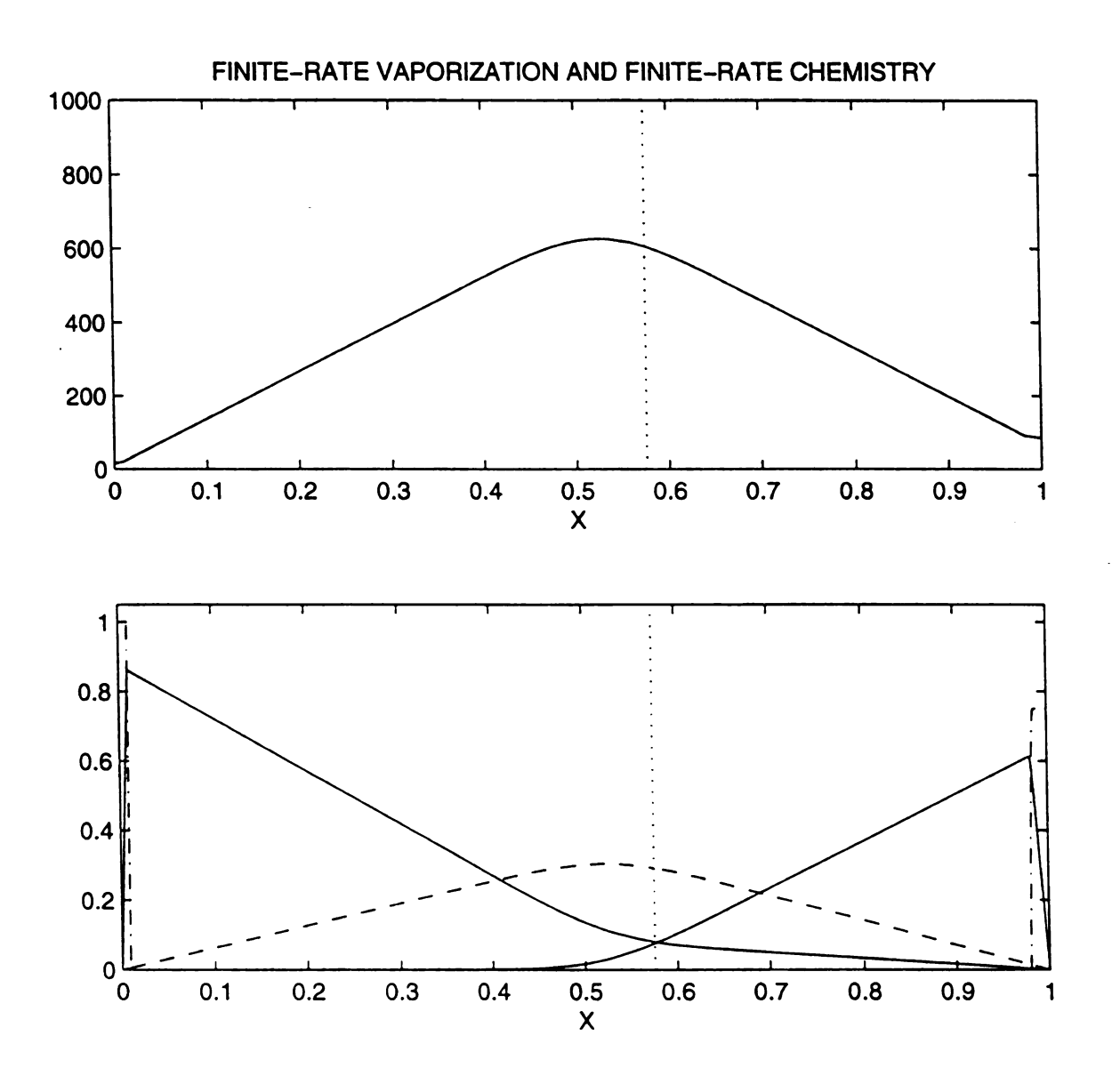


Figure 23. A result of finite-rate vaporization and finite-rate chemistry at extinction in X-coordinate, with $Y_{OO} = 0.15$, $Y_{FF} = 0.025$, K=26.50/sec, and the original diameter of $O_2 = 1.0 \mu$ m. Upper diagram: T [K]. Lower diagram: \tilde{Y}_{Fg} , \tilde{Y}_{Og} (_), \tilde{Y}_{Fl} , \tilde{Y}_{Ol} (-.), \tilde{Y}_{P} (--).

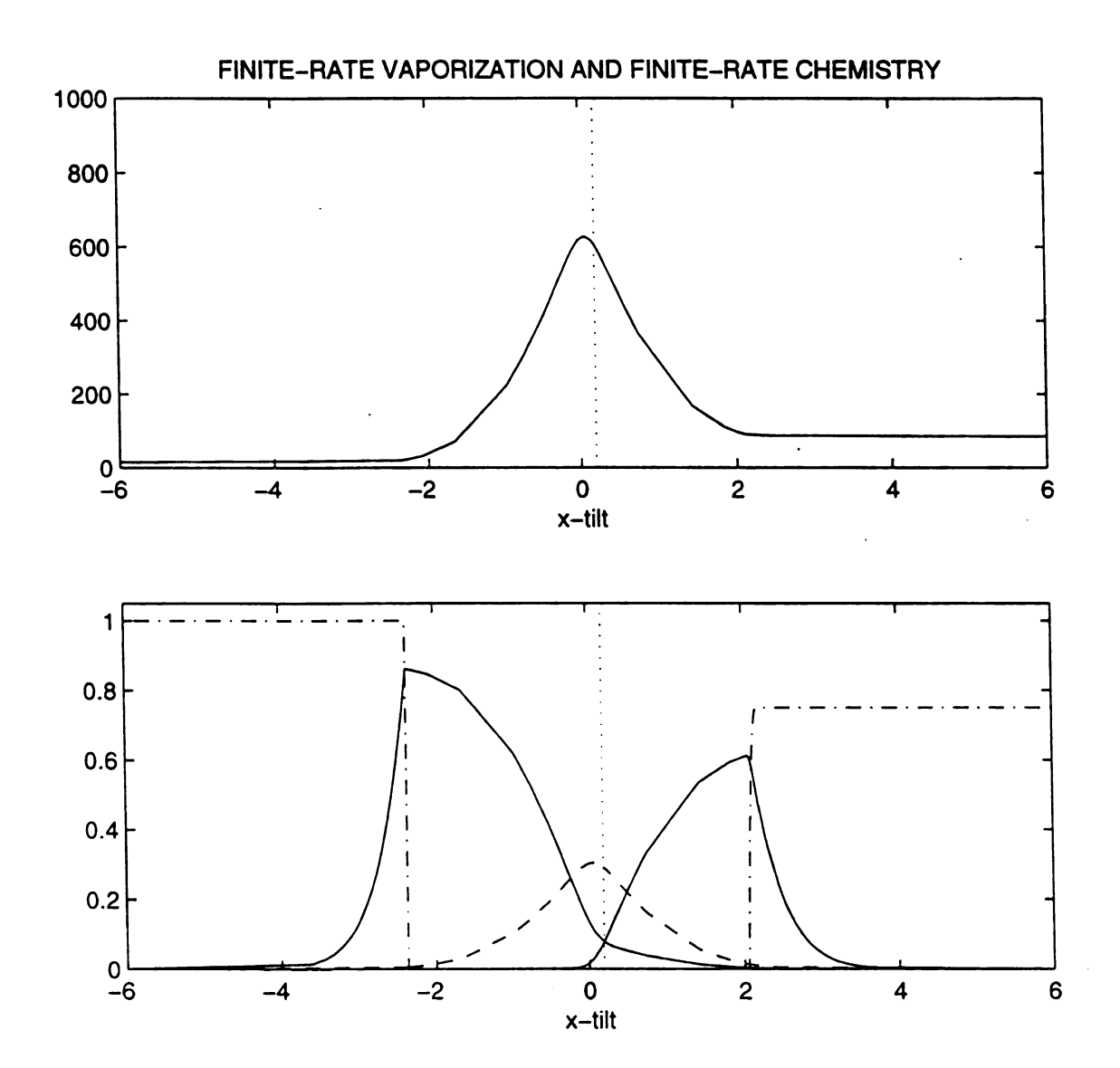


Figure 24. A result of finite-rate vaporization and finite-rate chemistry at extinction in \tilde{x} -coordinate, with $Y_{OO}=0.15$, $Y_{FF}=0.025$, K=26.50/sec, and the original diameter of $O_2=1.0~\mu$ m. Upper diagram: T [K]. Lower diagram: \tilde{Y}_{Fg} , \tilde{Y}_{Og} (_), \tilde{Y}_{Fl} , \tilde{Y}_{Ol} (-.), \tilde{Y}_{P} (--).



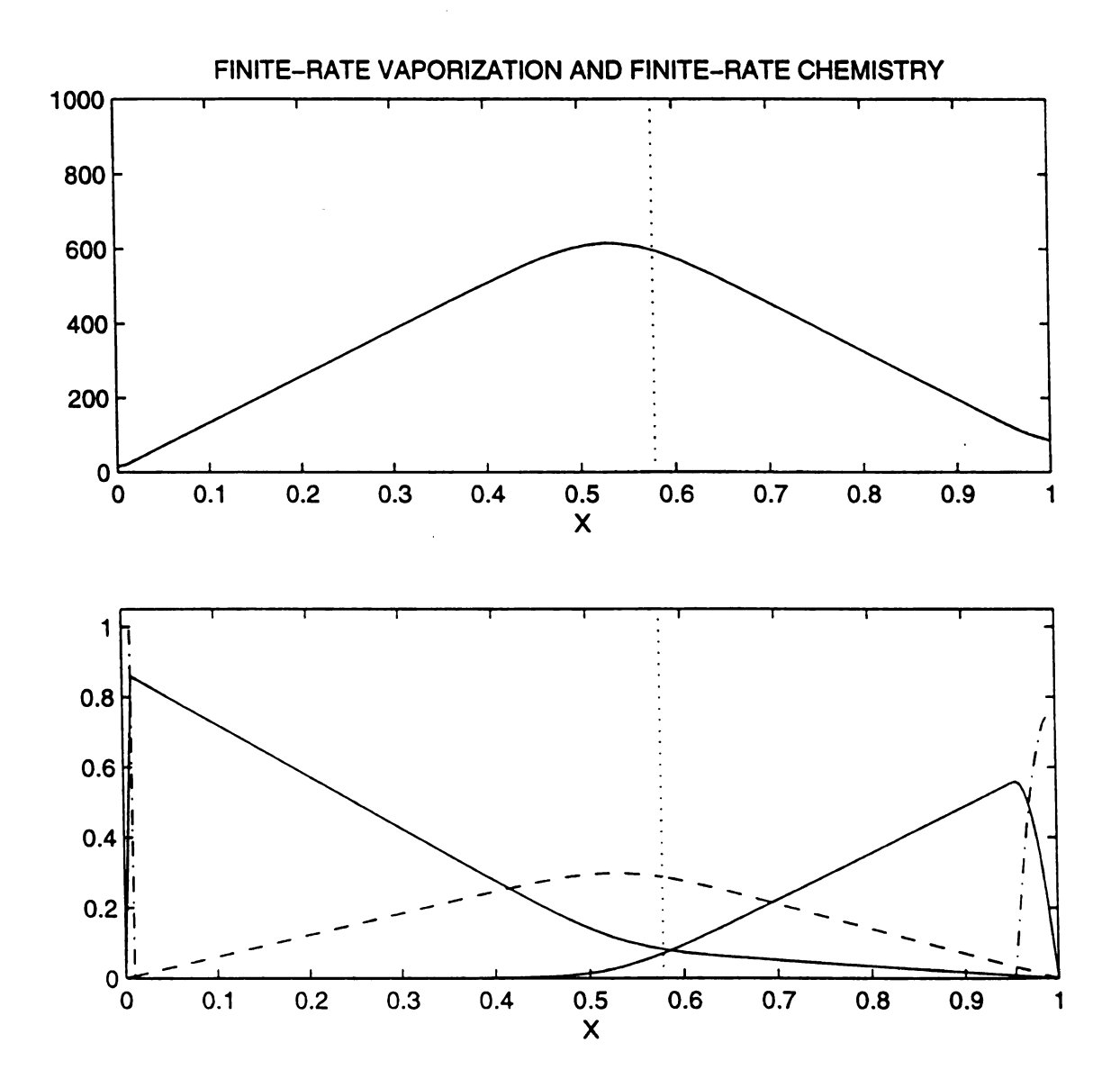


Figure 25. A result of finite-rate vaporization and finite-rate chemistry at extinction in X-coordinate, with $Y_{OO} = 0.15$, $Y_{FF} = 0.025$, K=21.39 /sec, and the original diameter of $O_2 = 10 \mu$ m. Upper diagram: T [K]. Lower diagram: \tilde{Y}_{Fg} , \tilde{Y}_{Og} (_), \tilde{Y}_{Fl} , \tilde{Y}_{Ol} (-.), \tilde{Y}_{P} (--).



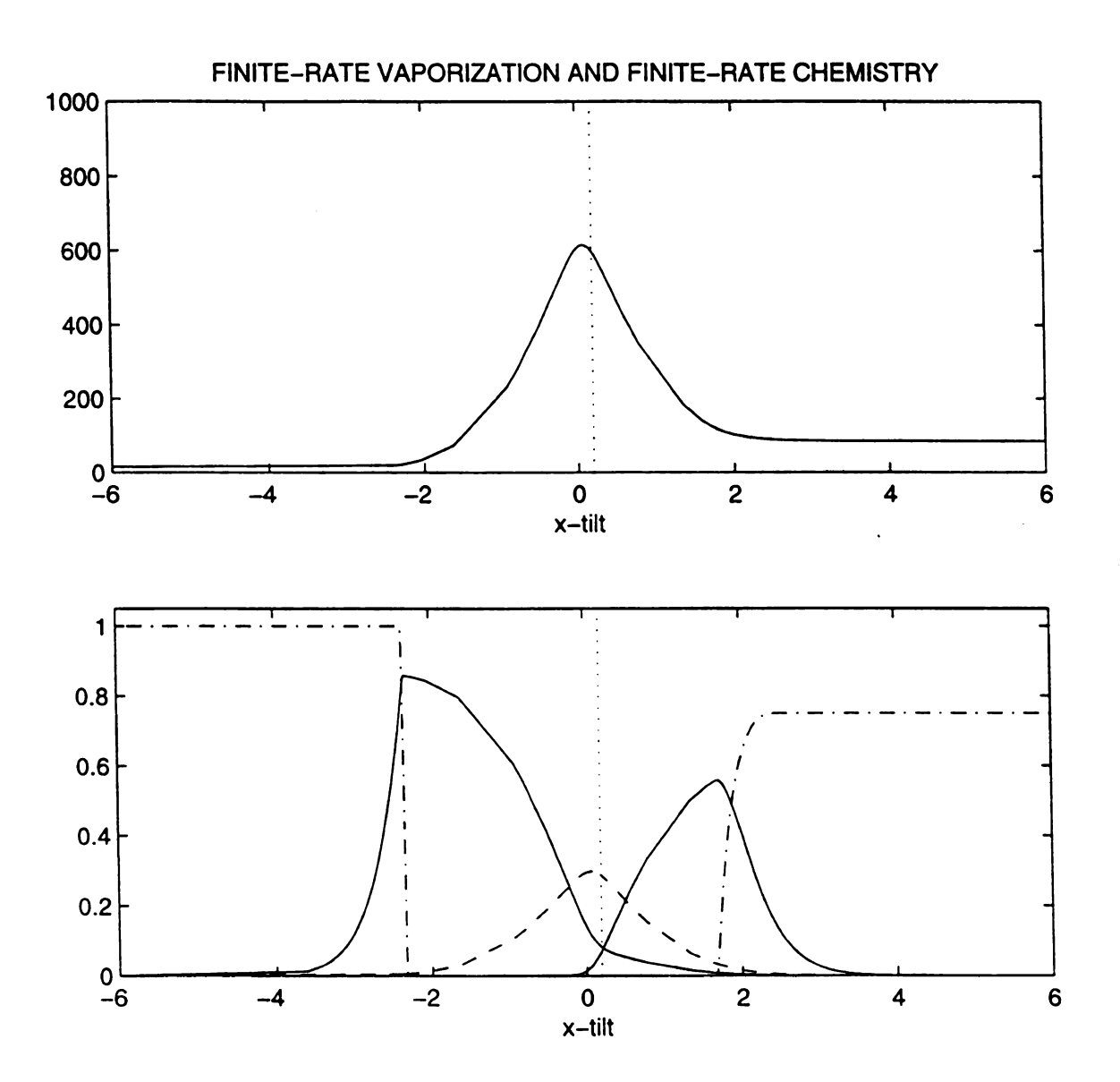


Figure 26. A result of finite-rate vaporization and finite-rate chemistry at extinction in \tilde{x} -coordinate, with $Y_{OO}=0.15$, $Y_{FF}=0.025$, K=21.39 /sec, and the original diameter of $O_2=10~\mu$ m. Upper diagram: T [K]. Lower diagram: \tilde{Y}_{Fg} , \tilde{Y}_{Og} (_), \tilde{Y}_{Fl} , \tilde{Y}_{Ol} (-.), \tilde{Y}_{P} (--).

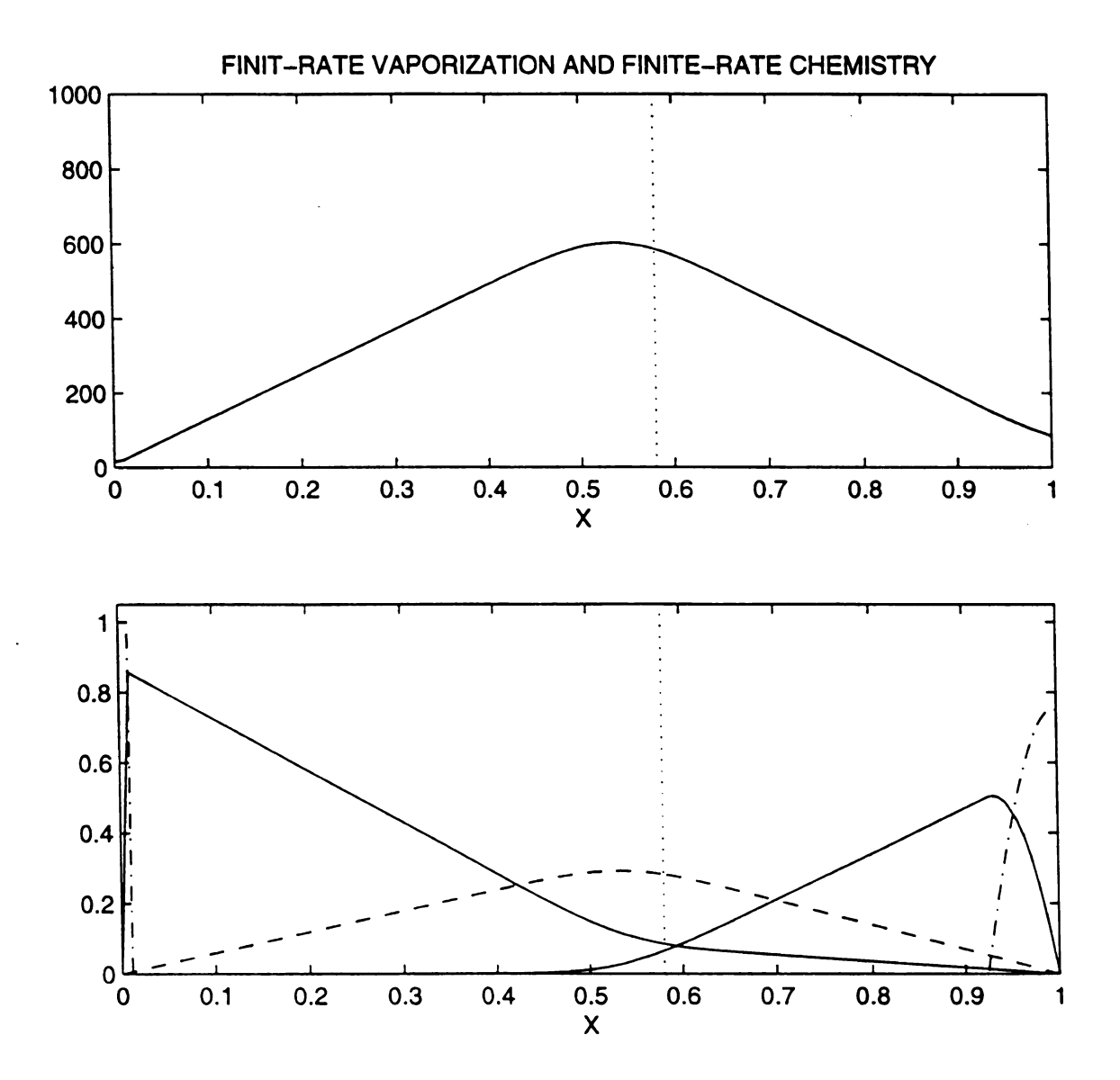


Figure 27. A result of finite-rate vaporization and finite-rate chemistry at extinction in X-coordinate, with $Y_{OO} = 0.15$, $Y_{FF} = 0.025$, K=17.02/sec, and the original diameter of $O_2 = 20 \mu$ m. Upper diagram: T [K]. Lower diagram: \tilde{Y}_{Fg} , \tilde{Y}_{Og} (_), \tilde{Y}_{Fl} , \tilde{Y}_{Ol} (-.), \tilde{Y}_{P} (--).



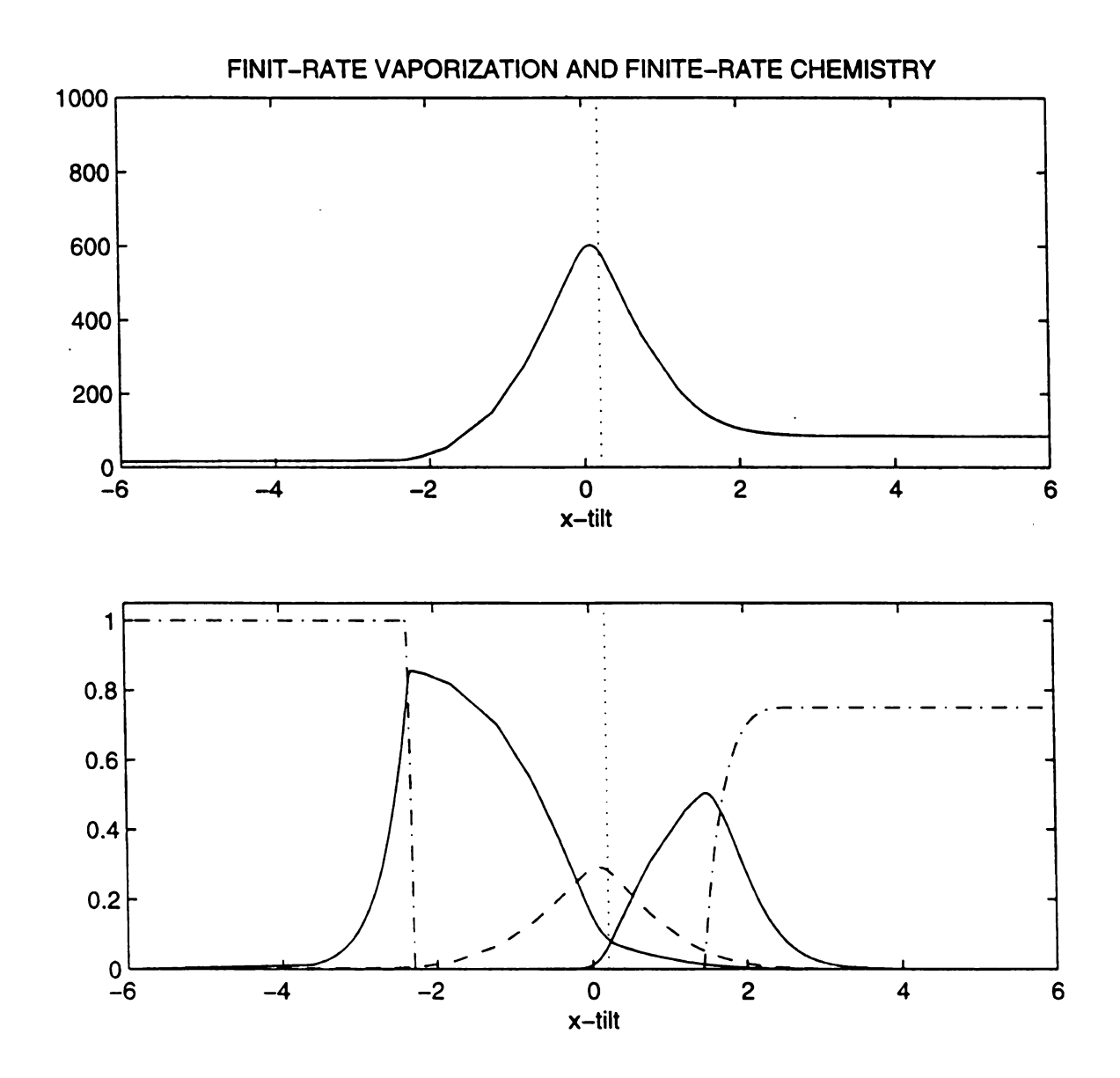


Figure 28. A result of finite-rate vaporization and finite-rate chemistry at extinction in \tilde{x} -coordinate, with $Y_{OO}=0.15$, $Y_{FF}=0.025$, K=17.02/sec, and the original diameter of $O_2=20~\mu$ m. Upper diagram: T [K]. Lower diagram: \tilde{Y}_{Fg} , \tilde{Y}_{Og} (_), \tilde{Y}_{Fl} , \tilde{Y}_{Ol} (-.), \tilde{Y}_{P} (--).

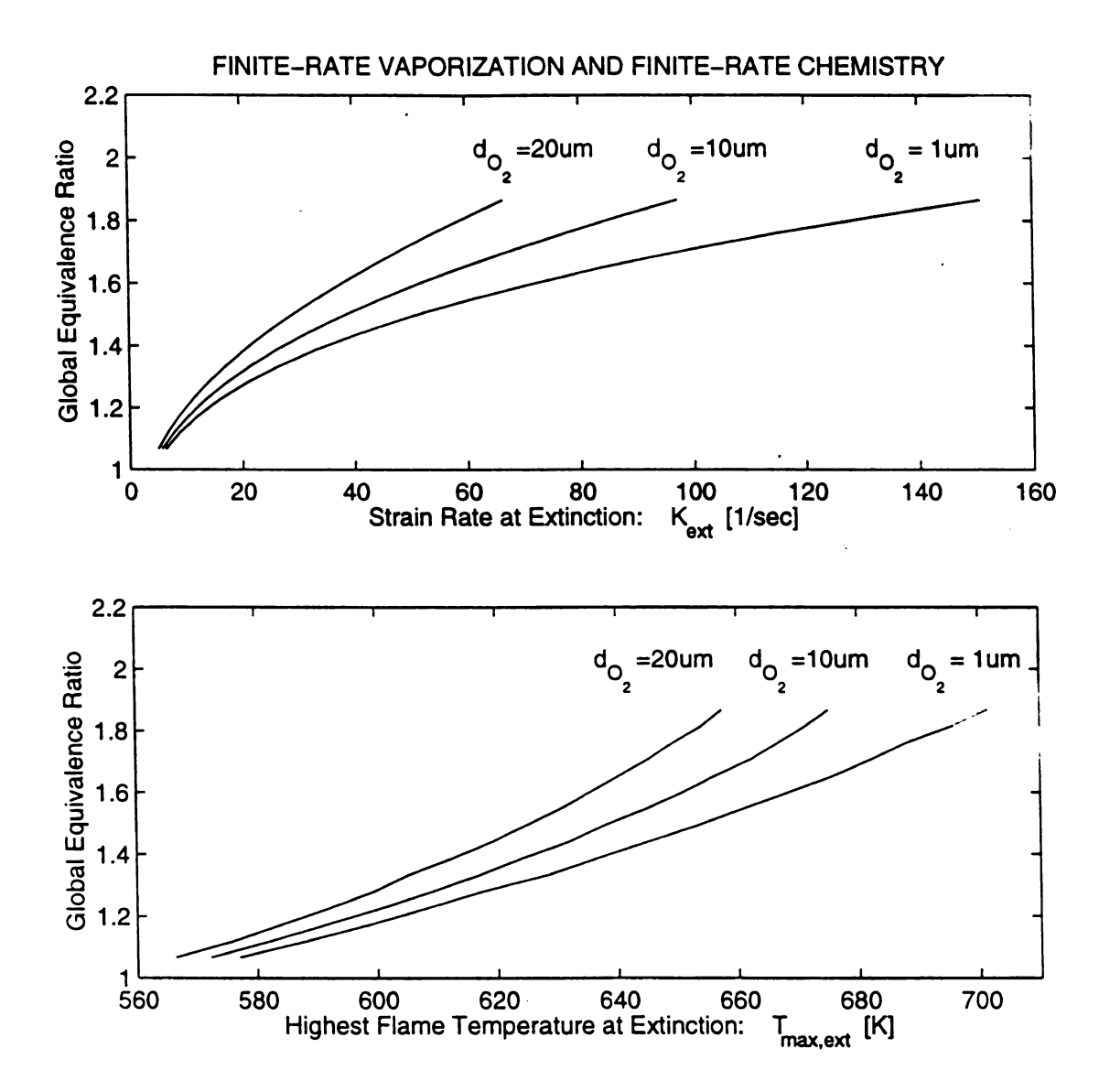


Figure 29. Results of finite-rate vaporization and finite-rate chemistry shown as (upper) the global equivalence ratio ϕ versus strain rate at extinction, K'_{ext} [1/sec], and (lower) ϕ versus the highest flame temperature at extinction, $T_{max, ext}$ [K], with $Y_{OO} = 0.15$, and the original diameter of $O_2 = 1 \mu m$, $10 \mu m$, $20 \mu m$.

CHAPTER SEVEN

COMPARISON BETWEEN THE DOUBLE-SPRAY, FUEL-SPRAY-ONLY, AND PURELY-GASEOUS MODELS

Figure 30 compares Figure 29 with the fuel-spray-only case, featuring oxygen in the gaseous phase and the original droplet diameter of hydrogen at 0.21 μ m, 2.1 μ m, and 4.1 μ m, and with the purely-gaseous case, featuring both hydrogen and oxygen in gaseous phases. Either in the global equivalence ratio versus K_{ext} or in that versus $T_{max, ext}$, we may conclude the following:

- (1) First look at the purely-gaseous curve, and then the existence of fuel spray shifts the curve leftward (meaning more extinguishable and lower flame temperature), and the existence of "double-spray" shifts the curves further leftward.
- (2) The variety in the droplet size causes divergence of the curves, and the variety in the oxidizer droplet size exerts a dominant influence upon such divergence rather than that in the fuel droplet size does.

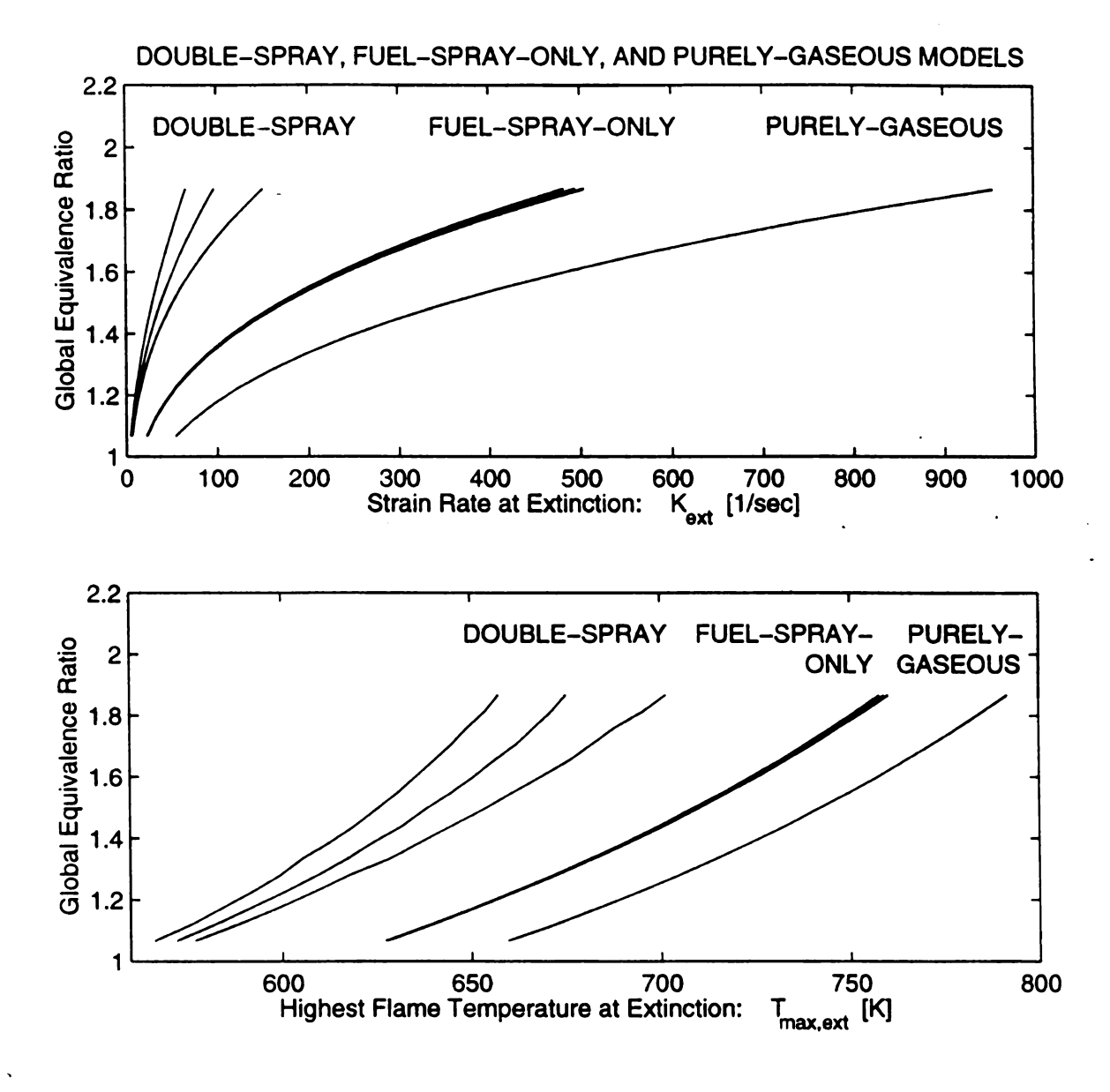


Figure 30. Comparison between the Double-spray, Fuel-Spray-Only, and Purely-Gaseous Models

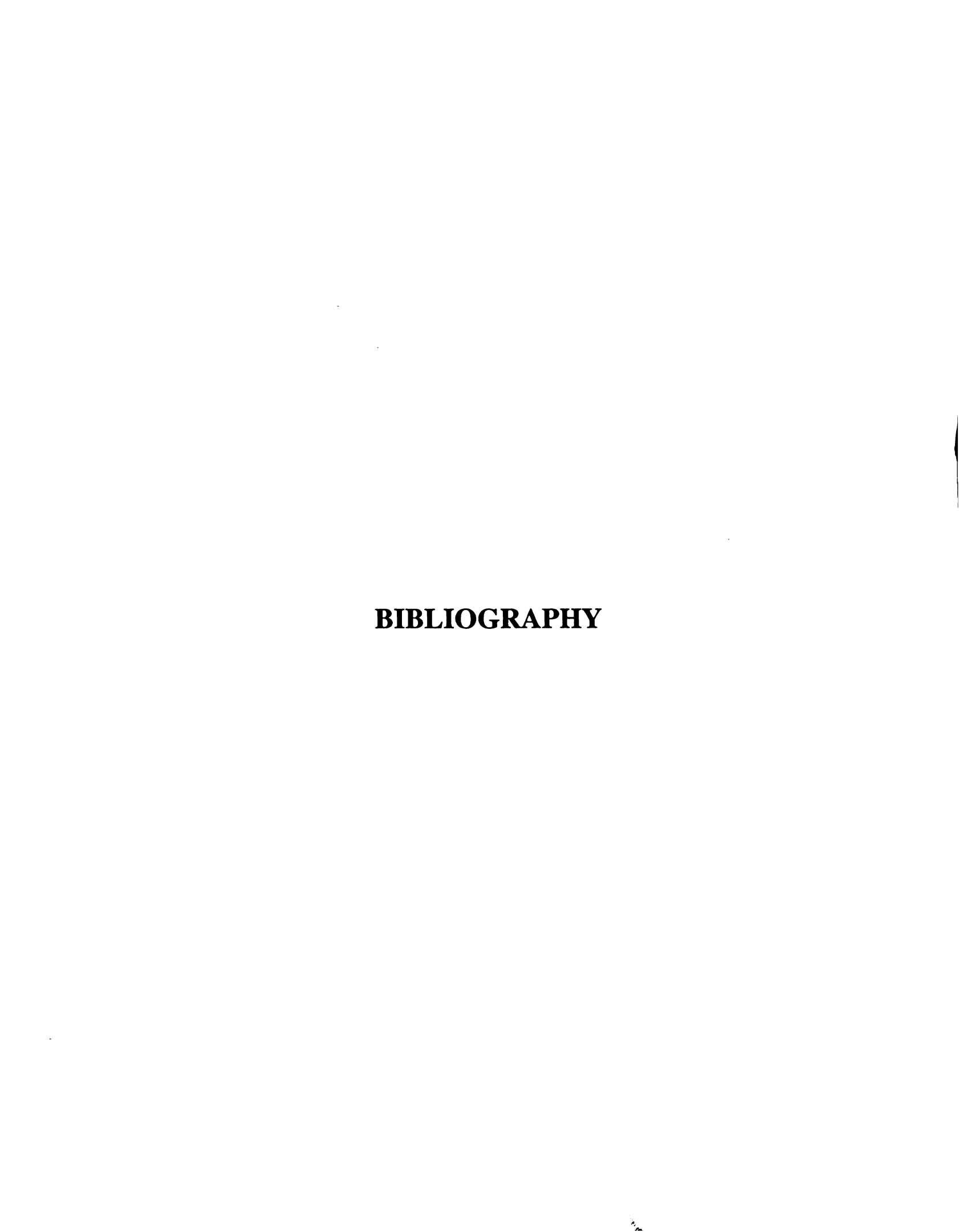
CONCLUSION

We have investigated our model both theoretically and numerically: we make a few thermodynamic assumptions in Chapter 1, develop governing differential equations in Chapter 2, and set up algebraic analysis as well as computation routines for three typical cases in Chapters 3, 4, and 5, respectively, present and discuss the numerical results of these three cases in Chapter 6, and finally, compare the results in our model to those in the fuel-spray-only and purely-gaseous models. The numbers we obtain are consistent with physical reality, which means that our theoretical derivations are correct.

One of the recommended directions to extend our work is to change the double-spray model toward the liquid rocket engine, where the reactants' vaporization is driven by pressure difference, and where the reactants are pure at their origins (i.e., no background gases). We anticipate this as a significant approach in the combustion studies.

MORAL OF THE STORY:

EACH NUMBER CARRIES A PHYSICAL REALITY!



BIBLIOGRAPHY

- Versaevel, P. (1993), "Counterflow Spray Diffusion Flames: Comparison between Asymptotic, Numerical, and Experimental Results," Ecole Centrale de Paris, France. Unpublished.
- 2. Doyle, S. E. and Hall, R. C. (1992), "History of Liquid Rocket Engine developed in the United States 1955-1980," American Astronautical Society.
- 3. Williams, F. A. (1985), "Combustion Theory," Benjamin/Cummings Publishing Co.
- 4. Reid, R. C., Prausnitz J. M., and Poling, B. E. (1987), "The Properties of Gases and Liquids," McGraw-Hill Publishing Co.
- 5. Verkin, B. I. (1991), "Handbook of Properties of Condensed Phases of Hydrogen and Oxygen," Hemisphere Publishing Co.
- 6. Sychev, V. V., Vasserman, A. A., Kozlov, A. D., Spiridonov, G. A., and Tsymarny, V. A. (1987), "Thermodynamic Properties of Helium," Hemisphere Publishing Co.
- 7. Strahle, W. C. (1993), "An Introduction to Combustion," Chapter 3, Gordon and Breach, Overseas Publishers Association, Amsterdam (2nd printing 1996).
- 8. Lefebvre, A. H. (1989), "Atomization and Sprays," Hemisphere Publishing Co.

